

**OPERATION OF SOFT OPEN POINT IN A
DISTRIBUTION NETWORK UNDER FAULTED
NETWORK CONDITIONS**



Avinash Venkataramana Aithal

School of Engineering
Cardiff University

A thesis submitted for the degree of Doctor of Philosophy

February 2018

Table of Contents

| | |
|---|-------------|
| Abstract | VII |
| Declaration | VIII |
| Dedication | IX |
| Acknowledgement | X |
| List of Figures | XI |
| List of Tables | XV |
| Abbreviations | XVI |
| Chapter 1 Introduction | 2 |
| 1.1 RENEWABLE GENERATION AND ELECTRICITY DEMAND GROWTH | 2 |
| 1.2 EMERGENCE OF SMART GRID..... | 3 |
| 1.3 RESEARCH MOTIVATION | 5 |
| 1.4 MAJOR CONTRIBUTIONS OF THIS THESIS..... | 7 |
| 1.5 LIST OF PUBLICATION | 8 |
| 1.6 OUTLINE OF THE THESIS | 9 |
| Chapter 2 State of the Art and Literature Review | 11 |
| 2.1 INTRODUCTION | 11 |
| 2.2 MEDIUM VOLTAGE DISTRIBUTION NETWORKS | 12 |
| 2.2.1 Switchgear used in distribution networks..... | 12 |
| 2.2.2 Automation in distribution networks..... | 13 |
| 2.2.3 Types of feeder automation..... | 15 |

2.2.4 Need for upgradation of assets in distribution network 17

2.3 INTRODUCTION TO SOP 19

 2.3.1 Key drivers of using SOP 19

 2.3.2 SOP and other type of FACTS devices at distribution level 20

 2.3.3 Back-to-Back VSC based SOP 22

2.4 PREVIOUS RESEARCH ON SOP 23

 2.4.1 Steady state operation 23

 2.4.2 Dynamic operation 24

2.5 SUMMARY 26

Chapter 3 Fault Studies of a Distribution Network with Soft Open Point 29

3.1 INTRODUCTION 29

3.2 MODELLING AND CONTROL OF A BACK-TO-BACK VSC BASED SOP 29

 3.2.1 Modelling of the SOP 29

 3.2.2 Control of SOP 30

3.3 DYNAMIC BEHAVIOUR OF A NETWORK WITH SOP 33

 3.3.1 Behaviour of a network with SOP during normal operation..... 33

 3.3.2 Behaviour of a network with SOP during a fault 35

3.4 FAULT ANALYSIS OF DISTRIBUTION NETWORKS WITH SOP 36

 3.4.1 Fault analysis using symmetrical components..... 36

 3.4.2 Fault analysis of a network with SOP using symmetrical components..... 37

 3.4.3 Fault detection and Fault-Index 40

3.5 SIMULATION RESULTS 41

 3.5.1 Test Network..... 41

3.5.2 Case 1: Behaviour of equivalent sequence network and its validity for different control schemes 42

3.5.3 Case 2: Capability of the SOP to detect various types of faults 47

3.5.4 Case 3: Correlation between of the sequence components (voltage/currents) and the SOP set points 49

3.6 SUMMARY 54

Chapter 4 Fault Diagnostics in Distribution Networks with Soft Open Point 56

4.1 INTRODUCTION 56

4.2 CONVENTIONAL D-FA SCHEME 56

 4.2.1 Sequence of events in a conventional D-FA Scheme..... 56

 4.2.2 Impact of using SOP on conventional D-FA scheme 59

4.3 CONVENTIONAL D-FA SCHEME WITH SOP 62

 4.3.1 Sequence of events in a conventional D-FA Scheme with SOP 64

 4.3.2 Drawbacks of D-FA schemes using auto-reclosers 66

4.4 NETWORK DIAGNOSTICS USING SOP 67

 4.4.1 Diagnostic mode of SOP operation 67

 4.4.2 The proposed D-FA scheme with the sequence of events coordinated by the SOP 70

 4.4.3 Benefits of using SOP for FA in comparison to using auto-reclosers..... 73

4.5 SIMULATION RESULTS 74

 4.5.1 Test network 74

 4.5.2 Case 1: Fault type identification 74

 4.5.3 Case 2: Detection of fault and determination of fault location 75

 4.5.4 Case 3: Improvements in restoration time 78

| | |
|---|------------|
| 4.6 SUMMARY | 79 |
| Chapter 5 Experimental Validation of Fault Diagnostics Capability of Soft Open Point | 81 |
| 5.1 INTRODUCTION | 81 |
| 5.2 DESCRIPTION OF THE EXPERIMENTAL SETUP | 81 |
| 5.2.1 VSC prototype (Hardware under test) | 81 |
| 5.2.2 Real-time digital simulator | 86 |
| 5.2.3 Power interface | 89 |
| 5.3 SIMULATION RESULTS | 91 |
| 5.3.1 Case 1: Fault detection during normal operation (grid-connected) | 92 |
| 5.3.2 Case 2: Fault detection and type identification during diagnostic mode operation..... | 93 |
| 5.3.3 Case 3: Fault location estimation during diagnostic mode operation | 97 |
| 5.4 SUMMARY | 98 |
| Chapter 6 Conclusions and Future Work..... | 100 |
| 6.1 CONCLUSION..... | 100 |
| 6.1.1 Fault analysis of a network with SOP | 101 |
| 6.1.2 Role of SOP in Feeder Automation | 102 |
| 6.1.3 Experimental validation | 102 |
| 6.2 FUTURE WORK..... | 103 |
| 6.2.1 Improvements in the diagnostic mode operation | 103 |
| 6.2.2 Broader scope of SOP applications..... | 104 |
| 6.2.3 Supplementary study to justify the methods proposed | 105 |

| | |
|-------------------------|------------|
| References | 106 |
| Appendix A..... | 116 |
| Appendix B..... | 117 |

Abstract

A Soft Open Point (SOP) is a power electronic device, usually implemented using back-to-back voltage source converters (VSCs) installed at normally-open points (NOP) of a distribution network. SOPs are typically utilised to enhance distribution network operation, under normal network conditions. Their applications include power loss reduction, feeder load balancing, network reinforcement, voltage profile improvement and distributed generation (DG) connection support. This thesis investigates the operating principle and applications of a back-to-back VSC based SOP under faulted network conditions.

The dynamics of a network with SOP were observed during normal and faulted network conditions. The conventional fault analysis technique using symmetrical components was extended to include SOP, such that it can be applied on distribution networks with SOP. Equivalent sequence networks were developed for different type of faults, including phase-to-ground faults, phase-to-phase faults and three-phase faults. The correlation between the symmetrical components (of voltages and currents) at the SOP grid connection point and the SOP set points were studied. A simple but effective method of fault detection during grid-connected operation was formulated using the sequence voltages at the grid connection point of the SOP.

The impact of the SOP dynamics on a conventional distributed feeder automation (D-FA) scheme was investigated. It was found that the current contributed from the SOP during a fault could potentially disturb the protection coordination of the network. Consequently, the sequence of events in a feeder automation scheme is disrupted if the SOP is kept operational beyond the fault ride-through period. A new operating mode was defined to operate the SOP during network faults such that it can be co-ordinated with network protection. Based on the local measurements at SOP grid connection point, methods to determine the presence of a fault, fault type and location of a fault were investigated. A D-FA scheme was proposed, in which the fault diagnostic capability of an SOP was utilised to coordinate the feeder automation sequence. Substantial improvements were achieved in both the restoration time and life of existing switchgear by using SOPs for feeder automation.

The fault diagnostic capability of an SOP was validated using a power hardware-in-the-loop (PHIL) experimental setup. A VSC prototype with a constant DC voltage source was used to emulate an SOP. The prototype was integrated with a distribution network modelled in the real-time digital simulator (RTDS), through a power interface. Individual protection features of the SOP including fault detection, fault type identification and estimation of fault location were validated using this experimental setup. The results obtained using the real-time PHIL experiment were consistent with the results obtained using software simulations.

Declaration

This work has not been submitted in substance for any other degree or award at this or any other university or place of learning, nor is being submitted concurrently in candidature for any degree or other award.

Signed _____ (Candidate) Date: 14th February 2018

Statement 1

This thesis is being submitted in partial fulfilment of the requirements for the degree of PhD.

Signed _____ (Candidate) Date: 14th February 2018

Statement 2

This thesis is the result of my own independent work/investigation, except where otherwise stated, and the thesis has not been edited by a third party beyond what is permitted by Cardiff University's Policy on the Use of Third Party Editors by Research Degree Students. Other sources are acknowledged by explicit references. The views expressed are my own.

Signed _____ (Candidate) Date: 14th February 2018

Statement 3

I hereby give consent for my thesis, if accepted, to be available online in the University's Open Access repository and for inter-library loan, and for the title and summary to be made available to outside organisations.

Signed _____ (Candidate) Date: 14th February 2018

Statement 4: Previously approved bar on access

I hereby consent for my thesis, if accepted, to be available online in the University's Open Access repository and for inter-library loans **after expiry of a bar on access previously approved by the Academic Standards & Quality Committee.**

Signed _____ (Candidate) Date: 14th February 2018

Dedication

To all that is good in this world

Acknowledgement

I would like to express my sincere gratitude and appreciation to my supervisors, Professor Jianzhong Wu and Professor Nick Jenkins, for their never-ending guidance, support and patience. I'm extremely honoured to have this research conducted under their supervision.

I'm indebted to Wenlong Ming and Ali Al-Wakeel for their help, as well as reviewing this thesis.

I will always be grateful to my research team, Lee Thomas, Qi Qi, Chao Long, Saif Sami, and Mrs Jeanette Whyte for their inputs and kindness. I will never forget the assistance, guidance and patience they showed throughout my years in Cardiff.

Special thanks to my lovely Shalini, my source of motivation. I will always be indebted to the love bestowed on me by her and my family.

I thank Simantini, Ella (and little Logan) and Shree for being my connection to the world outside during my PhD. It has been my privilege to be offered your time.

Finally, I wish to acknowledge and thank every individual who has in some way contributed to the completion of this research in the best manner in which this current volume could be presented.

List of Figures

| | |
|---|----|
| Figure 1.1 Hierarchical building blocks of smart grid; reproduced from [11] | 4 |
| Figure 1.2 Outline of the thesis | 9 |
| Figure 2.1 Network topology and voltage levels for transmission and distribution networks in GB [19]. | 11 |
| Figure 2.2 Response to a fault on a network with and without feeder automation; Figure reproduced from [18] | 14 |
| Figure 2.3 SOP in a distribution network..... | 19 |
| Figure 2.4 SOP and other type of FACTS devices at distribution level..... | 20 |
| Figure 2.5 IGBT connections in a B2B VSC based SOP..... | 22 |
| Figure 2.6 Ideal operating region for BTB VSC based SOP in P - Q plane | 23 |
| Figure 3.1 Average model of SOP | 30 |
| Figure 3.2 Classical two-level cascaded control system of an SOP. | 31 |
| Figure 3.3 P and Q flowing through grid connection point GCP1 for different set points | 34 |
| Figure 3.4 P and Q flowing through grid connection point GCP2 for different set points | 34 |
| Figure 3.5 Voltages at the grid connection points of the SOP | 34 |
| Figure 3.6 Dynamic response of the current injected from SOP after a fault at $t=1$ s .. | 35 |
| Figure 3.7 P and Q flowing through grid connection point GCP2 after a fault on Feeder-1 at $t=1$ s | 36 |
| Figure 3.8 Equivalent sequence network of a feeder with an SOP for a line-to-ground fault at f | 39 |
| Figure 3.9 Equivalent sequence network of a feeder with an SOP for a line-to-line fault at f | 39 |

| | |
|---|----|
| Figure 3.10 Equivalent sequence network of a feeder with an SOP for a three phase fault at f | 39 |
| Figure 3.11 Generic 11kV distribution network with SOP (Test network). | 41 |
| Figure 3.12 Comparison of sequence voltages for different control modes of SOP | 46 |
| Figure 3.13 Comparison of sequence currents for different control modes of SOP | 46 |
| Figure 3.14 Dynamic response of FI | 49 |
| Figure 3.15 Comparison of FI for different control modes of SOP | 49 |
| Figure 3.16 Positive sequence voltage for range of P_1^* set points, $Q_1^* = 0$ (solid lines); Range of Q_1^* set points, $P_1^* = 0$ (Dotted lines)..... | 52 |
| Figure 3.17 Negative sequence voltage for range of P_1^* set points, $Q_1^* = 0$ (solid lines); Range of Q_1^* set points, $P_1^* = 0$ (Dotted lines)..... | 52 |
| Figure 3.18 Positive sequence current for range of P_1^* set points, $Q_1^* = 0$ (solid lines); Range of Q_1^* set points, $P_1^* = 0$ (Dotted lines)..... | 53 |
| Figure 3.19 Negative sequence current for range of P_1^* set points, $Q_1^* = 0$ (solid lines); Range of Q_1^* set points, $P_1^* = 0$ (Dotted lines)..... | 53 |
| Figure 4.1 Typical distribution network..... | 57 |
| Figure 4.2 Sequence of D-FA events for a temporary fault | 58 |
| Figure 4.3 Sequence of D-FA events for a permanent fault | 58 |
| Figure 4.4 Typical distribution network with SOP | 59 |
| Figure 4.5 Recloser status and converter current for a temporary fault on feeder connected to P - Q controlled VSC. | 60 |
| Figure 4.6 Recloser status and converter current for a temporary fault on feeder connected to V_{dc} - Q controlled VSC..... | 61 |
| Figure 4.7 Voltages during temporary fault on feeder connected to V_{dc} - Q controlled VSC. | 61 |

| | |
|--|----|
| Figure 4.8 Recloser status and converter current during reclosing after a temporary fault. | 62 |
| Figure 4.9 Control scheme for the restoration mode | 63 |
| Figure 4.10 Conventional sequence of operation in a network with SOP | 64 |
| Figure 4.11 Sequence of D-FA events in a network with SOP for a temporary fault.... | 65 |
| Figure 4.12 Sequence of D-FA events in a network with SOP for a permanent fault... 65 | |
| Figure 4.13 A typical radial feeder connected to an SOP in diagnostic mode (during an AC fault) | 68 |
| Figure 4.14 Equivalent single line diagram of the radial feeder in diagnostic mode..... | 69 |
| Figure 4.15 Proposed sequence of operation using diagnostic mode | 71 |
| Figure 4.16 FA scheme using diagnostic mode of SOP for a temporary fault..... | 72 |
| Figure 4.17 FA scheme using diagnostic mode of SOP for a permanent fault..... | 72 |
| Figure 4.18 Test Network..... | 74 |
| Figure 4.19 Voltage and current phasors for L_a -G fault. | 76 |
| Figure 4.20 Voltage and current phasors for L_a - L_b fault..... | 76 |
| Figure 4.21 Voltage and current phasors for L_a - L_b - L_c fault..... | 76 |
| Figure 4.22 Comparison of restoration times between conventional FA and FA using SOP in diagnostic mode | 78 |
| Figure 5.1 Experimental setup | 82 |
| Figure 5.2 The HuT: VSC prototype and the DC voltage source | 82 |
| Figure 5.3 (a) Circuit topology; (b) Circuit board of the VSC | 84 |
| Figure 5.4 Altera DE0 Nano development board, used as the VSC controller; reproduced from [100]. | 86 |
| Figure 5.5 Operational block diagram of the VSC controller..... | 86 |

| | |
|--|----|
| Figure 5.6 Test network modelled in RSCAD | 88 |
| Figure 5.7 Basic HIL experiment architectures (a) CHIL (b) PHIL [105] | 89 |
| Figure 5.8 Functional setup of the HIL experiment [112] | 90 |
| Figure 5.9 Equivalent circuit of the HIL experimental setup..... | 90 |
| Figure 5.10 The experimental test rig..... | 91 |
| Figure 5.11 Test setup for Case 1: Fault detection for normal operation (grid-connected) | 92 |
| Figure 5.12 Test Setup for Case 2 and 3: Fault detection, type identification and determination of fault location during diagnostic mode operation..... | 93 |
| Figure 5.13 Dynamic response of FI for a L_a -G fault at section 1 | 95 |
| Figure 5.14 Voltage and current phasors for L_a -G fault. | 96 |
| Figure 5.15 Voltage and current phasors for L_a - L_b fault..... | 96 |
| Figure 5.16 Voltage and current phasors for L_a - L_b - L_c fault..... | 96 |

List of Tables

| | |
|--|-----|
| Table 2.1 Functionalities of switchgear used in distribution networks; table reproduced from [20] | 13 |
| Table 2.2 Summary of SOP and other type of FACTS devices; reproduced form [53] | 21 |
| Table 3.1 Set points (P_1^* , Q_1^*) and (V_{dc}^* , Q_2^*) during normal operation | 33 |
| Table 3.2 Symmetrical voltage components (in kV) and FI for two operating mode and various scenarios of SOP operation..... | 44 |
| Table 3.3 Symmetrical current components (in kA) for two operating mode and various scenarios of SOP operation | 45 |
| Table 3.4 FI for various SOP operating scenarios under different loading conditions.. | 48 |
| Table 4.1 Fault type determination criteria [89] | 70 |
| Table 4.2 Equations for voltage and current at GCP1 for respective faults [97], [98]... | 70 |
| Table 4.3 Values of Fault-Index, during and after a fault..... | 77 |
| Table 4.4 Calculated values of apparent impedance, estimated location and error in location estimation | 77 |
| Table 5.1 System parameters..... | 83 |
| Table 5.2 <i>FI</i> for a grid-connected system with SOP in power control mode..... | 93 |
| Table 5.3 <i>FI</i> for an isolated system with SOP in the diagnostic mode | 95 |
| Table 5.4 Calculated values of apparent impedance, estimated location and error in location estimation | 97 |
| Table A.1 The set points used to simulate Scenarios 1-4 in Case 1..... | 116 |
| Table B.1 Protection settings for recloser R1 | 117 |
| Table B.2 Protection settings for recloser R2..... | 117 |

Abbreviations

| | |
|------|--|
| AC | Alternating Current |
| A/D | Analogue to digital |
| C-FA | Centralised feeder automation |
| CML | Customer minutes lost |
| D/A | Digital to analogue |
| DC | Direct Current |
| DER | Distributed Energy Resources |
| D-FA | Distributed feeder automation |
| DG | Distributed Generation |
| DMS | Distributed Management System |
| DNO | Distribution Network Operator |
| DSO | Distribution System Operator |
| ENSG | Electricity Networks Strategy Group |
| FA | Feeder Automation |
| FDIR | Fault detection, isolation and reconfiguration |
| FI | Fault-Index |
| FPGA | Field programmable gate array |
| GCP | Grid connection point |
| GHG | Greenhouse gas |
| GHz | Giga Hertz |
| HIL | Hardware in the loop |
| HuT | Hardware under test |
| HV | High Voltage |

| | |
|-------|--|
| HVDC | High Voltage Direct Current |
| ICT | Information and Communication Technology |
| IED | Intelligent Electronic Device |
| I/O | Input/Output |
| IGBT | Insulated Gate Bipolar Transistors |
| LCNF | Low Carbon Network Fund |
| LV | Low Voltage |
| MV | Medium Voltage |
| MVDC | Medium Voltage direct current |
| NIC | Network Innovation Competition |
| NOP | Normally Open Point |
| OFGEM | Office of Gas and Electricity Markets |
| OLTC | On-load tap changer |
| PHIL | Power hardware in the loop |
| PLL | Phase locked loop |
| PWM | Pulse width modulation |
| RES | Renewable energy sources |
| RMS | Root Mean Square |
| ROS | Rest of system |
| RTDS | Real-time digital simulator |
| SCADA | Supervisory Control And Data Acquisition |
| SOP | Soft Open Point |
| SPEN | Scottish Power Energy Networks |
| TRL | Technology readiness level |

| | |
|-------|--|
| UKGDS | United Kingdom Generic Distribution System |
| UKPN | UK Power Networks |
| UPFC | Unified power flow controllers |
| VSC | Voltage source converters |
| VUF | Voltage unbalance factor |



Introduction

Chapter 1 Introduction

1.1 Renewable Generation and Electricity Demand Growth

Over the past two decades, greenhouse gas (GHG) (carbon dioxide (CO₂), methane (CH₄), nitrous oxide (N₂O)) emissions and their impact on the climate have been one of the key drivers of changes in the energy paradigm [1]. Worldwide efforts have been made to reduce the GHG emissions. Two hundred countries, including the UK gathered at Kyoto in 1997 to discuss the possible solution to the challenge. The “Kyoto Protocol” was signed in 1997 and later amended in 2012 [2]. Each of the signing member committed to cutting down their GHG emissions to at least 5% below the 1990 level during the commitment period of 2008-2012, and then updated the targets for the 2013-2020 period [3]. The “Renewable Energy Directive”, applicable for the European Union (EU) member countries, was ratified in 2009. It targeted a 20% reduction of GHG emissions by 2020 compared with the 1990 level and further by 80-95% reduction compared to 1990 by the end of 2050 [4].

A number of measures were taken by the UK government to achieve the targets set by these regulatory schemes. The UK targeted an overall increase in the amount of energy generated from renewable sources from 2% to 15% by 2020. The UK renewable energy strategy proposed the following renewable energy targets in each energy consumption sector [5] :

- more than 30% of electricity generated from renewables - A substantial increase in the use of small-scale electricity power generation connected to distribution networks;
- 12% of heat generated from renewables;
- 10% transport energy from renewables.

As a result, there has been a significant increase in the use of renewable energy, ‘clean’ generation technologies and a considerable reduction in the use of fossil fuels (e.g. coal, diesel and petrol). There is a push for change towards large-scale integration of electrified transport (e.g., electric vehicles and rail electrification) and decarbonised domestic heating (e.g., electric heating pumps) which will lead to an increase in the electricity demand. In addition, the continuous growth of population will further increase the global energy (particularly electricity) demand. Taking these factors into consideration, it is projected that the electricity demand in the UK could double by the year 2050 [6]. This will require significant changes in electric power technologies in order

to maintain sustainable, secure and affordable supply of energy. The development of the “smart grid” concept is emerging as one of the effective solutions to ensure optimal utilisation of existing infrastructure and address future challenges.

1.2 Emergence of smart grid

A smart grid is an intelligent electricity network that is designed and operated to efficiently deliver sustainable, economic and secure electricity supplies. There are many definitions of smart grid in the literature. The European Technology Platform for Smart Grids has published a definition of a smart grid as [7]–[9]

“...an electricity network that can intelligently integrate the actions of all users connected to it – generators, consumers and those that do both – in order to efficiently deliver sustainable, economic and secure electricity supplies. A smart grid employs innovative products and services together with intelligent monitoring, control, communication and self-healing technologies to:

- *Better facilitate the connection and operation of generators of all sizes and technologies*
- *Allow electricity consumers to play a part in optimising the operation of the system.*
- *Provide consumers with greater information and choice of supply.*
- *Significantly reduce the environmental impact of the total electricity supply system.*
- *Maintain or even improve the existing high levels of system reliability, quality and security of supply;*
- *Maintain and improve the existing services efficiently; and*
- *Foster market integration towards a European integrated market.”*

The “Smart Grid Vision” published by the UK’s Electricity Networks Strategy Group (ENSG) outlines the challenges that need to be addressed over the next several years to achieve a smart grid in the UK [10]. The role of distribution networks is believed to be crucial to meet the carbon reduction targets and for wider deployment of smart grid technologies.

Figure 1.1 illustrates the hierarchical building blocks of a smart grid in distribution networks. Power networks (circuit topology), information technology (IT) and telecommunication infrastructure blocks constitute its foundation layer. The fundamental

applications form the next layer that includes smart meters, data management systems, distribution management systems, substation automation and distribution automation. There are a number of smart grid enabled applications including home areas networks, electric vehicles, energy storage, distributed generation, demand side response and microgrids. The colour gradient indicates the consumer-utility orientation of the applications, with decreasing consumer involvement from the left to the right of the figure. This thesis will focus on the power networks (foundation layer) and build smart grid capabilities with vertical integration of the upper-layer applications.

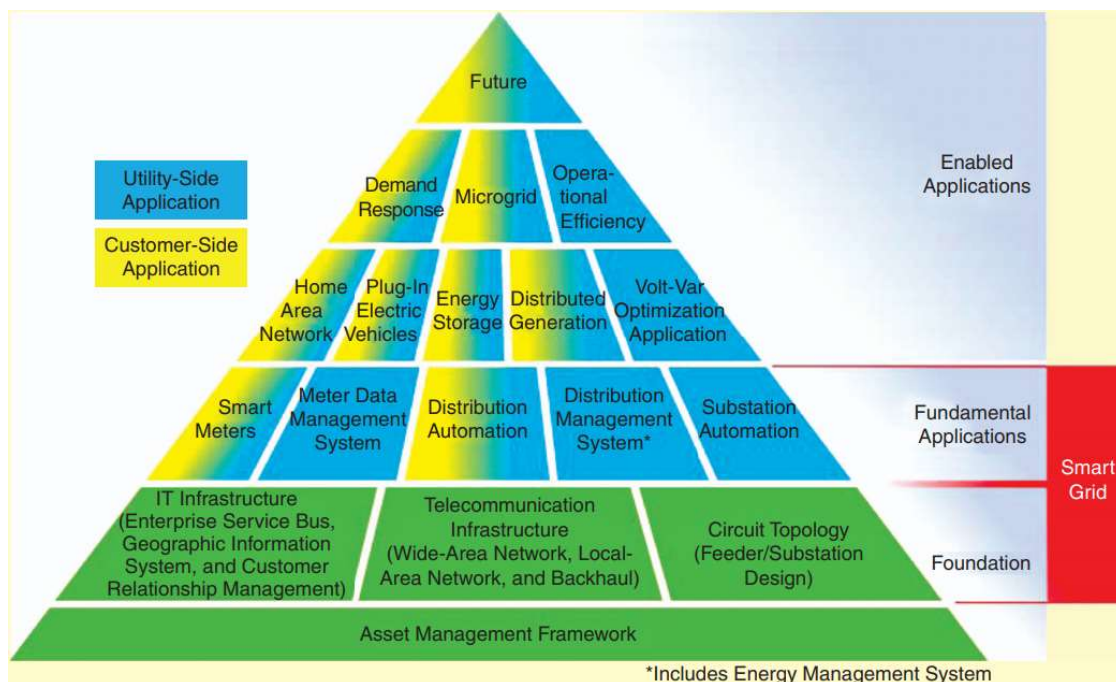


Figure 1.1 Hierarchical building blocks of smart grid; reproduced from [11]

Considerable investments are being made in smart grid research at the distribution level, through a range of initiatives by the Office of Gas and Electricity Markets (OFGEM). OFGEM established the Low Carbon Network Fund (LCNF) and its successor, the electricity Network Innovation Competition (NIC). OFGEM runs an annual competition for allocation of up to £64 million to help fund a small number of flagship projects [12], [13]. Through the LCNF and NIC projects, the distribution network operators (DNOs) are exploring new fundamental and enabled smart grid applications that can simultaneously solve more than one technical issue on distribution networks. Various smart grid projects undertaken through the LCNF and NIC projects are described in [14], [15].

1.3 Research motivation

De-carbonization of energy systems could have a profound impact on the nature and pattern of demand on the future distribution networks. DNOs are faced with a number of challenges due to increasing uptake of low carbon initiatives at the distribution level. In addition to growing electricity demand and need for network reinforcement, problems such as increase of fault level, harmonics, voltage flickers, violation of voltage and thermal limits are introduced in the network. Significant changes are needed in electricity distribution technologies in order to maintain sustainable, secure and affordable supply of electricity. Therefore, distribution networks have a great opportunity for smart interventions.

The Soft Open Point (SOP) is one of the smart grid applications of interest to distribution engineers [16]. An SOP is a power electronic device, installed at normally-open points (NOP) or normally-closed points and is most commonly modelled using a back-to-back voltage source converters (VSCs) topology. Other topologies of SOP are discussed in Section 2.3.2.

SOPs are emerging as a viable solution to address the existing and future challenges of distribution networks. They are predominantly utilised to enhance distribution network operation, under normal network conditions; including power loss reductions, feeder load balancing, network reinforcement, voltage profile improvement and DG connection support. A number of LCNF and NIC projects are currently exploring the deployment of SOPs for these benefits (details of the projects and studies can be found in Section 2.4.). The operation of SOPs under normal network conditions is presently at a technology readiness level of 6 (TRL-6) [17], on a scale from 1 to 9, with 9 being the most mature technology. TRLs are used by European Commission and UK to estimate the maturity of a technology [15]. This thesis is motivated to investigate the following points regarding the use of SOPs for distribution network operation.

1) Performance of a network with SOP under AC network faults

An SOP is a multi-functional power electronic device, and hence its deployment in a network helps realise all the aforementioned functionalities. However, previous studies in the literature mainly focused on the optimal use of SOPs under normal operating conditions and post-fault conditions of the network (details of these studies can be found in Section 2.4.). Therefore, the operating principle of an SOP under faulted network conditions needs to be investigated. Majority of the work on behaviour of VSC based devices during AC faults was focused on transient studies. There is a clear need

to investigate the dynamic behaviour of a network with an SOP during network faults. A method needs to be developed to carry out holistic system studies incorporating an SOP in the network, particularly during faulted conditions.

2) Co-ordination between feeder automation and SOP

Power distribution at 11/6.6 kV level is through open ring circuits feeding from primary substations to normal open points (NOP) that provide interconnection with adjacent feeders. These feeders are usually operated in a radial configuration under normal un-faulted network conditions. Network operators often use feeder automation (FA) schemes to improve the reliability of their networks (the detailed discussion is in Section 2.3). FA schemes ensure that a distribution network follows predetermined steps to automatically isolate the faulted section [18]. In case of permanent faults, power is re-routed to unaffected feeder sections through the healthy feeder by closing the NOP. The desired sequence of events in a FA scheme is achieved through proper coordination of all the associated devices. The impact of installing an SOP on such feeders with existing FA schemes and their interactions with the sequence of events have not been fully explored. In the conventional operating philosophy, an SOP is not co-ordinated with FA schemes and remains disconnected until the network is restored. SOP has a potential to significantly improve fault response of a network because of its capability of fast response and flexible control. However, there have been no attempts to investigate the possible enhancements in network performance during a fault, due to the presence of an SOP.

3) Hardware-in-the loop testing

Typically, the objective of performing software simulation is to obtain results as fast as possible. Depending upon the available computational power, the execution time for individual calculation could differ from the real-world time. Therefore software simulations, particularly relating to protection studies are not always sufficient to validate a technology. Furthermore, there is a need to perform laboratory-based prototype testing in order to develop the technology to a higher technology readiness level.

1.4 Major contributions of this thesis

The major contributions of this thesis are described below.

1) Conventional fault analysis technique was extended for distribution networks with SOP

The performance of a medium voltage distribution network with SOP was investigated during grid-side AC faults. Use of symmetrical components of voltage and currents was extended to include the SOP such that the conventional fault analysis technique can be used on distribution networks with SOPs. Equivalent sequence networks were developed for networks with an SOP during short circuit faults (including phase-ground, phase-phase and three phase faults). Dependence of the sequence voltages and currents on SOP set points was also investigated.

A method was developed to detect AC faults in a grid supplied distribution network with an SOP. A Fault-Index (FI) was defined using the sequence voltages at the grid connection point of the SOP, without using any additional devices. The effectiveness of FI to detect faults on distribution networks was verified using software simulations.

2) A feeder automation scheme was developed in which the SOP was used to coordinate the sequence of events.

The impact of using an SOP on the conventional distributed feeder automation (D-FA) scheme was investigated. A diagnostic mode was developed to operate the SOP during grid-side AC faults such that it can be used for fault diagnostics of the connected network. Local voltage and current measurements at the grid connection point of the SOP were used to detect AC faults, estimate fault type and locate a fault in radial distribution networks.

A D-FA scheme was developed that includes the SOP. The diagnostic mode operation of the SOP was used to coordinate the sequence of FA events after a fault. This scheme incorporates the diagnostic mode operation with the existing operating modes of the SOP to improve the performance of the network during a fault. The benefits of incorporating the SOP into D-FA was compared to conventional feeder automation schemes using reclosers.

3) The diagnostic capability of the SOP was validated using hardware-in-the-loop experiments.

The behaviour of a network with an SOP was tested using real-time hardware-in-the-loop (HIL) experiments. Power hardware-in-the-loop (PHIL) experiments were carried out using a VSC prototype and a distribution network modelled in a real-time digital simulator (RTDS), both connected through a power interface. The diagnostic mode operation and its individual protection features (including fault detection, fault type identification and estimation of fault location) were validated using this experimental setup. Experimental results were compared to the software simulation results to validate the diagnostic capability of SOP.

1.5 List of publication

The research carried out in this thesis has resulted in the following publications

1. **Aithal, Avinash**, Gen Li, Jianzhong Wu, and James Yu. "Performance of an Electrical Distribution Network with Soft Open Point during a Grid-Side AC Fault." *Applied Energy* (2017).
2. **Aithal, Avinash**, Chao Long, Wanyu Cao, Jianzhong Wu, and Carlos E. Ugalde-Loo. "Impact of Soft Open Point on Feeder Automation." In *Energy Conference (ENERGYCON), 2016 IEEE International*, pp. 1-6. IEEE, 2016.
3. **Aithal, Avinash**, Gen Li, and Jianzhong Wu. "Grid Side Unbalanced Fault Detection using Soft Open Point in an Electrical Distribution Network." *Energy Procedia* 105 (2017): 2859-2864.
4. **Aithal, Avinash** and Jianzhong Wu. "Operation and Performance of a Medium Voltage DC link" *CIREC-Open Access Proceedings Journal 2017*, no. 1 (2017): 1355-1358.
5. **Aithal, Avinash**, Wenlong Ming, Jianzhong Wu and Lee Thomas "Fault Diagnostics in Medium Voltage Distribution Networks using a Soft Open Point" (submitted to IEEE Transactions on Smart Grid; under peer review process).

1.6 Outline of the thesis

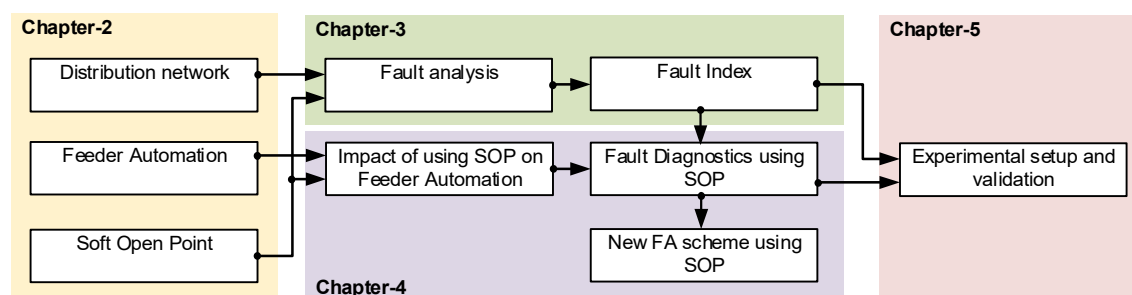


Figure 1.2 Outline of the thesis

Figure 1.2 illustrates the research described in this thesis, grouped into respective chapters.

Chapter 2 describes typical distribution networks in the UK. An overview of the different switching devices used in the networks are discussed. The role of feeder automation in restoring power during a fault is presented. This chapter also provides a concise introduction to the SOP, its types and benefits. An up-to-date literature review of existing research about SOP in distribution network is summarised.

Chapter 3 describes the performance of a medium voltage distribution network with a connected SOP, under grid-side AC faults. Use of sequence networks is extended to include the SOP such that the conventional fault analysis technique can be used on a distribution network with an SOP. Offline software simulations are carried out on a generic distribution network with connected SOP to study the equivalent sequence networks.

In **Chapter 4**, the impact of using SOP on an existing D-FA scheme is investigated. The drawbacks of conventional FA schemes are discussed. A method was developed to diagnose AC faults on radial medium voltage distribution networks using SOPs. A new feeder automation scheme is described using an SOP to carry out the fault diagnostics on the connected network.

An experimental setup used to validate the diagnostic capability of an SOP is described in **Chapter 5**. The experimental results obtained using a VSC prototype and a distribution network model in RTDS were compared with the software simulation results obtained in Chapter 3.

Chapter 6 presents the conclusions drawn, main findings and recommendations for future work.

2

State of the Art and Literature Review

Chapter 2 State of the Art and Literature Review

2.1 Introduction

The network topology and voltage levels for transmission and distribution networks in the GB main land is illustrated in Figure 2.1. The transmission network operates at 400 kV and 275 kV (extra-high voltage (EHV)), with 132 kV (high voltage) used for some transmission and sub-transmission routes. Distribution networks operate at medium voltage at the primary substation (33 kV and 11 kV with some legacy use of 66 kV and 6.6 kV) [19], [20]. The low voltage distribution networks operate at 400 V and constitute the network supplying the domestic and some commercial customers. The figure also illustrates the load density at different transmission and distribution levels. The studies carried out in this thesis mainly focus on 11 kV distribution networks.

In Great Britain (GB), there are 14 licensed DNOs that operate the distribution networks. They are each responsible for a regional distribution service area. The 14 DNOs are owned by six different commercial groups. The regulator OFGEM supervises the development of markets and competition to ensure the required services are provided to customers at a reasonable price. OFGEM also promotes security of supply and sustainability, for present and future generations of consumers.

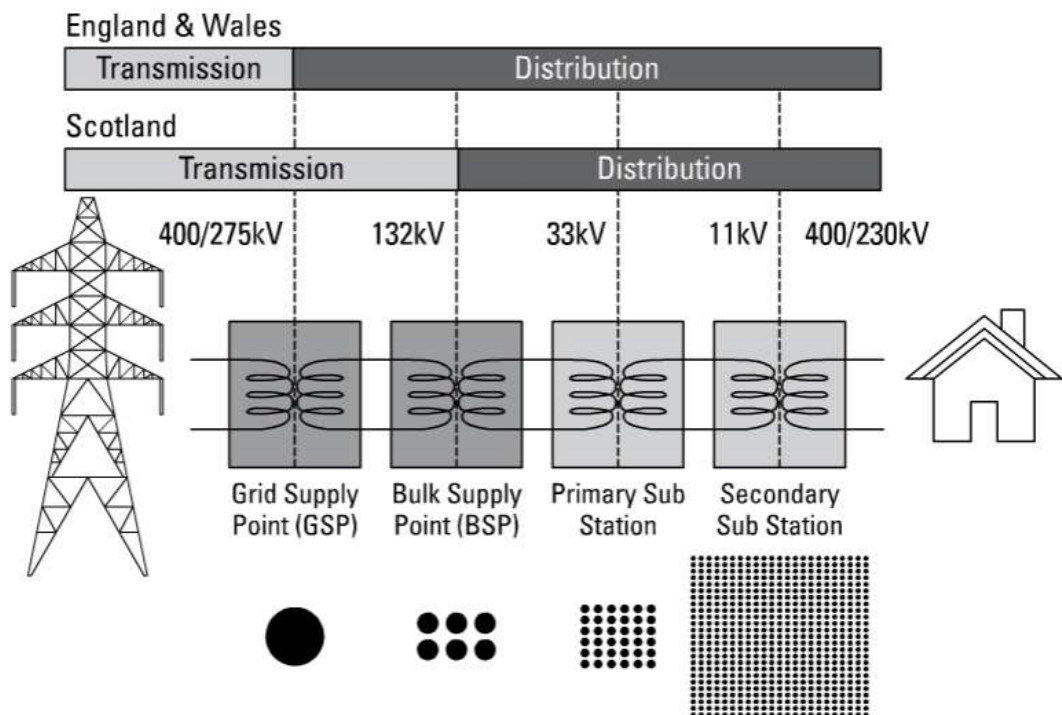


Figure 2.1 Network topology and voltage levels for transmission and distribution networks in GB [19].

2.2 Medium voltage distribution networks

A distribution network distributes electrical power from sources to a number of load points using a system of interconnected electric lines. A typical distribution network has step down transformers at the bulk supply points and primary substations, which then feed a number of feeders. The consumers are supplied through a number of secondary substations spaced along the primary distribution feeders with varying lengths.

Primary substations have transformers with on-load tap-changers (OLTC) as the principal means of voltage regulation. Some of these tap changers are being upgraded to enable remotely controlled switching actions. However, a significant number OLTCs continue to operate locally using a relatively simple line-drop compensation. A number of papers in the literature investigate alternative methods of voltage regulation using power electronic devices. Details regarding this are discussed in the following sections of this chapter.

Conventional distribution network design was guided by the assumption that the network would almost exclusively service loads with no generation connected at these voltages. Feeders typically use radial lines (double circuits at 33 kV and single circuit at 11 kV) with normally-open and normally-closed points. Most distribution networks operate radially to have less short circuit current and better protection co-ordination [20]. Power delivery systems comprise of a number of primary devices that deliver power and secondary devices that protect and allow control of the primary devices. The following subsection outlines the switching devices used in a distribution network.

2.2.1 Switchgear used in distribution networks

Switchgear is a general term covering switching devices. A number of these devices associated with interconnection and protection are used in distribution networks. Devices that are most commonly used by the distribution utilities are listed below [21].

- Switch
- Switch Fuse unit (SFU)
- Circuit breaker
- Recloser
- Disconnecter (Sectionalizer)

A switchgear's service is defined by its current breaking capacity, current making capacity, normal current rating, and Standard operating duty cycle. The switching capacity is the value of current, at a given rated voltage, at which a switchgear can operate (break/make) safely. Duty cycle for a switchgear is the prescribed number of unit-operations (one close-open operation) performed in a standardised sequence at allowable current levels [20][22]. The details of the operating sequence are defined by their respective governing IEC/IEEE standards. A comparison between the above listed devices, based on these parameters are listed in Table 2.1

Table 2.1 Functionalities of switchgear used in distribution networks; table reproduced from [20]

| Type | Rated current | | Fault current | | Duty cycle (Number of unit operations) |
|------------------------|---------------|------|---------------|------|---|
| | Break | Make | Break | Make | |
| Switch | Yes | Yes | No | Yes | Single |
| Switch Fuse unit (SFU) | Yes | Yes | No | No | Single |
| Circuit breaker | Yes | Yes | Yes | Yes | Single |
| Recloser | Yes | Yes | Yes | Yes | Multiple |
| Sectionalizer | Yes | Yes | No | No | Single |

The medium voltage (MV) switchgear is governed by the standards "IEC 62271-200-2003: ac metal-enclosed switchgear and control gear for rated voltages above 1 kV and up to and including 52 kV" [23] ; "IEC 60694-2002: common specifications for high-voltage switchgear and control gear standards" [24] and "IEEE C37.20.2-1999: IEEE standard for metal-clad switchgear" [25]. Detailed comparative requirements of IEC and IEEE standards for MV switchgear are discussed in [26] .

It is desirable to have remote operation capability in the switching devices to enable operation through control signal initiated by automation or a control engineer. A combination of primary switchgear and number of secondary devices such as voltage transformers, current transformers, fault passage indicators and auxiliary contactors are used for the automation of distribution network operation. Such systems ensure minimal impact to customers during an event on the network and allow for faster restoration of network. The details of automation in distribution networks are discussed in the following section.

2.2.2 Automation in distribution networks

Distribution automation (DA) is used by DNOs to improve the reliability of networks. DA operates on multiple control hierarchical layers. They include substation,

feeder and customer layers [20]. DNOs develop business cases for each layer, targeting areas where improved performance produces measurable benefits. Deployment and acceptance of these layers across the industry are varied. However, in the UK, there is a strong business case for the deployment of automation at feeder level based on the performance indicators outlined by OFGEM. An interruption of power supply over three minutes is registered as an event and the DNOs are heavily penalised for the excess customer minutes lost (CML) [27].

DNOs use various types of FA schemes in order to minimise the interval between a fault on a feeder and its corrective action. Typical response to a fault with and without feeder automation is compared in Figure 2.2. The figure indicates the time required for the restoration of power onto unfaulted feeders in the event of a permanent fault. In a network without automation, there are considerable delays on account of patrolling of the circuit before manual switching of circuit breakers. Therefore restoration of power to unfaulted feeders could take up to 50-80 mins [18]. Usually, this can be reduced to meet OFGEM requirements with the use of FA. Introduction of FA ensures that the unfaulted feeders are restored automatically while the repair of the faulted feeder can continue. Consequently, the total time required to repair a faulted feeder to its normal condition is also improved.

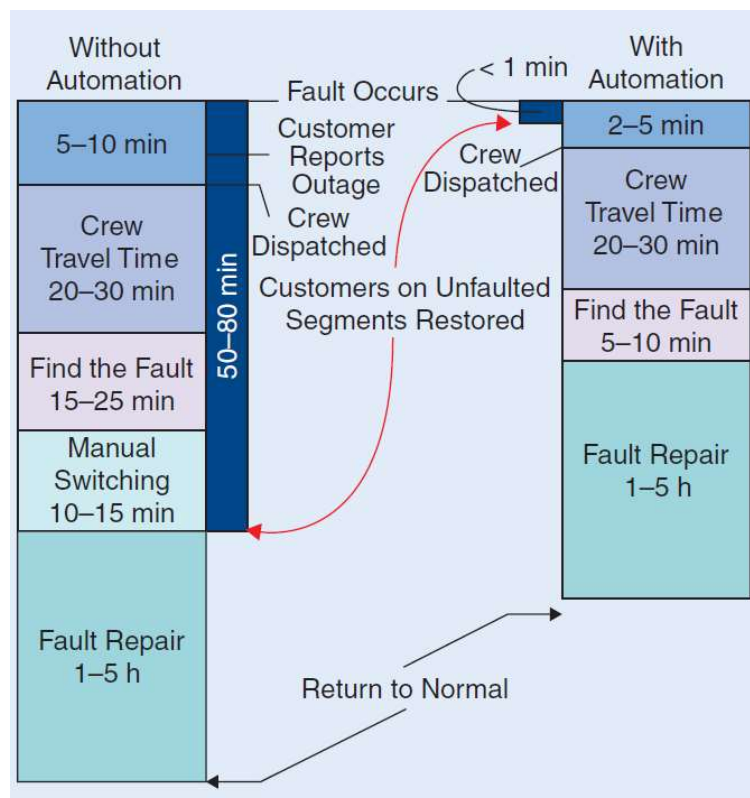


Figure 2.2 Response to a fault on a network with and without feeder automation; Figure reproduced from [18]

2.2.3 Types of feeder automation

Improvements in restoration time are achieved by automatic fault detection, isolation and restoration (FDIR) of faulted segments of distribution feeders via sensors, controls, switches, and communications systems. The associated devices can operate autonomously in response to local events or in response to signals from a central control system.

FA deployment is broadly classified into two categories based on the control philosophy of the switchgears and its associated use of communication infrastructure [28], [29]. The categories are

1) Centralised feeder automation (C-FA)

In modern energy infrastructure the automation is achieved by central control of multiple intelligent electronic devices (IEDs) spread through the distribution network. The data from each device is read and the desired outcome of the network situation is decided by the logic programmed in a control centre. The action commands are then transmitted to the applicable devices. C-FA may be implemented as one of the applications of Distribution Management Systems (DMS) or supervisory control and data acquisition (SCADA) systems. C-FA systems require an accurate load model information and a complex communication infrastructure such that each switch controller can communicate with the control centre directly. This method allows for the highest possible optimisation of FA with complex switching logics [28]. However, the overall response time of a complete automation system may be comparatively high. The developments in this area are dominated by the improvements in the information and communication technology (ICT) infrastructure. Authors of [28], [30], [31] explore the developments in C-FA and the ICT infrastructure.

2) Distributed feeder automation (D-FA)

A more basic form of feeder automation without using a complex communication infrastructure is still extensively used in the networks. The distributed FA uses intelligent-controlled devices at each switchgear locations. These devices communicate with each other to determine the appropriate switching actions necessary for restoration.

Typically, DNOs use combinations of different switching devices coupled with auxiliary devices such as fault passage indicators to achieve various D-FA schemes.

Auto-reclosers are most commonly deployed to achieve D-FA schemes in radial networks. Auto-reclosers are fault interruption devices similar to circuit breakers, with an additional control unit that can be programmed to automatically close and open the device multiple times. The control unit initiates a reclose attempt after a pre-set waiting time, called dead time. Each reclosing attempt is called a shot. The number of shots vary depending on the network and are usually limited to four shots [32].

A temporary fault usually clears before the final shot of an auto-recloser. Therefore, normal operation of the network is restored without intervention of the DNO. This is particularly desirable since historical data indicate that 85-90% of faults on distribution feeders are temporary [20]. A fault is usually permanent if it persists longer than the duration required to complete the allowable number of recloser shots. In this case, the device locks out in the open state during the final shot. A lock out normally requires intervention of the network operator to restore the network.

Protection coordination between the switchgear is achieved by proper selection of tripping curves. Inbuilt timers in the local control units are used to achieve the desired operating sequence. Simple network operation is possible using only current-time coordination without a communication link. However, remote operation capability in the switching devices is preferred. Switching coordination is thus achieved by sharing the status between remotely-operated devices using a simple communication link, in addition to current-time coordination. The location of these devices are chosen to minimise the number of customers impacted by a fault. The developments in the IEC 61850 Generic Object-Oriented Substation Event (GOOSE) based technology is a good fit for D-FA applications. A number of publications explore this technology [33]–[35].

A more coordinated D-FA scheme can also be achieved by grouping devices (switch/recloser) in a geographic location. The devices within a group at various locations need to be connected over a communication network. Introduction of the pulse reclosing technology [36], [37] and associated “team operation” of the grouped devices improve the performance of such D-FA schemes. The achieved solution is easy and less expensive to deploy than C-FA. However, “team operation” require the deployment of the specific switchgear that are compatible with this such operation and cannot be implemented using existing devices on the network [38], [39].

This thesis focuses on the conventional D-FA scheme. Detailed sequence of events of an existing D-FA scheme using auto-reclosers is discussed in Chapter 4.

2.2.4 Need for upgradation of assets in distribution network

DNOs have identified a number of challenges in the existing distribution network. A large number of assets are reaching the end of their productive life cycle and will soon need replacement and/or reinforcement [40]. An increase in the penetration of renewable energy sources (RES) connected directly to the distribution network will also exert stress on the existing assets. Additional network capacity is needed in order to supply the evolving loads and increasing DG connections to their networks. Such problems require a more immediate response. The traditional reinforcement techniques are unlikely to deliver the desired outcomes. Furthermore, due to their scale such investments can take a significant amount of time before they are fully implemented. For example, the traditional approach to reinforce a network to overcome an under-voltage condition would be to replace the line or cable with one of a higher cross-sectional area or addition of a substation. This approach would require substantial amount of time on account of planning, possible disruption and actual implementation times. Therefore, DNOs in the UK are now considering use of power electronics to solve the network problems. DNOs are procuring a number of power electronic devices to trial on their networks using the funding available through the LCNF and NIC projects [16].

Power electronic converters, their associated technologies and applications are relatively mature in transmission networks. Devices such as FACTS (flexible AC transmission systems), static synchronous compensator (STATCOMS) and high voltage DC (HVDC) transmission have been commonly used to improve the performance of transmission networks since early 1990s [41]. However, their use in the distribution networks are at a relatively early stages of development. A range of power electronic devices to be used at distribution level are under investigation [42]. These include

- Soft open points;
- Active in-line voltage regulators;
- Solid state transformers;
- Solid state fault current limiters;
- On-load tap changers for secondary substation transformers;
- Flywheel energy storage system.

A number of pilot projects were undertaken by the DNOs to deploy SOP type devices in distribution networks.

'Flexible Urban Networks-Low Voltage' (FUN-LV) is an LCNF funded project initiated by UK Power Networks. The project explored the use of SOPs to enable the deferment of reinforcement and facilitate the connection of low carbon technologies and distributed generation in urban areas. This was achieved by meshing existing networks using SOPs at selected normally open points on the network. Trial area covered networks in the London and Brighton areas [17], [43].

'Network Equilibrium' project is initiated by Western Power Distribution and is funded by LCNF. This project explores a number of voltage and power flow management approaches to improve the utilisation of electricity networks. One of the approach was to deploy SOP (Flexible Power Link) to accommodate increased levels of low carbon technologies, during normal operation and outage conditions. The project aims to install and trial links between two different grid groups that cannot be paralleled due to circulating current issues [14].

More recently the 'Angle-DC' project was initiated by Scottish Power Energy Networks, using the funds awarded through the NIC [44]. This project aims to demonstrate a network reinforcement technique using SOP type device, in North Wales. A DC link will be implemented using two VSCs connected along a distribution network using existing AC assets. The two VSCs are to be installed in separate substations, at different geographical locations. The technique is being used as an efficient method to create network capacity headroom and facilitate GB's objective for the shift towards a low carbon economy.

SP Energy Networks has initiated the 'LV Engine' project which aims to carry out design and trial of Solid State Transformers or "Smart Transformers" within the distribution network at secondary substations. If successful, LV Engine will be a major enabler for the future Distribution Systems Operator (DSO) [45], [46].

These new technologies and their applications are able to support network operation either by improving the effectiveness of existing operation or by offering new functions to the distribution network. This thesis focuses on the enhancement of performance on a network with SOP during faults. As a background to this research, the state of the art of SOP used in distribution networks are presented in the following section.

2.3 Introduction to SOP

SOPs are multi-functional power electronic devices installed in place of normally-open or normally-closed points in distribution networks. They have also been called “SIPLINK” [47], “DC link” [48], [49], and “SNOP” [50] in the literature. The term ‘soft’ open point is derived from the fact that there are no mechanical opening and closing (hard switching operation) of switching contacts in an SOP like in conventional switchgear. The real power (P) flowing through an SOP, and the reactive power (Q) being provided at the converter terminals are achieved through controlled switching of power electronic switches.

Typically, an SOP is used as a soft meshing device installed in place of the normally-open tie switch connecting two feeders. Figure 2.3 illustrates a simple network that consists of two radial feeders connected in an open loop configuration through an NOP. D_{1n} and D_{2n} represent the switching devices used on Feeder-1 and Feeder-2. The SOP is installed in place of the NOP as indicated. There are many benefits of using an SOP on a distribution network; the key drivers are listed below.

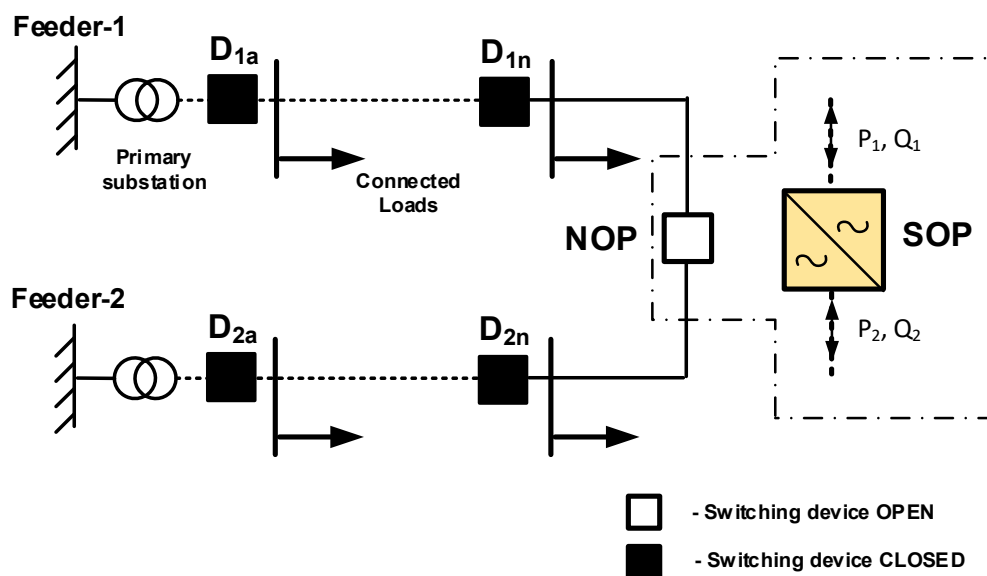


Figure 2.3 SOP in a distribution network

2.3.1 Key drivers of using SOP

- Operational flexibility: The use of SOP allows for independent control of P and Q in either direction up to its maximum rated power capacity. The network operator has the flexibility to dynamically change the operational set points continuously or in steps as per the network requirements [51]. This allows the

SOP to be used for dynamic voltage support with flexibility to absorb or inject reactive power at both its interface terminals.

- Improvement in power quality: SOPs can be used to improve the performance of the network by mitigating voltage imbalance, flicker, sag and lower order harmonics [51], [52].
- Fault levels not increased: SOPs enable the connection of two networks while only modestly increasing the fault levels of the individual networks. There is a substantial increase in fault level if two feeders are connected by closing a NOP. Due to the instantaneous control of currents, the two connected feeders act as a meshed network without increase in the fault level [42].
- Connectivity of dissimilar feeders: The two networks connected by an SOP could be operating at different frequencies and phase angles. This is particularly helpful when connecting feeders supplied from different substations. The two networks remain electrically decoupled and can be connected regardless of the rated voltage or phase angle difference [52].
- Phase imbalance mitigation: Phase imbalance is one of the major causes of capacity limitation in a feeder at low voltage application [52]. An SOP allows instantaneous power transfer between phases and therefore can be used for balancing power flows within a feeder.

2.3.2 SOP and other type of FACTS devices at distribution level

SOPs are typically made from arrangements of voltage source converters (VSCs) in varying rating and quantity. Various topologies of VSC based devices are discussed in the literature [49], [52]–[54]. These mainly include back-to-back (BTB), multi-terminal (MT) VSCs and unified power flow controllers (UPFC) as illustrated in Figure 2.4.

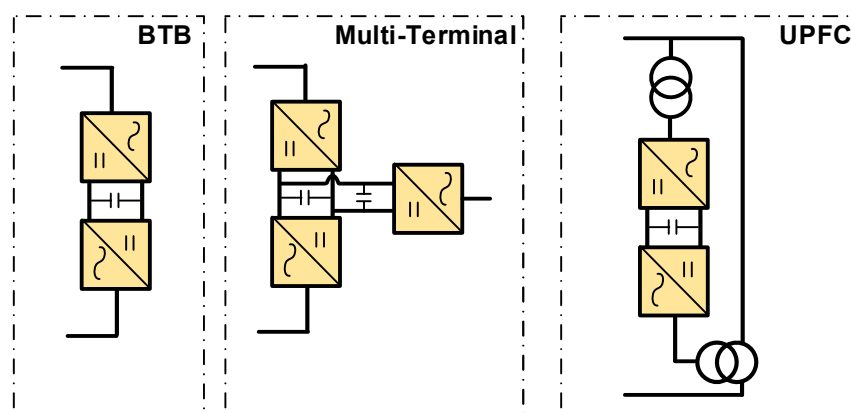


Figure 2.4 SOP and other type of FACTS devices at distribution level

A back-to-back VSC based SOP consists of two VSCs connected via a common DC link to form an asynchronous AC/AC conversion device. Similar operation of the network can be achieved using point-to-point VSC links, in which the DC link is extended and the two VSCs are geographically displaced. This thesis is focused on the performance and operation of back-to-back VSC based SOP. Back-to-back VSC based SOPs are most commonly used in distribution networks due to their simplicity of implementation. Furthermore, it has been suggested that the back-to-back arrangement is the most cost effective topology in distribution networks [42], [53]. The details of this configuration are discussed in the following subsection.

The multi-terminal VSC based SOP is an extension of the back-to-back topology, in which additional VSCs are connected through a common DC link. The operational principle is similar to that of a back-to-back VSC based SOP, with power transferrable across each of the connected VSCs.

The UPFC (also called shunt-series VSCs in the literature [53], [55]) consist of two VSCs with a common DC link. Unlike back-to-back and multi terminal based SOP, UPFCs can only be installed in normally closed points of a network. One VSC is connected in series and the other is connected in shunt with the interconnected feeders. The series connected VSC controls the power flows between the interconnected feeders by injecting a voltage with controllable magnitude and phase angle [55]. The active power demand of the series VSC is supplied by the shunt connected VSC through the DC link. It is possible to control the reactive power independent of the series connected VSC.

Each topology has its unique characteristics based on its construction and functional implementation. Suitable configuration is selected based on network requirements. Table 2.2 lists the different parameters of comparison between the three topologies discussed in this subsection.

Table 2.2 Summary of SOP and other type of FACTS devices; reproduced form [53]

| Parameter | B2B | MT | UPFC |
|----------------------------|--------------|--------------|-------------|
| Real power exchange | Yes | Yes | Yes |
| Reactive power support | Yes | Yes | Yes |
| Post-fault restoration | Yes | Yes | Yes |
| Partially rated converters | No | No | Yes |
| VSCs in conduction | 2 | ≥ 2 | 1 |
| Number of VSC/Device | 2 | ≥ 3 | 2 |
| Feeder connection type | DC Link | DC Link | Direct |
| Feeder connection | Asynchronous | Asynchronous | Synchronous |

2.3.3 Back-to-Back VSC based SOP

The circuit topology of a back-to-back VSC based SOP is shown in Figure 2.5. It consists of two VSCs connected through a DC link. Each VSC consists of six arms of Insulated Gate Bipolar Transistors (IGBTs) connected in a bridge configuration. The VSCs are interconnected to the feeder through an inductor. An isolation transformer is usually used to isolate the SOP terminals from its respective feeder [52].

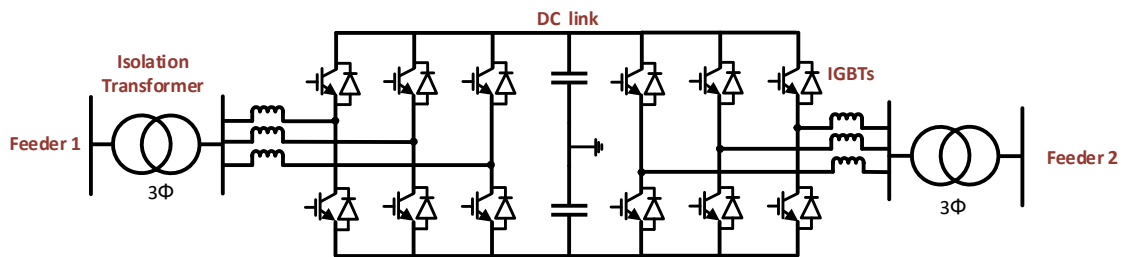


Figure 2.5 IGBT connections in a B2B VSC based SOP.

It is common to use two-level converters for medium voltage and/or low voltage applications. Multilevel topologies are predominantly used for higher voltage levels [53]. Each VSC in the SOP is operated through controlled commutation of the IGBTs using Pulse width modulation (PWM). Real power transfer through the VSC is achieved by controlling the phase angles of the converter terminal voltage with respect to the SOP grid connection point. Transfer of reactive power is achieved by controlling the magnitude of voltage at the converter terminal with respect to the voltage at the SOP grid connection point. Smooth voltages are generated at the VSC terminals using low pass filters. The DC capacitors limit the ripples in DC current and provide for decoupled real power exchange between VSCs [49].

Figure 2.6 shows the ideal operating region of a back-to-back VSC based SOP in the P - Q plane. The operating region is represented by a circle with a radius equal to the total rated apparent power (S) of the SOP. The SOP can operate on any set points within the circle. Therefore, this configuration of SOP allows control of real and reactive power in all four quadrants of the P - Q plane. It can also facilitate black start, unlike line commutated converters (LCC) [51].

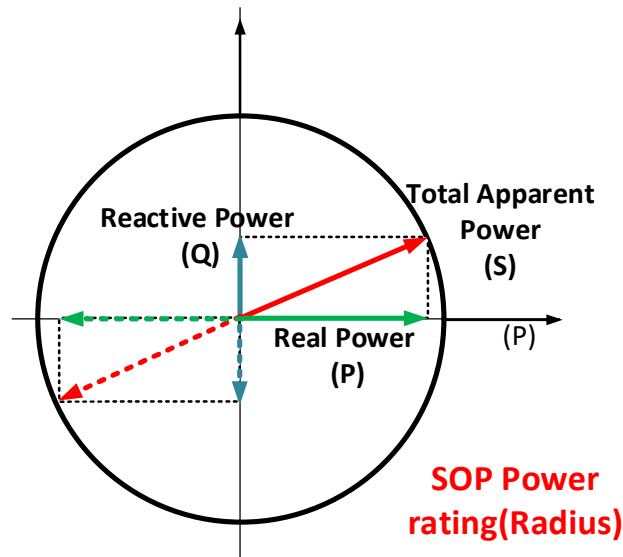


Figure 2.6 Ideal operating region for BTB VSC based SOP in P - Q plane

2.4 Previous research on SOP

In this section the previous work on SOPs is discussed highlighting the research gaps which are discussed broadly in terms of the steady state and dynamic operation.

2.4.1 Steady state operation

A number of publications discuss the steady state operation of SOPs in distribution networks. These mainly focus on optimal network operation and benefit quantification of using SOP in distribution networks under normal operating conditions.

Authors of paper [56], [57] proposed a method to determine the optimal installation sites and capacities of SOPs under normal operating conditions. A mixed integer non-linear optimisation problem was formulated based on typical operation scenarios generated by Wasserstein distance. In addition, an optimal configuration model of SOP was presented.

Using the method proposed in [56] to determine the optimum location of SOP, an optimal planning model of distributed energy storage systems was developed for active distribution networks in [58]. Hourly network reconfiguration was conducted to optimise the power flow by changing the network topology whilst incorporating SOPs and reactive power capability of DGs

The benefits of using SOPs in distribution networks have previously been reported for specific objectives, such as: loss minimisation , feeder load balancing [50],

[59], maximisation of network loadability and DG penetration [49], [60]. A multi-objective optimisation framework was proposed in [61] to improve the operation of a distribution network with distributed generation and a soft open point (SOP). An optimisation method that integrates a Multi-Objective Particle Swarm Optimisation (MOPSO) algorithm and a local search technique, the Taxi-cab method, was proposed to determine the optimal set points of the SOP. Power loss reduction, feeder load balancing and voltage profile improvement were taken as objectives.

A steady state analysis framework was developed in [62] to quantify the operational benefits of a distribution network with SOPs under normal network operating conditions. It was shown that the use of one SOP achieved a similar improvement in network operation as using network reconfiguration with all branches equipped with remotely controlled switches. A generic power injection model was developed and used to determine the optimal SOP operation using an improved Powell's Direct Set method.

The authors of [63] used an algorithm to assess the increase in hosting capacity that resulting from the addition an SOP to link two networks. A stress majorisation technique was applied to a United Kingdom Generic Distribution System (UKGDS) to visualise non-concurrent per-node hosting capacity.

A Jacobian matrix - based sensitivity method was used to define the operating region of an SOP when the feeders at the two terminals of the SOP had different load and generation conditions. The exact operational set points were determined by adopting a non-linear optimisation considering different objectives separately. Three optimisation objectives were considered with different DG penetrations and different network observabilities.[64]

The impact of control strategy adopted for the SOP (DC link) operation on the power-flow convergence of integrated AC–DC systems was investigated in [65]. Considering various control strategies, a sequential method was used to solve the DC variables in the Newton Raphson (NR) power flow model.

2.4.2 Dynamic operation

The research involving the dynamic operation of SOP network mainly focuses on the control philosophy and applications of SOP in improving the performance of a distribution network during unfaulted and post-fault scenarios. A number of papers discuss the use of SOPs for load balancing, voltage profile management, increase in DG penetration, network reinforcement and post-fault restoration.

In [50], [66] the effectiveness of using SOPs as a viable alternative to other voltage control strategies on distribution networks was investigated. Applications of SOPs for load balancing through voltage profile management were also discussed. Multiple network models with various topologies were used. Economic benefits of increasing feasible DG penetration were also reported.

Authors of [67] proposed a coordinated voltage and reactive power control method based on SOP for active distribution networks. A time-series model of coordinated control was developed to minimise operational costs and eliminate voltage violations of networks. The model was then linearised, such that it can be efficiently solved to meet the requirement of voltage regulation rapidity.

The application of SOPs to increase the penetration of photovoltaic generation on a distribution network was discussed in [68]. The authors demonstrated the use of SOPs with energy storage for providing damping functionality simultaneous to its other functions. A formula to estimate the level of energy storage required to handle worst-case transient conditions, as well as two high-level control schemes for the SOPs were proposed. These were then simulated using typical distribution systems with historical measurements.

The use of SOPs for network reinforcement was discussed in [44], [69], [70]. The use SOP and VSC based converter systems installed within the network was investigated to provide increased power transfer capability without the upgrading the cables and associated assets. The ability of the SOP to dynamically force active power flows to balance feeders (and phase loadings), and thereby improve the utilisation of the existing network capacity was discussed in [71].

The use of SOPs in mitigating serious unbalanced network operation caused by asymmetric integration of distributed generators was investigated in [72]. A strategy was developed using SOPs to reduce power losses and simultaneously mitigate the three-phase unbalance of the high voltage grid.

An SOP was investigated for supply restoration in medium voltage distribution networks in [51], [73], [74]. Two control modes were defined for SOP operation under normal and post-fault restorative network operating conditions. A mode switch method based on the phase-locked loop (PLL) technique was proposed to facilitate a smooth transition between the two control modes and thus facilitate supply restoration.

Majority of the work on the behaviour of VSC based devices during AC faults focused on transient studies and their fault ride-through capabilities, as discussed in [75], [76]. Small signal stability of the power electronic converters during network unbalance is investigated in [77]. Strategies for fault ride-through of inverter interfaced distributed energy resources (DER) was discussed in [78]. An inverse time-domain transient analysis to locate sub-cycle incipient faults in distribution systems was investigated in [79]. These studies focused on detailed power electronic design. Authors of [80] explored the accurate representation of distributed generators interfaced with inverters in fault current calculation. The authors used the knowledge of control strategy to develop a linear analytical equivalent model as a function of the inverter's hardware parameters and controller gains.

The existing literature does not describe the operation of a distribution network with SOP during a fault on the network. Typically network studies and power electronics design are two separate areas of study. There are no methods described in the literature to incorporate an SOP into fault studies or the operation of an SOP during abnormal network conditions.

2.5 Summary

In this chapter, the state of the art of distribution network operation, specifically in the UK was summarised. Switching devices typically used in distribution networks were briefly discussed. The need and benefits of automation at distribution level were presented. Salient features, types of feeder automation and their role in network restoration following a fault were discussed. Challenges in the future distribution networks were then introduced, with special attention paid to the emergence of power electronics at the distribution network level.

Power electronics devices can offer a variety of operational functions and, hence, will play a key role to enable controllability and flexibility features throughout the future distribution networks. An SOP is one such power electronics device in distribution networks. The key drivers of SOP deployment in distribution networks and different topologies of SOPs were introduced. A review of the state-of-the-art of the SOP studies was presented, and these were followed by identifying the corresponding research gaps.

The potential of using power electronics devices to improve network protection has been mentioned in the literature [48], [80]. However, this topic was not fully explored. In order to realise network protection capabilities of an SOP, it is important to incorporate

the SOP into network fault studies. The impact on existing automation schemes and interactions between the SOP and the existing network operating dynamics need to be investigated.

To bridge this gap, this study investigates the dynamic operation of a back-to-back voltage source converter (VSC) based SOP under faulted network conditions. In Chapter 3, fault analysis technique using equivalent sequence networks is extended to a distribution network with connected SOP. This allows a detailed study of the interactions between an SOP and existing feeder automation schemes on the network.

3

Fault Studies of a Distribution Network with Soft Open Point

Chapter 3 Fault Studies of a Distribution Network with Soft Open Point

3.1 Introduction

The operation and benefits of using SOP in a distribution network were discussed in the previous chapter. It is important to understand the dynamic behaviour of a network with an SOP during a fault for wide deployment of SOP. To fill this gap, fault analysis of a distribution network with an SOP is carried out in this chapter. The modelling of an SOP suitable for the fault studies is discussed. The performance of the network with SOP was investigated during normal and faulted conditions. Use of sequence networks is extended to include the SOP such that conventional fault analysis technique can be used on a distribution network with an SOP. Correlation between the sequence components (of the voltages and currents) and the SOP set points was investigated. Furthermore, a fault detection method is developed using the equivalent sequence networks without using additional devices. Simulations were carried out on an 11kV generic UK distribution network model developed in PSCAD/EMTDC.

3.2 Modelling and control of a Back-to-Back VSC based SOP

3.2.1 Modelling of the SOP

As described in Chapter 2, Figure 2.5, a back-to-back VSC based SOP consists of two VSCs, each with six arms of IGBT connected through a DC bus to form an asymmetrical AC/AC converter. In order to perform the fault study on a network with a connected SOP, the detailed power electronic design of the SOP is not necessary. An average model of an SOP using switched equivalent circuit is sufficient for this study. The model describes the steady state and the dynamic behaviour of the VSC with sufficient accuracy [81].

An average model of an SOP is illustrated in Figure 3.1. It consists of two switched equivalent circuits of a VSC, each with decoupled AC and DC sides. The AC side is modelled as a three-phase voltage source (V_1 for VSC1 and V_2 for VSC2). The DC side is modelled as a current source connected in parallel to a capacitor at a DC voltage of V_{dc} . Subscripts 1 and 2 are added to the variable names of the SOP to indicate the respective values corresponding to VSC1 and VSC2.

The direct current (I_{dc}) represents the real power transfer between the VSCs. The magnitudes of real power flowing between the terminals of SOP are equal during steady state operation. Equation (3.1) illustrated by the power balance equation in an SOP; where P_1 and P_2 are the magnitudes of real power transferred across the terminals of the SOP and P_{dc} is the DC power transferred through the DC link.

$$P_1 = P_2 = P_{dc} = V_{dc} \times I_{dc} \quad (3.1)$$

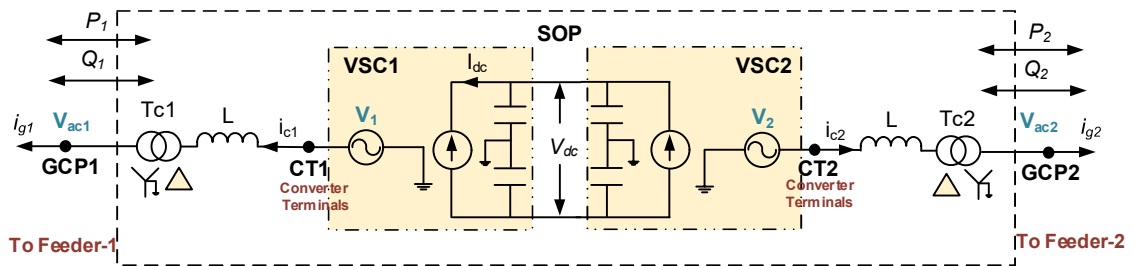


Figure 3.1 Average model of SOP

3.2.2 Control of SOP

A number of control schemes for VSCs have been proposed in the literature, including linear and non-linear methods [82]–[85]. Classical two-level $dq0$ -control is used in this study [86]. It is a common control technique, which allows the use of linear proportional-integral (PI) controllers to control the sinusoidal network quantities. This is achieved by transforming the three-phase (a, b, c) network quantities to a synchronously rotating reference frame ($d, q, 0$) using Parks transformation as shown in Equation. (3.2). $T(\theta)$ is Park's transformation matrix (details in Appendix A); \mathbf{X}_{abc} is a vector of three-phase quantities in the abc frame and \mathbf{X}_{dq0} is the vector of the converted quantities in the $dq0$ frame.

$$[\mathbf{X}_{dq0}] = [\mathbf{T}(\theta)][\mathbf{X}_{abc}] \quad (3.2)$$

The angle θ is synchronised to the grid angle using the angular frequency ω , obtained using a phase locked loop (PLL) [81]. The angular frequency ω is calculated using the positive sequence voltage as an input to the PLL. Details of symmetrical components are explained in Section 3.4.1. The angular frequency of the rotating frame is controlled such that the resultant angle θ , maintains the quadrature axis voltage (V_q) at zero. The direct axis voltage (V_d) is linearly controlled to achieve the desired VSC output voltage.

Each VSC is equipped with a separate two-level cascaded control system, which include an outer (power) and an inner (current) control loop as shown in Figure 3.2. The outer loop uses PI controllers to regulate active power (P) or DC voltage (V_{dc}) using the direct axis variable (i_d) and reactive power (Q) or AC voltage (V_{ac}) using the quadrature axis variable (i_q). The outer loop produces the direct axis (i_d^*) and the quadrature axis (i_q^*) current reference signals for the inner loop.

The mode of operation is selected between the active power control (APC) or the direct voltage control (DVC) through switch S1. Similarly, the reactive power control (RPC) or the alternating voltage control (AVC) is selectable through switch S2. Therefore, the SOP control modes are switchable between the P - Q , V_{dc} - Q , V_{dc} - V_{ac} and P - V_{ac} modes, during normal network operation.

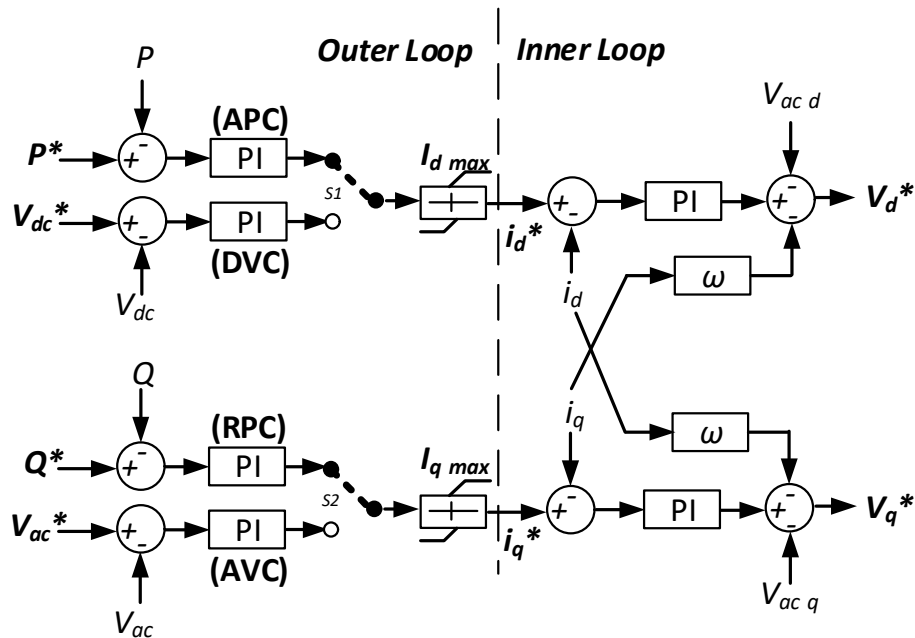


Figure 3.2 Classical two-level cascaded control system of an SOP.

The inner loop is used to regulate the values of the current references i_d^* and i_q^* , received from the outer loop. Decoupling signals are included to eliminate cross-coupling dynamics. The summation of the inner loop PI controller outputs and the decoupling terms produces the direct (V_d^*) and quadrature (V_q^*) axis voltage references. The voltage reference signals are then used to generate the converter phase voltages (V_a , V_b , V_c) through an inverse Park's transformation. In the average model, the firing operation is realised through the functional equivalent of the IGBT operation. The modulation index m is defined using V_d^* and V_{dc} as shown in Equation. (3.3). The converter terminal voltages are calculated using Equation. (3.4). The DC current flowing through the DC

link is determined according to the Equation. (3.5) [84]. i_a , i_b and i_c are the AC current magnitudes through phases a, b and c.

$$m = V_a^* \left(\frac{2}{V_{dc}} \right) \quad (3.3)$$

$$V_k = m \left(\frac{V_{dc}}{2} \right); \text{ where } k = a, b, c \quad (3.4)$$

$$I_{dc} = \frac{m}{2} (i_a + i_b + i_c) \quad (3.5)$$

An IGBTs has a maximum current carrying capacity (i_{max}) which is typically 1.5 times the magnitude of the rated current flowing through its terminals [81]. A current limiter is adopted to model the physical current carrying limitations of an IGBT. Equation. (3.6) represents the mathematical calculation of the current limiter in the VSC controller. This ensures that the maximum current through IGBTs saturates at i_{max} , which protects the IGBTs from damage due to overcurrent.

$$(i_d)^2 + (i_q)^2 \leq (i_{max})^2 \quad (3.6)$$

A sustained DC voltage ensures a balanced real power flow between the terminals of the SOP. Therefore, either VSC1 or VSC2 must control V_{dc} for proper operation of the SOP. However, the two VSCs cannot control the DC link voltage simultaneously as this may lead to hunting [81].

The VSC control described above is commonly referred as the power control mode in the literature [73]. In this mode, the SOP may operate in combinations of control schemes, and are interchangeable for VSC1 and VSC2 without affecting the overall performance of the device. This chapter focuses on analysis of an SOP in combinations of P - Q and V_{dc} - Q modes only. The reference values of the real power (P_1^* and P_2^*), reactive power (Q_1^* and Q_2^*) and the AC voltage (V_{ac1}^* and V_{ac2}^*) at terminals of VSC1 and VSC2 are defined by the user as per network requirements. All values within the rating of the SOP are permissible. The DC voltage (V_{dc}^*) is usually fixed for a SOP design.

3.3 Dynamic behaviour of a network with SOP

3.3.1 Behaviour of a network with SOP during normal operation

Simulations are carried out to illustrate the dynamic response of a network with an SOP. Different set points of active and reactive power are used while keeping a constant DC link voltage. Simulation results illustrate the independent control of P and Q during unfaulted network operation using a 6MVA SOP model. (P_1^*, Q_1^*) are real and reactive power set points for VSC1. (V_{dc}^*, Q_2^*) are DC voltage and reactive power set points for VSC2. The set points were changed in steps as shown in Table 3.1. However, any value of set points within the capacity of the device can be used. The direction of power flow from Feeder- 1 to Feeder-2 (in Figure 3.1) was considered as positive throughout the simulation.

Table 3.1 Set points (P_1^*, Q_1^*) and (V_{dc}^*, Q_2^*) during normal operation

| Simulation Time | P_1^* (MW) | Q_1^* (MVA _r) | V_{dc}^* (kV) | Q_2^* (MVA _r) |
|-----------------|--------------|-----------------------------|-----------------|-----------------------------|
| $t = 0$ s | 2 | -0.5 | 35 | 0.5 |
| $t = 1$ s | 0 | -0.5 | 35 | 0.5 |
| $t = 2$ s | 0 | 0.5 | 35 | -1.5 |
| $t = 3$ s | -1 | 0.5 | 35 | -1.5 |
| $t = 4$ s | -1 | -1.5 | 35 | 1 |
| $t = 5$ s | -1 | -1.5 | 35 | 1 |

Figure 3.3 shows the real and reactive power (P_1 and Q_1) flowing through SOP grid connection point GCP1, and Figure 3.4 shows (P_2 and Q_2) flowing through GCP2, under normal network conditions. The magnitude of P flowing through the two terminals was equal throughout the simulation. However, the Q flowing through the two terminals were different and independent of each other. From the curves, it is clear that an SOP allows independent control of P and Q flow in either direction of the DC link.

Figure 3.5 shows the voltages (V_{ac1} and V_{ac2}) at the grid connection points of the SOP (GCP1 and GCP2). The terminal voltage rises with an increase in Q injection into the network and conversely drops with export of Q from the network. In addition, a voltage rise was observed with increasing injection of P into the network. This can be seen at time ($t = 1$ s) and ($t = 3$ s) in Figure 3.5, corresponding to the change in P^* (at same respective times) in Figures 3.3 and 3.4. This is due to the relatively high ratio of resistance (R) to reactance (X) in a distribution network ($R/X \approx 0.3$ at 33 kV and $\approx 0.5-1$ at 11kV). Therefore the effect of real power on voltage profile cannot be ignored [40].

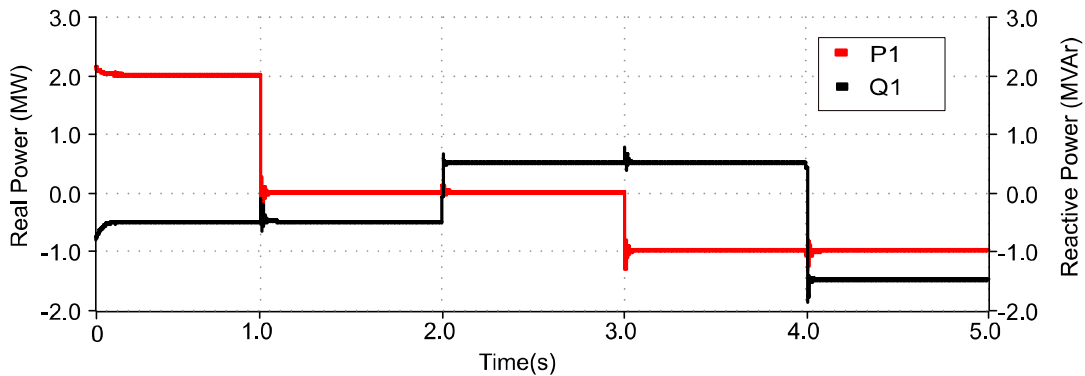


Figure 3.3 P and Q flowing through grid connection point GCP1 for different set points

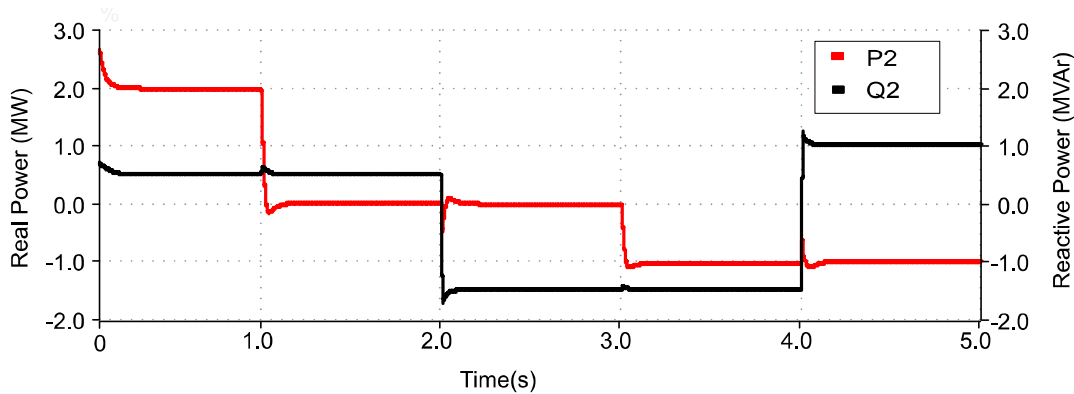


Figure 3.4 P and Q flowing through grid connection point GCP2 for different set points

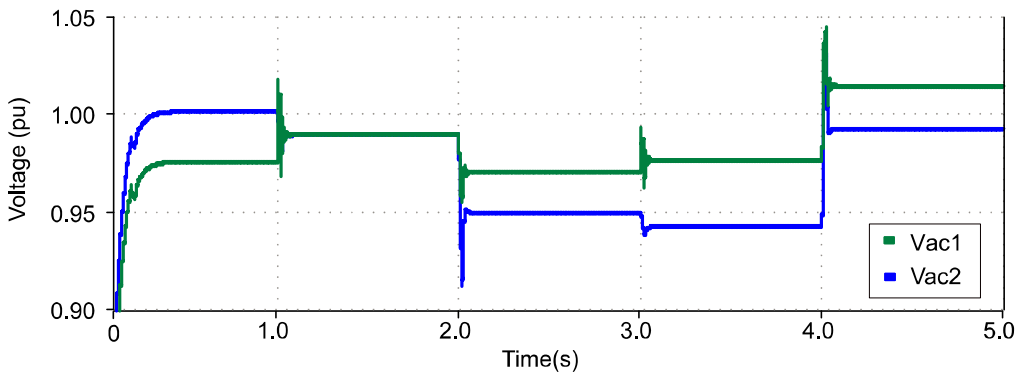


Figure 3.5 Voltages at the grid connection points of the SOP

3.3.2 Behaviour of a network with SOP during a fault

The detailed fault dynamic response of an SOP is determined by the hardware implementation (e.g. back-to-back VSC or UPFC) and the controller design. In the classical two-level $dq0$ -control used for the back-to-back VSC based SOP, the outer loop attempts to maintain the predefined set points. A change in the magnitude of power flow due to a drop in the voltage during AC faults results in an increase in current reference i_d^* and i_q^* . Figure 3.6 illustrates the current injected from the SOP following a balanced fault on the connected feeder (Feeder 1). The current limiter ensures that the maximum current flowing through the SOP terminals is limited to i_{max} .

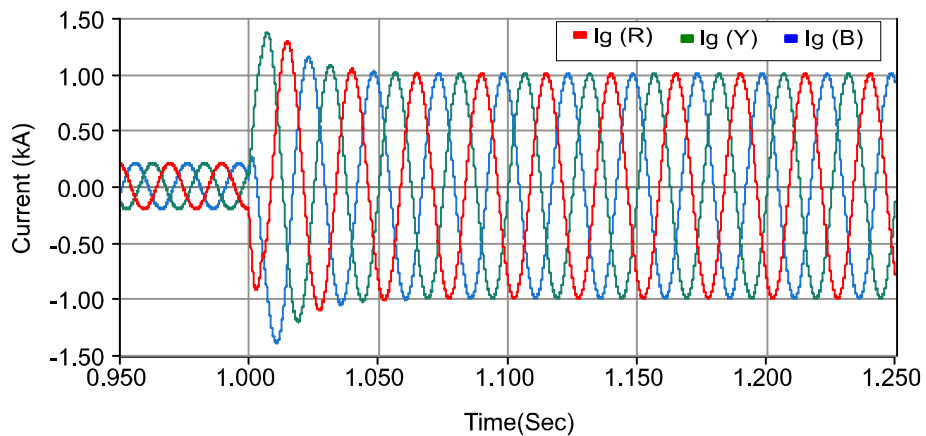


Figure 3.6 Dynamic response of the current injected from SOP after a fault at $t=1$ s

During a balanced fault, real and reactive power flows decrease due to a substantial drop in the feeder voltage [51]. In case of an unbalanced fault the real and reactive power flowing through the SOP terminals remain nearly the same as the pre-fault values. However there are ripples in the power flows due to voltage imbalance in the feeder resulting from the unbalanced fault.

The reactive power flowing through the SOP terminals of the unfaulted feeder remains unchanged for all types of faults. Figure 3.7 illustrates the real and reactive power (P_2 and Q_2) flowing through GCP2 following a fault on Feeder 1 at time $t=1$ s. The SOP continues to provide reactive power support to the unfaulted feeder during a fault on one of the feeders, provided that suitable control for V_{dc} is used. Analysing the dynamic response of the DC link voltage is not in the scope of this thesis.

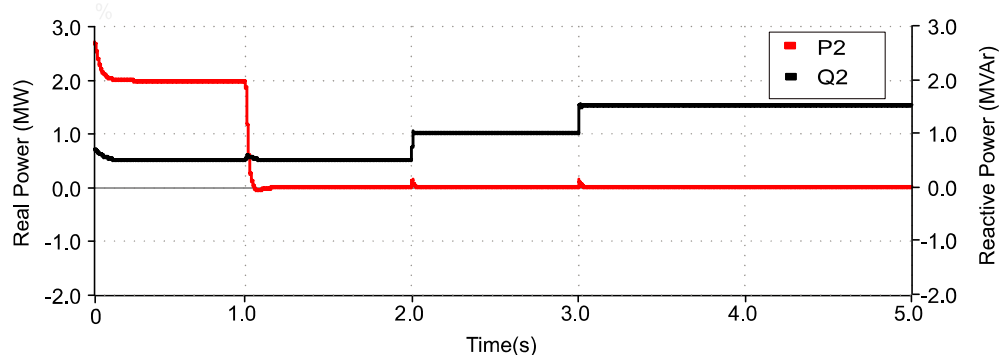


Figure 3.7 P and Q flowing through grid connection point GCP2 after a fault on Feeder-1 at $t=1s$

3.4 Fault analysis of distribution networks with SOP

MV radial feeders are typically operated with unidirectional power flow. The reverse current in a feeder due to the introduction of an SOP results in a disruption of the protection settings. Consequently, the use of SOP brings more complexity to the dynamic response of a network during a fault. The current settings of the relays between the SOP and the fault need recalibration in order to prevent unintended tripping of circuit breakers. This needs to be taken into account in the network studies so as to ensure proper operation of the network with an SOP. Therefore it is important to incorporate SOP into fault studies of a distribution network.

3.4.1 Fault analysis using symmetrical components

Fortescue proposed the theory of symmetrical components to study unbalanced networks [87]. During a fault, the unbalanced network can be resolved into three sets of balanced three-phase vector groups (positive, negative and zero sequences) called symmetrical components. Positive sequence components consist of balanced three-phase vectors in normal phase sequence. Whereas vectors in reverse phase sequence constitute the negative sequence components. The zero sequence components consists of three in-phase vectors. Ignoring the negative sequence components resulting from load imbalances, no negative and zero sequence components exist in a network during normal (no fault) operation.

Although these are not physically present in the network, monitoring and superimposition of symmetrical components represents the basis of understanding network behaviour during faults [88], [89]. Equations. (3.7) - (3.9) show the measured phase voltages (V_a , V_b , V_c) expressed as a function of the symmetrical components (V^p , V^n , V^z) using the complex operator 'a'.

$$V_a = V^p + V^n + V^z \quad (3.7)$$

$$V_b = a^2V^p + aV^n + V^z \quad (3.8)$$

$$V_c = aV^p + a^2V^n + V^z \quad (3.9)$$

where $a = e^{-\frac{3\pi j}{2}}$; subscripts a , b and c indicate the three-phase quantities and the superscripts p , n and z represent the positive, negative and zero sequence components respectively. Using Equations. (3.7) - (3.9) filters are modelled to resolve the measured phase voltages and line currents into positive, negative and zero sequence vectors. Details regarding the modelling of filters are in Appendix B. Similar equations can be written for the currents.

Fault studies are carried out by replacing the fault with a voltage source equal to the pre-fault voltage at the fault point. Symmetrical components are then used to draw equivalent sequence networks by considering the fault point to be the source of imbalance [89]. A low ohmic connection between phases or between phases and earth constitutes a fault [80]. Open circuits and high impedance faults are not analysed in this research.

3.4.2 Fault analysis of a network with SOP using symmetrical components

In order to enable detailed fault studies on a network with SOP, the current contribution of an SOP needs to be included in the sequence networks. Depending upon the type of fault, positive, negative and zero sequence currents are injected from the SOP grid connection point. A VSC can produce positive and negative sequence currents using a classical $dq0$ -controller. Zero sequence currents exist depending on the grounding arrangement and winding arrangement of the isolation transformer.

During a grid-side AC fault, an SOP viewed from the network behaves as a current source. The current flowing into the fault is a sum of the current infeed from the grid and the current injected from the SOP. Therefore, the contribution from the SOP is represented by a current source in parallel to their respective sequence component in the equivalent sequence network.

Figures 3.8 - 3.10 illustrate the equivalent sequence networks for grid-side AC faults on a network with an SOP. The portion highlighted in yellow represents the sequence network of the SOP. ' f ' represents the location of the fault on one of the feeders connected to the SOP terminal. $GCP1$ is the grid connection point of the SOP and the faulted feeder; E_{g1} is the AC grid voltage at G1. Z_{Tg1} represents the AC grid impedance (including the distribution lines and the grid transformer) of the faulted feeder. Z_{Tc1} is the isolation transformer impedance and Z_c is the converter impedance. Superscripts p , n and z represent positive, negative and zero sequence components.

Figure 3.8 shows the equivalent sequence network for a line-to-ground fault (L_a-G). The positive, negative and zero sequence components are in series for such a fault [89]. Zero sequence components exist in the network only if a ground path is available for the flow of current. The VSC does not produce zero sequence current since it is connected to the delta side of the isolation transformer (in Figure 3.1). However, the fault current at f has a zero-sequence component, since the grid transformer and the SOP isolation transformer are star grounded on the feeder side.

Figure 3.9 shows the equivalent sequence network for an unbalanced line-to-line fault (L_a-L_b). The positive and negative sequence networks are in parallel with each other for an unbalanced fault [89]. Thus, the positive and negative sequence voltages are equal in magnitude. There are no zero sequence components in the network, since there is no ground connection associated with this type of fault.

The equivalent sequence network for a balanced three-phase fault ($L_a-L_b-L_c$) is shown in Figure 3.10. Only the positive sequence current is present in this network. There are no negative and zero sequence currents since the network is balanced.

Due to the nature of SOP, the two feeder connected through the SOP are decoupled from each other. Therefore, impedances of unfaulted feeder do not appear in the equivalent sequence network.

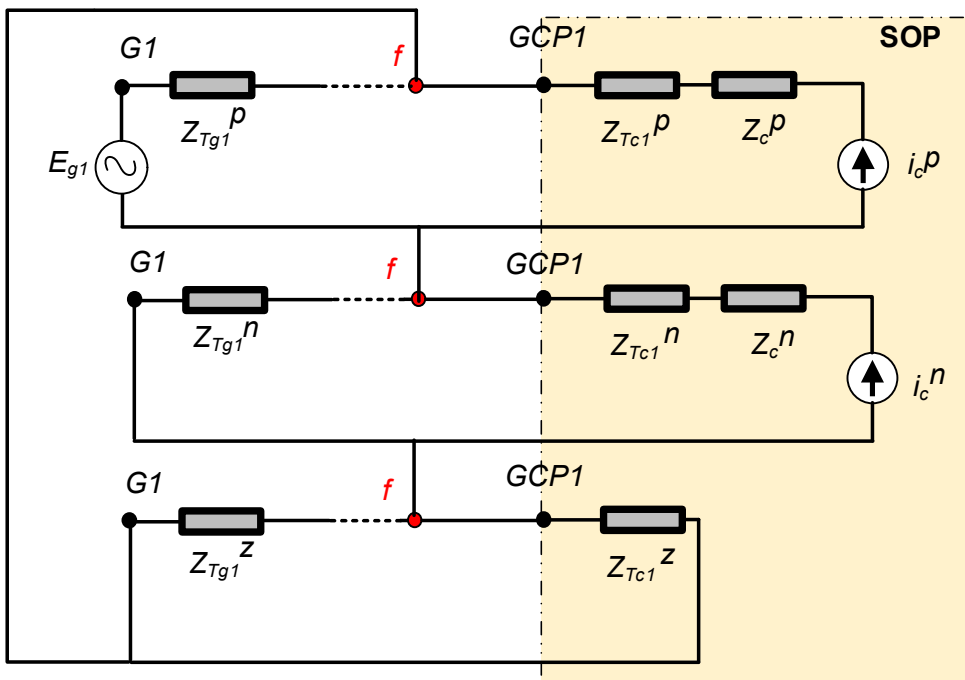


Figure 3.8 Equivalent sequence network of a feeder with an SOP for a line-to-ground fault at f

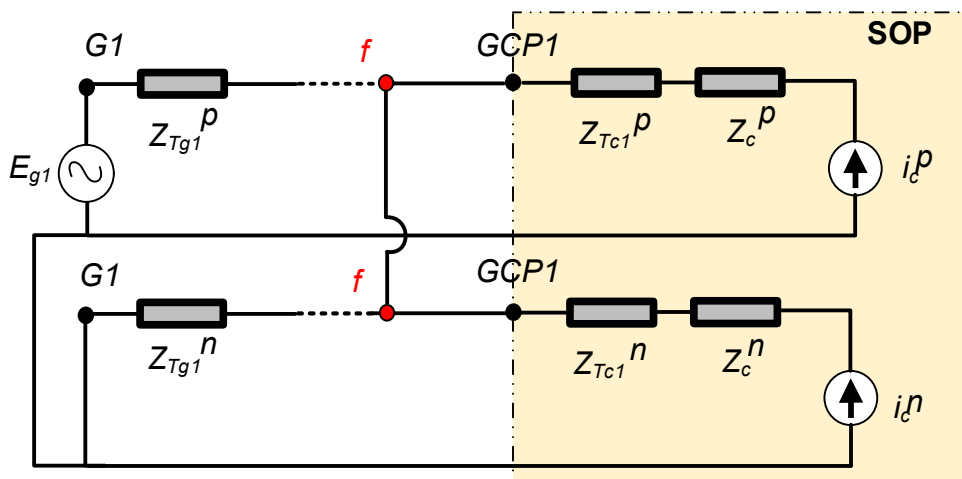


Figure 3.9 Equivalent sequence network of a feeder with an SOP for a line-to-line fault at f

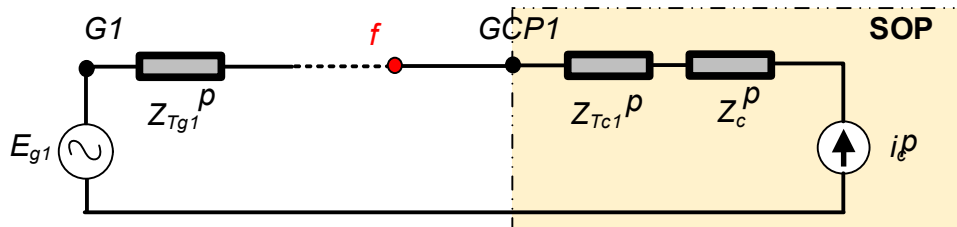


Figure 3.10 Equivalent sequence network of a feeder with an SOP for a three phase fault at f

3.4.3 Fault detection and Fault-Index

In a conventional distribution network without distributed energy resources, the rotational energy stored in generators is dissipated during a fault in the form of a large fault current. Each type of fault is accurately characterised by the corresponding fault current. Coordination of overcurrent protection devices is achieved by detailed fault analysis carried out on the network.

Measurements of symmetrical current components were introduced over the years as an improvement to the conventional over current measurements. During an unbalanced fault, the negative sequence current is present in a large proportion as compared to load imbalance. Thus, measuring the sequence currents was an effective method to detect faults on distribution networks. Authors of [90] defined a function to quantify the negative sequence currents for fault detection. The method eliminated faulty operation of overcurrent protection devices due to transient currents in a network. However, quantification of the negative sequence currents will not be applicable for balanced faults. In addition, the current based detection method in a network with an SOP will lead to further complication since the SOP contributes sequence currents into faults. Thus, a symmetrical voltage-based method of fault detection is proposed to overcome the shortcomings of using current measurement based method.

Fault-Index (FI), defined in Equation. (3.10) is the ratio of the difference between the root mean square (RMS) values of positive, negative and zero sequence voltages to the nominal positive sequence voltage of the distribution network, for each phase.

$$FI_x = \frac{(V_{x\text{RMS}}^p - (V_{x\text{RMS}}^n + V_{x\text{RMS}}^z))}{(V_{x\text{RMS(nominal)}}^p)} \quad (3.10)$$

Where x corresponds to the phases a, b and c.

The power quality criterion is based on the voltage unbalance factor (VUF) which is the ratio of negative to positive sequence voltages. Voltage unbalance may occur in a network due to unbalanced system impedance or due to switching of high loads. They rarely exceed 2%, for a short duration of time. Engineering Recommendation P29 [91] states that the VUF should not go above 1.3% for systems with nominal voltages below 33kV. To clearly distinguish between voltage imbalance and a fault, an unbalance of 10% or greater ($VUF \geq 0.1$) is assumed to indicate a fault in the network. Using this inequality in Equation. (3.10), the value of numerator is ≤ 0.9 . Similarly, the value of the

denominator can be calculated to be ≥ 1 . Thus, a threshold value of $FI \geq 0.9$ was calculated for a healthy network. Any value of $FI < 0.9$ indicates a fault in the network.

3.5 Simulation Results

3.5.1 Test Network

An 11 kV generic UK distribution network was used in this study [92], [93]. The test network consists of two radial feeders connected through a 6 MVA SOP. Each feeder consists of three sections each of 1 km length. Figure 3.11 shows Feeder-1 of the 11 kV test network connected to Feeder-2 through the SOP. Feeder-2 (not shown in the figure) is identical to Feeder 1 with same set of devices and line characteristics. The model was developed in PSCAD/ EMTDC package.

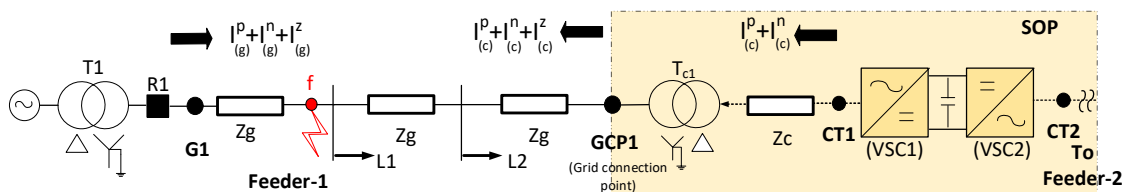


Figure 3.11 Generic 11kV distribution network with SOP (Test network).

G1 is the grid infeed point. T1 is a 15 MVA, delta-star grid transformer grounded through a 25Ω resistor on the feeder side. R1 is an overcurrent-based substation circuit breaker. Z_g represents the line impedance of a section. Each 1km section has a positive (Z_g^p), negative (Z_g^n) and zero (Z_g^z) sequence impedance of $0.164+j0.321 \Omega$, $0.164+j0.321 \Omega$ and $0.542+j0.426 \Omega$ respectively. For simplicity, the positive and negative sequence impedances were assumed equal. $L1$ and $L2$ are uniform lumped loads of 1 MW/ph at power factor of 1. The rating of the SOP was selected such that it is sufficient to feed the loads $L1$ and $L2$. The isolation transformer (T_{c1}) is a delta-star transformer with a directly grounded star winding on the feeder side. It is connected between the converter terminals (CT1) and the grid connection point (GCP1) on Feeder-1. Z_c represents the impedance of the inductor connected between the converter and the isolation transformer and is equal to $0.5+j1.57\Omega$. The converters are connected through a DC link at 35 kV, which consists of two $600 \mu\text{F}$ capacitors in series. The converter terminals of VSC2 (CT2) are connected to Feeder-2 through an isolation transformer identical to T_{c1} (not shown in the figure).

The dynamic response of the test network was investigated under various type of faults. Simulations were carried out for the L_a -G, L_a - L_b and L_a - L_b - L_c faults at location f (shown in Figure 3.11) on Feeder-1. A temporary fault occurs at simulation time $t=1$ s,

for a duration of 0.6 seconds. The duration of the fault was selected less than the time needed for the network protection devices to operate. Fault resistance was assumed to be negligibly small. Feeder-2 was assumed to be healthy (without fault) throughout the simulation. The network with SOP was studied under three main cases.

3.5.2 Case 1: Behaviour of equivalent sequence network and its validity for different control schemes

This case verifies the behaviour of equivalent sequence networks and illustrate their validity for different control schemes of VSC1, under different operating scenarios of the SOP. The three-phase voltages and currents measured at GCP1 were decomposed into symmetrical components for various faults. The equivalent sequence network developed for each fault was verified by matching the behaviour of measured values to the expected behaviour of their respective sequence network. The sequence voltages and currents at GCP1 are compared under different control schemes of VSC1 during a fault (i.e. in the P - Q mode and the V_{dc} - Q mode).

Extending from Section 2.3.3, an SOP can operate in all four quadrants of the P - Q plane during normal (without fault) operating conditions of the network. This translates to four possible operating scenarios of an SOP.

1. No power exchange; The SOP is in an 'open tie-switch' configuration with no P and Q exchange between Feeder-1 and Feeder-2;
2. Q exported to Feeder-1; The SOP operates as a STATCOM providing Q support to the connected feeder (to Feeder-1 in this scenario);
3. P imported from Feeder-1 and Q exported to Feeder-1; Q support to Feeder-1 with controlled P transfer from Feeder-1 to Feeder-2;
4. P and Q exported to Feeder-1; Q support to Feeder-1 with controlled P transfer from Feeder-2 to Feeder-1 (reverse direction of P flow as compared to Scenario 3).

Importing Q from the feeder to SOP is not considered. Drawing of Q from the network is detrimental to the voltage profile in a radial distribution network, and is therefore not recommended.

Each of the four scenarios listed above are achievable in the P - Q mode and the V_{dc} - Q mode. Fixed set points are used to simulate the above four scenarios. Details of the set points used for VSC1 and VSC2 are in Appendix C. The measurements were noted for simulation time $t=1.1$ s such that no transients are present. The sequence

voltages and currents for the four scenarios are tabulated. A bar chart for Scenario 4 (from the list above) is used to illustrate the similarities of sequence quantities in the two modes of operation.

Table.3.2 shows the detailed values of sequence voltages (in kV) for the four operating scenarios of SOP. The magnitudes of sequence voltages observed at GCP1, are consistent with the analytical values of the respective equivalent sequence networks. V^p is maximum for the L_a-G fault and least for the L_a-L_b-L_c fault. V^n is maximum for the L_a-L_b fault. The magnitude of V^p and V^n are nearly equal for the L_a-L_b fault. No V^z is present in the L_a-L_b-L_c and L_a-L_b faults. Furthermore, the values are identical for a type of fault in each scenario.

Similarly, Table. 3.3 shows the detailed values of sequence currents (in kA) for the four operating scenarios of SOP. The L_a-L_b-L_c faults are most severe with saturation current flowing through GCP1. During balanced faults, the grid voltage is nearly zero. This gives rise to errors in the computation of the angle θ using PLL, resulting in a non-zero V_q value. Thus, small negative sequence voltage and currents are noted for balanced faults. For the L_a-G fault, I^p and I^n are nearly equal and considerable levels of I^z is present in the network. Although the sequence currents flowing from the grid to the fault point f remain the same, the sequence currents flowing at fault point f , changes due to the introduction of SOP at the end of the feeder.

Table 3.2 Symmetrical voltage components (in kV) and FI for two operating mode and various scenarios of SOP operation

| Fault on Feeder 1 @ $t=1$ s | | VSC1 in the P - Q mode | | | | VSC1 in the V_{dc} - Q mode | | | |
|-----------------------------|---|----------------------------|-------|-------|-------|---------------------------------|-------|-------|-------|
| | | FI | V^p | V^n | V^z | FI | V^p | V^n | V^z |
| L-G Fault | No power exchange | 0.15 | 4.55 | 1.62 | 1.97 | 0.16 | 4.47 | 1.45 | 2.02 |
| | Q exported to Feeder-1 | 0.18 | 4.80 | 1.64 | 2.04 | 0.18 | 4.72 | 1.47 | 2.10 |
| | P imported from Feeder-1 + Q exported to Feeder-1 | 0.17 | 4.73 | 1.64 | 2.01 | 0.17 | 4.61 | 1.45 | 2.07 |
| | P and Q exported to Feeder-1* ** | 0.17 | 4.78 | 1.65 | 2.06 | 0.19 | 4.81 | 1.49 | 2.12 |
| L-L Fault | No power exchange | 0.05 | 2.68 | 2.36 | 0 | 0.04 | 2.84 | 2.57 | 0 |
| | Q exported to Feeder-1 | 0.07 | 3.06 | 2.58 | 0 | 0.08 | 3.22 | 2.68 | 0 |
| | P imported from Feeder-1 + Q exported to Feeder-1 | 0.08 | 3.09 | 2.57 | 0 | 0.06 | 3.03 | 2.64 | 0 |
| | P and Q exported to Feeder-1* | 0.08 | 3.12 | 2.62 | 0 | 0.08 | 3.22 | 2.71 | 0 |
| L-L-L Fault | No power exchange | 0.01 | 0.07 | 0 | 0 | 0.01 | 0.10 | 0 | 0 |
| | Q exported to Feeder-1 | 0.06 | 0.48 | 0.07 | 0 | 0.06 | 0.47 | 0.07 | 0 |
| | P imported from Feeder-1 + Q exported to Feeder-1 | 0.06 | 0.49 | 0.07 | 0 | 0.06 | 0.48 | 0.07 | 0 |
| | P and Q exported to Feeder-1* | 0.09 | 0.66 | 0.09 | 0 | 0.08 | 0.60 | 0.09 | 0 |

* Scenario used for Box plot; ** Scenario used for dynamic analysis of FI

Table 3.3 Symmetrical current components (in kA) for two operating mode and various scenarios of SOP operation

| Fault on Feeder 1 @ $t=1$ s | | VSC1 in the P - Q mode | | | VSC1 in the V_{dc} - Q mode | | |
|-----------------------------|---|----------------------------|-------|-------|---------------------------------|-------|-------|
| | | I^p | I^n | I^z | I^p | I^n | I^z |
| L-G Fault | No power exchange | 0.03 | 0.13 | 0.90 | 0.04 | 0.18 | 0.92 |
| | Q exported to Feeder-1 | 0.13 | 0.14 | 0.93 | 0.11 | 0.19 | 0.95 |
| | P imported from Feeder-1 + Q exported to Feeder-1 | 0.17 | 0.14 | 0.92 | 0.16 | 0.21 | 0.95 |
| | P and Q exported to Feeder-1* | 0.20 | 0.15 | 0.93 | 0.17 | 0.21 | 0.96 |
| L-L Fault | No power exchange | 0.39 | 0.44 | 0 | 0.36 | 0.37 | 0 |
| | Q exported to Feeder-1 | 0.33 | 0.46 | 0 | 0.30 | 0.41 | 0 |
| | P imported from Feeder-1 + Q exported to Feeder-1 | 0.14 | 0.40 | 0 | 0.1 | 0.38 | 0 |
| | P and Q exported to Feeder-1* | 0.52 | 0.44 | 0 | 0.51 | 0.43 | 0 |
| L-L-L Fault | No power exchange | 0.07 | 0 | 0 | 0.09 | 0 | 0 |
| | Q exported to Feeder-1 | 0.72 | 0.06 | 0 | 0.74 | 0.06 | 0 |
| | P imported from Feeder-1 + Q exported to Feeder-1 | 0.71 | 0.06 | 0 | 0.75 | 0.06 | 0 |
| | P and Q exported to Feeder-1* | 0.74 | 0.06 | 0 | 0.69 | 0.06 | 0 |

Figures 3.12(a) and (b) compare the sequence voltages for two control modes of the SOP. The bar charts illustrate the comparison for SOP operation scenario 4 presented in Table 3.2. The bars in blue represent voltage at GCP1 when VSC1 is in the P - Q mode (and VSC2 is in the V_{dc} - Q mode) while bars in red represent voltage when VSC1 is in the V_{dc} - Q mode (and VSC2 is in the P - Q mode). The positive, negative and zero (if applicable) sequence voltages were observed to be nearly equal for both modes of VSC operation. Small variations are introduced due to difference in the controller parameters in each mode.

Similar observations are made for currents flowing through GCP1. Figures 3.13(a) and (b) compare the sequence currents for both SOP control modes presented in Scenario 4. The bars in blue and red represent currents through GCP1 when VSC1 is in the P - Q mode (and VSC2 is in the V_{dc} - Q mode) and when VSC1 is in the V_{dc} - Q mode (while VSC2 is in the P - Q mode) respectively. Currents from the SOP remain mostly unchanged for both modes of operation, with maximum difference of 0.06kA between the respective values.

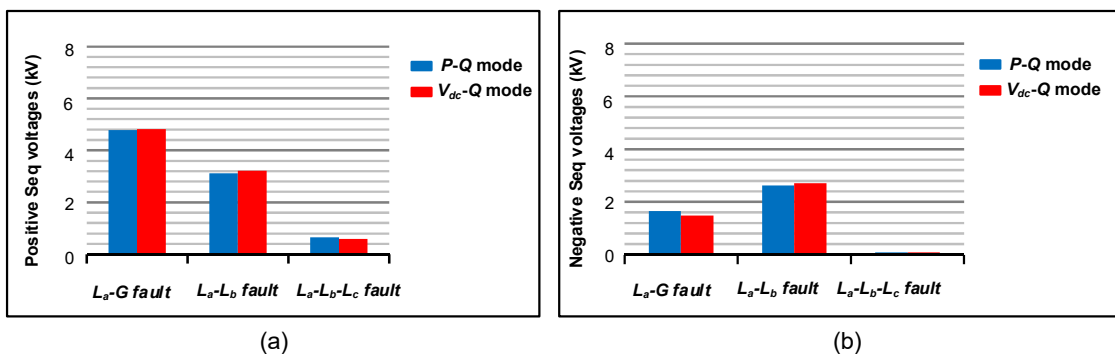


Figure 3.12 Comparison of sequence voltages for different control modes of SOP

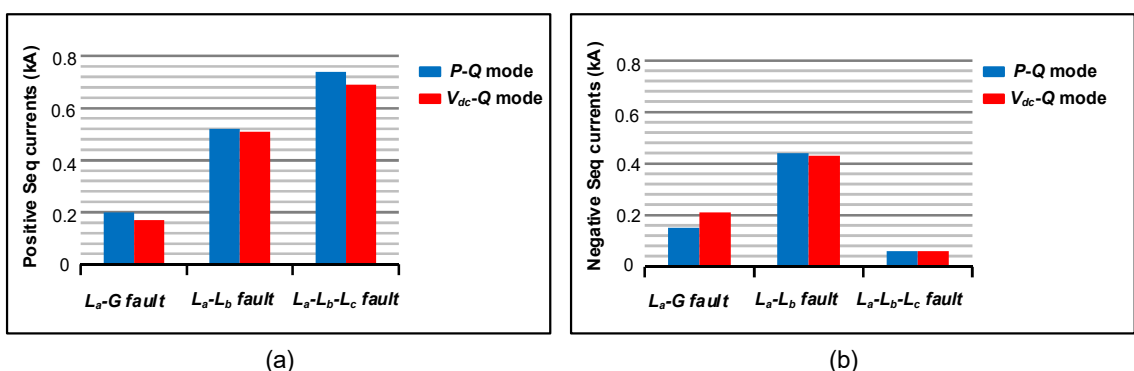


Figure 3.13 Comparison of sequence currents for different control modes of SOP

The trends of sequence values observed for various faults are consistent with the expected behaviour based on the equivalent sequence networks. It is clear that

sequence networks using classical fault analysis can be adopted to perform fault studies on a network with an SOP. Furthermore, this method is applicable for the network regardless of the control scheme of the VSC connected to the faulted feeder.

3.5.3 Case 2: Capability of the SOP to detect various types of faults

This case illustrates the capability of the FI to detect various types of faults. The dynamic response of the FI was analysed for a typical fault. FI was noted for each of the four scenarios in Case 1. The simulations were repeated to validate the FI under different loading conditions. The ability to detect balanced, unbalanced and ground faults was illustrated by comparing the values of FI with the defined threshold. A bar chart was plotted for Scenario 4 to illustrate the similarities of FI during different modes of operation.

Figure 3.14 shows the dynamic response of the FI for the L_a -G fault in Scenario 4. This scenario was selected as an extreme case, since the largest FI value was observed in this scenario. The steady state FI drops well below the threshold value within two cycles (0.04s) of the fault occurrence. This time does not include the measuring, computation and actuation time needed during real implementation. However, the measurements used for the calculation are available at the SOP controller for its operation and control, thus communication delay is negligible. The firing of the IGBTs can be blocked immediately after the value of FI drops below the threshold. It can be seen that the computation burden of calculating FI is negligible. Therefore the proposed method is considerably faster than the conventional current based detection method using relay and isolator which usually takes up to thirty cycles (0.6s) to detect a fault and isolate the SOP [90]. This illustrates the capability of the SOP to detect fault effectively.

The FI values in each of the four scenarios, under different type of faults are included in Table 3.2. The reliability of FI was further investigated under different loading conditions. The FI was calculated for decreasing loading conditions with 75% and 50% of 1 MW/phase load at unity and 0.9 power factors. The results are shown in Table 3.4. The FI varies between 0.15-0.2 for the L_a -G fault, 0.04-0.08 for the L_a - L_b fault and 0.01-0.09 for the L_a - L_b - L_c fault for different operating scenarios of the SOP. The FI was found to be well below the defined threshold of 0.9 for all types of faults, different SOP set points and loading conditions. Figure 3.15 illustrates a bar chart comparing the FI values for various faults under the two operating modes of SOP. The red bar is the defined threshold value of FI . The values are identical for both control modes. It is clear that FI is a simple and efficient method of fault detection in a distribution network with SOP, without the use of any additional devices.

Table 3.4 FI for various SOP operating scenarios under different loading conditions

| Fault on Feeder 1 @ $t=1s$; | | FI for VSC1 in P - Q mode | | | | FI for VSC1 in V_{dc} - Q mode | | | |
|------------------------------|---|---|-----------------|--------------------|-------------------|------------------------------------|-----------------|--------------------|-------------------|
| | | Per phase loads ($L1$ and $L2$) in (MW) | | | | | | | |
| | | 0.75MW @ 1 PF | 0.5MW @ 1 PF | 0.75MW @ 0.9 PF | 0.5MW @ 0.9 PF | 0.75MW @ 1 PF | 0.5MW @ 1 PF | 0.75MW @ 0.9 PF | 0.5MW @ 0.9 PF |
| L-G Fault | No power exchange | 0.15 | 0.15 | 0.15 | 0.15 | 0.17 | 0.18 | 0.17 | 0.17 |
| | Q exported to Feeder-1 | 0.16 | 0.16 | 0.16 | 0.16 | 0.2 | 0.19 | 0.19 | 0.19 |
| | P imported from Feeder-1 + Q exported to Feeder-1 | 0.15 | 0.15 | 0.15 | 0.15 | 0.19 | 0.19 | 0.18 | 0.18 |
| | P and Q exported to Feeder-1 | 0.17 | 0.17 | 0.17 | 0.17 | 0.2 | 0.2 | 0.20 | 0.20 |
| L-L Fault | No power exchange | 0.04 | 0.03 | 0.03 | 0.03 | 0.03 | 0.03 | 0.03 | 0.03 |
| | Q exported to Feeder-1 | 0.06 | 0.06 | 0.06 | 0.06 | 0.06 | 0.06 | 0.06 | 0.06 |
| | P imported from Feeder-1 + Q exported to Feeder-1 | 0.05 | 0.05 | 0.06 | 0.06 | 0.05 | 0.04 | 0.04 | 0.04 |
| | P and Q exported to Feeder-1 | 0.07 | 0.07 | 0.07 | 0.07 | 0.07 | 0.07 | 0.07 | 0.06 |
| L-L-L Fault | No power exchange | 0.01 | 0.01 | 0.014 | 0.01 | 0.01 | 0.01 | 0.01 | 0.01 |
| | Q exported to Feeder-1 | 0.06 | 0.05 | 0.06 | 0.05 | 0.05 | 0.07 | 0.05 | 0.06 |
| | P imported from Feeder-1 + Q exported to Feeder-1 | 0.06 | 0.06 | 0.06 | 0.06 | 0.06 | 0.05 | 0.06 | 0.06 |
| | P and Q exported to Feeder-1 | 0.07 | 0.07 | 0.07 | 0.07 | 0.07 | 0.08 | 0.07 | 0.07 |

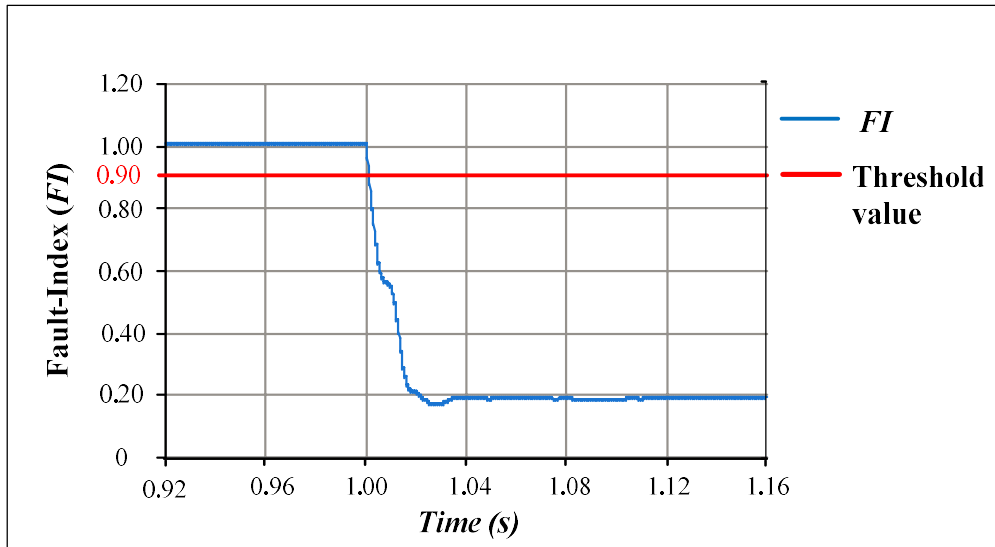


Figure 3.14 Dynamic response of FI

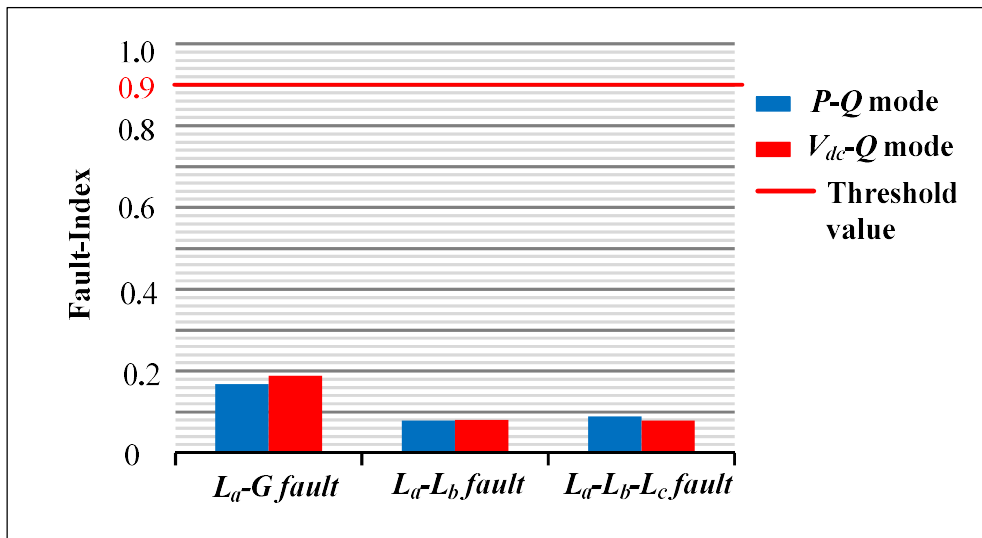


Figure 3.15 Comparison of FI for different control modes of SOP.

3.5.4 Case 3: Correlation between of the sequence components (voltage/currents) and the SOP set points

This case investigates the dependence of sequence voltages and currents on the SOP set points. The correlation between the sequence quantities at GCP1 for different P_1^* and Q_1^* set points of VSC1 during a fault, when VSC1 is in the $P-Q$ mode, is investigated.

The SOP can be operated in permissible set point prior to a fault. The power transfer through GCP1 during normal (without fault) operation follows the real and reactive power set points. In order to examine the effect of real power set point on the

sequence components, simulations are carried out for different values of P_1^* whilst Q_1^* equals to zero. P_1^* is varied from -5 MW to 5 MW in steps of 1 MW. The sequence voltages and currents at GCP1 are analysed.

To analyse the results, the sequence quantities are grouped by the respective sequence. Therefore, the positive sequence voltages (or currents) during the three faults for different values of P_1^* are grouped in one plot. The negative sequence voltages (or currents) are grouped in the second plot. Similarly, the effect of reactive power set point is examined by varying Q_1^* from -5 MVar to 5 MVar in steps of 1 MVar, keeping P_1^* at zero. The sequence quantities are similarly grouped for analysis.

Figure 3.16 compares the positive sequence voltages for variation of P_1^* set points and Q_1^* set points. In this figure the solid line represents the sequence quantities for a range of P_1^* whilst set point $Q_1^* = 0$ (marked on lower x-axis and y-axis). Similarly the dotted lines represent the sequence quantities for range of Q_1^* with set point $P_1^* = 0$ (marked on upper x-axis and y-axis). The colours red, blue and black plots indicates the L_a-G , L_a-L_b and $L_a-L_b-L_c$ faults respectively. Figure 3.17 shows negative sequence with identical representation.

V^p at GCP1 varies linearly based on the pre-fault operating condition of the SOP. It gradually drops with increasing power exported from Feeder-1 prior to the fault. Conversely, increasing power injection from SOP to feeder results in a gradual rise of voltage at GCP1. However, in comparison to real power injection, the slope of the voltage drop is slightly greater for reactive power injection. Figure 3.17 shows similar results for V^n . Slight droop is observed in variation of negative sequence voltages for changes in P_1^* and Q_1^* set points. Similar droop is observed for the zero-sequence voltage in the L_a-G fault. However, the percentage variation is very low over the range of set points. Therefore, the negative and the zero sequence voltages at the SOP grid connection point are almost unaffected by the pre-fault operating condition of SOP during fault analysis on a network with SOP.

In the $L_a-L_b-L_c$ fault, the droop in the sequence voltages is less evident since the network voltage during the fault is significantly low. It is noteworthy that the SOP terminal voltage during a $L_a-L_b-L_c$ fault is zero when the SOP is operated at zero set points. This is because the SOP behaves as an open point on the network when it is operated at zero set point. As illustrated in Case 1, the voltage values depend upon the type of fault and consequently upon the equivalent sequence network connection. However, regardless

of the type of fault, the trend of voltage variation is consistent for corresponding change in real and reactive power flow through the SOP terminals.

In a distribution network, the injection of real and reactive power affects the voltage at the node due to their large R and X ratio [88], as discussed in section 3.3.1. Figure 3.16 and 3.17 substantiate this behaviour in the test network with the SOP. Negative values of the set points indicate injection of power into Feeder-1 from the SOP in all the following figures and analysis.

Figure 3.18 and 3.19 show the positive and negative sequence currents with variation of the P_1^* and Q_1^* set points. For the L_a -G fault there is a steep, linear rise in the magnitude of the currents with the increase in P_1^* and Q_1^* regardless of the direction of power flow prior to the fault. In contrast to the L_a -G fault the sequence currents in the L_a - L_b fault has a nonlinear relation to the set points. In addition, the variation in currents for changes in P_1^* and Q_1^* shows dependence on the polarity of set points and appears converse to each other.

For the L_a - L_b - L_c fault, the sequence currents are largely uniform and unaffected by changes of set points (for non-zero set points). For zero set point, the behaviour of SOP is consistent with an open circuit with no current flowing through the SOP.

The variation of currents with changes in set points is similar for a given type of fault, but varies considerably for different type of faults. Unlike the sequence voltages, the sequence current injection shows a nonlinear dependency to the pre-fault condition. Further investigation is required to generalise the current response of the SOP under different faults. However, this clearly illustrates the need for a non-current based method for fault detection at the grid connection point of the SOP.

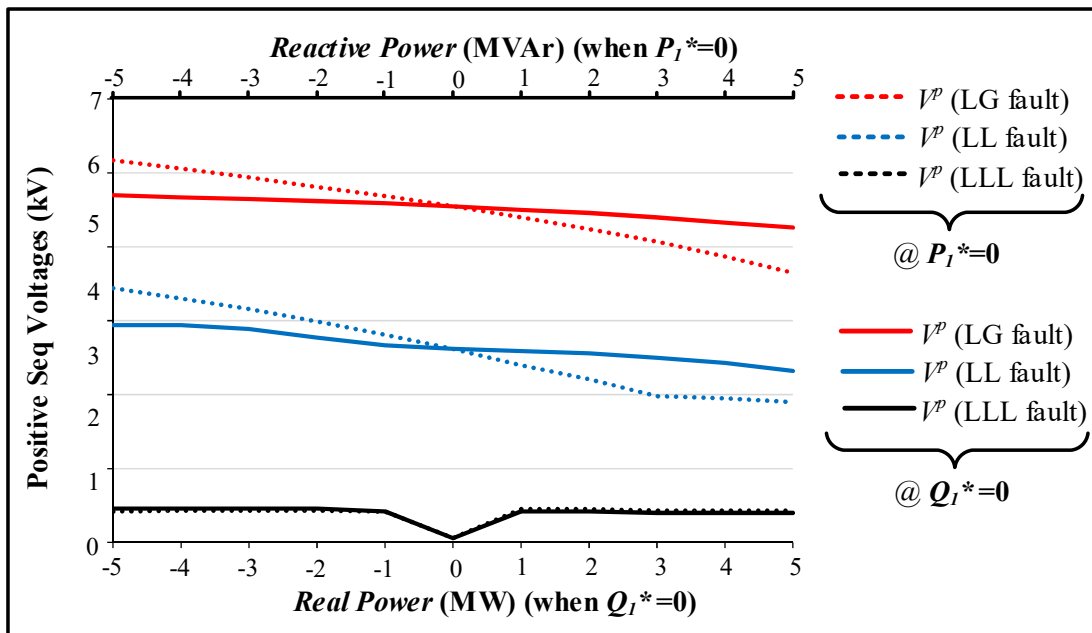


Figure 3.16 Positive sequence voltage for range of P_1^* set points, $Q_1^* = 0$ (solid lines); Range of Q_1^* set points, $P_1^* = 0$ (Dotted lines).

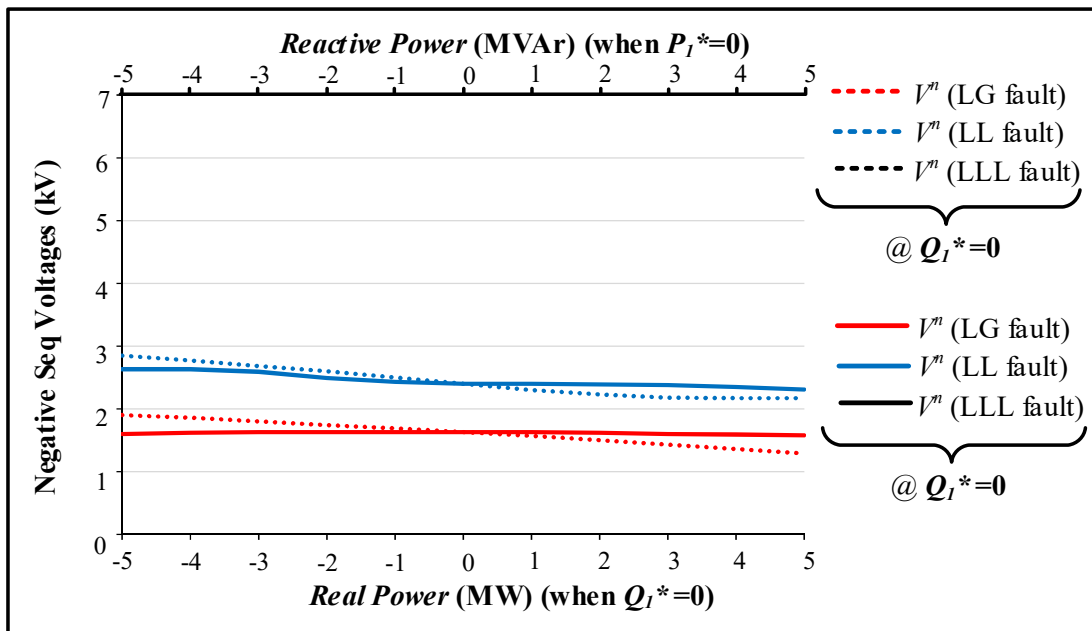


Figure 3.17 Negative sequence voltage for range of P_1^* set points, $Q_1^* = 0$ (solid lines); Range of Q_1^* set points, $P_1^* = 0$ (Dotted lines).

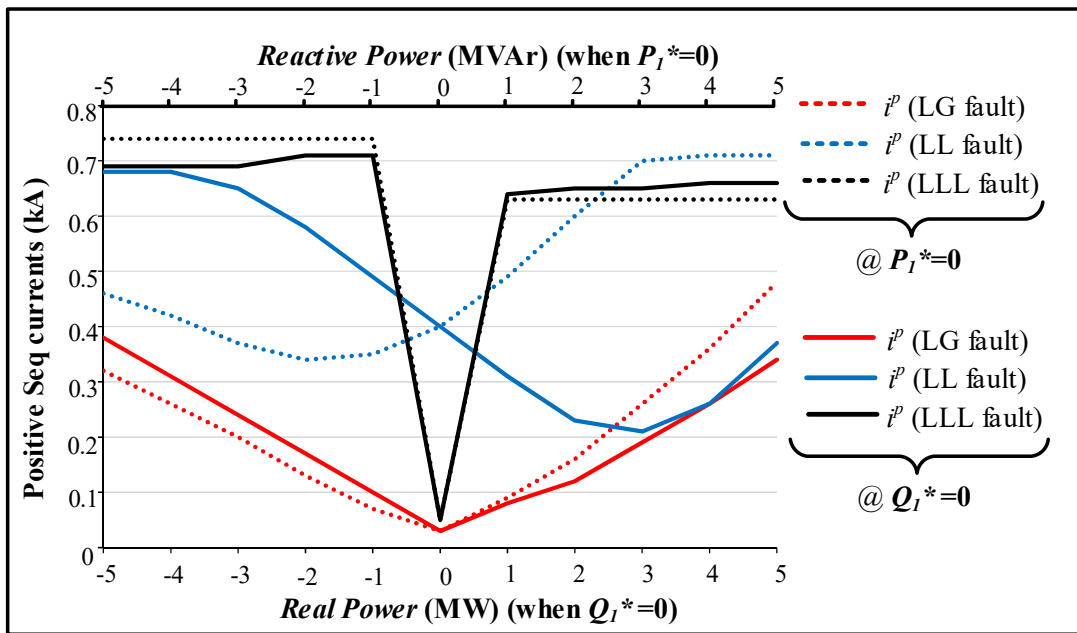


Figure 3.18 Positive sequence current for range of P_1^* set points, $Q_1^* = 0$ (solid lines); Range of Q_1^* set points, $P_1^* = 0$ (Dotted lines).

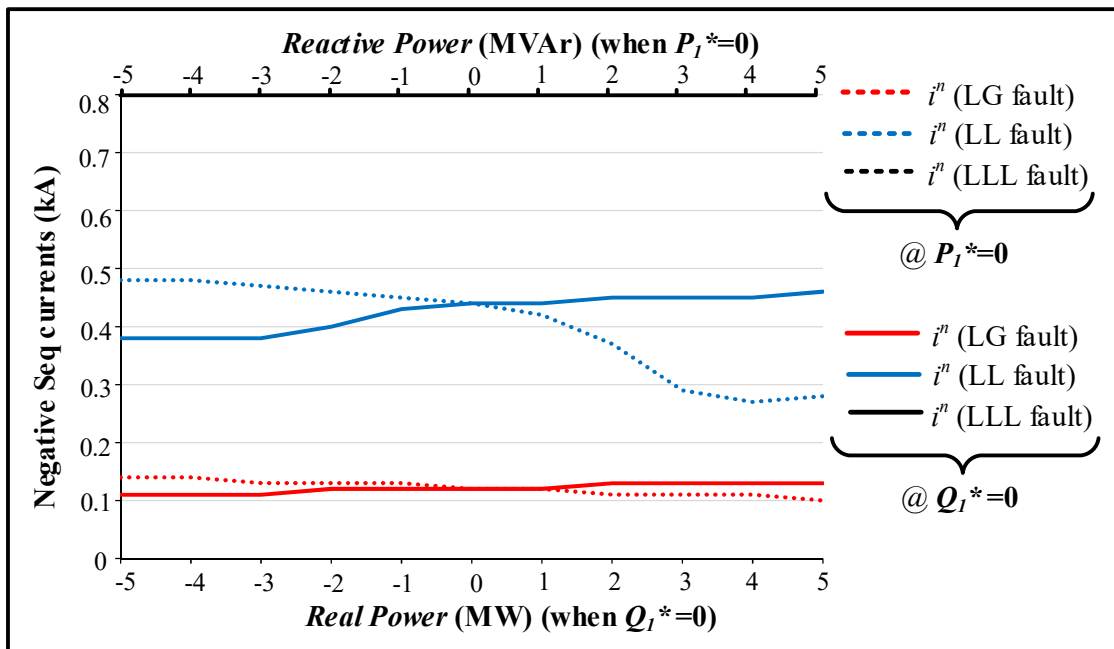


Figure 3.19 Negative sequence current for range of P_1^* set points, $Q_1^* = 0$ (solid lines); Range of Q_1^* set points, $P_1^* = 0$ (Dotted lines).

3.6 Summary

The performance of a medium voltage distribution network with an SOP was investigated, under grid-side AC faults. An averaged model of an SOP, suitable for dynamic study was used for this purpose. Equivalent sequence networks were developed for a network with an SOP under a line-ground fault, a line-to-line fault and a three-phase fault. The positive, negative and zero sequence components of the network were combined with the corresponding sequence components of the SOP to generate equivalent sequence network for each type of fault. Fault analysis using this representation was verified by simulations carried out on a generic UK distribution network with connected SOP. Their behaviour was compared for both P - Q and V_{dc} - Q modes of SOP operation. The correlation between the sequence voltages and currents at the SOP grid connection point were and the pre-fault set points of the SOP were studied.

A simple yet effective method of fault detection was formulated. The FI quantifies the unbalance in the network normalised by the nominal voltage. The positive, negative and zero sequence components of the voltage at the grid connection point of the SOP were used for this purpose. This method was found to be effective for AC fault detection in a network with an SOP for different type of faults and loading conditions.

4

Fault Diagnostics in Distribution Networks with Soft Open Point

Chapter 4 Fault Diagnostics in Distribution Networks with Soft Open Point

4.1 Introduction

In Chapter 3, an SOP was integrated in the fault studies for a simple radial network without considering any switching devices on the network. This chapter extends the studies to a radial network considering switching devices whose operation is governed by FA. It is common for distribution feeders to have FA, therefore it is important to investigate the impact of introducing an SOP on such distribution networks.

The interactions of an SOP with a D-FA scheme during an AC fault were investigated. Operation of the SOP is extended beyond its fault ride-through capability, to be integrated with dynamic operation of a distribution network. A diagnostic mode was developed to operate the SOP during grid-side faults such that the SOP can be used for fault diagnostics of the network. A new D-FA scheme was proposed in which the sequence of FA events is coordinated using an SOP. Simulations were carried out on an 11kV generic UK distribution network model with an existing FA scheme. The model was developed in PSCAD/EMTDC.

4.2 Conventional D-FA scheme

A number of FA schemes are utilised in distribution networks as discussed in Section 2.2.3. The detailed sequence of events in an existing FA scheme during temporary and permanent network faults are discussed in this section. The sequence of events corresponds to the automated circuit type-A in 11 kV, East of England distribution network operation, in the licensed areas of UK Power Networks (UKPN) plc [31]. It is a form of D-FA scheme in a simple network with two auto reclosers and a tie switch at the NOP. All devices in this scheme are equipped with remote operation capability.

4.2.1 Sequence of events in a conventional D-FA Scheme.

Figure 4.1 shows a radial feeder with remotely-operable auto-reclosers designated R1 and R2. It is connected to another feeder (not shown in the figure) through a tie switch which is a normally-open point that allows the two feeders to operate radially. Auto-reclosers are equipped with control units that initiate a number of reclose attempts

called shots, after a pre-set dead time (ΔDt_n ; where n corresponds to the n^{th} shot) between each shot [32]. 'f' is the location of a fault on the radial feeder as illustrated.

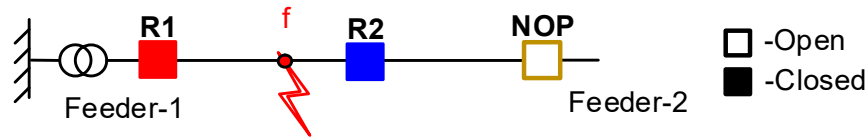


Figure 4.1 Typical distribution network

The devices undergo a sequence of events following a fault on the network as illustrated in Figures 4.2 and 4.3. The status '0' represents an open (OFF) state and '1' represents a closed (ON) state of the auto-recloser. The open and close operations of the devices are not instantaneous. However, for simplicity the transitions are shown as vertical lines in this illustration. The time stamps $t_0, t_1 \dots t_n$ are indicative of events in the FA sequence and are not to scale. It is assumed that a fault occurs at $t = t_1$.

Figure 4.2 illustrates the auto-recloser status for a temporary fault at location f on the feeder. R1 detects the fault current flowing through it and opens at $t = t_2$ following the relay operation time $\Delta t_1 = (t_2 - t_1)$. R1 attempts the first shot after a dead time of $\Delta Dt_1 = (t_3 - t_2)$. R1 opens again since the fault persists and attempts a second shot, with dead time $\Delta Dt_2 = (t_5 - t_4)$. R1 closes onto a healthy network during its second shot since the fault was cleared before t_5 . The internal counters and timers within the control units are reset. Temporary faults are normally cleared before the final shot. Therefore, normal operation of the network is restored without the DNO's intervention [32].

A permanent fault persists longer than the duration required to complete the allowable number of shots. The shots continue till the maximum count is attained, as illustrated in Figure 4.3. A maximum of three shots are used in this illustration. The device locks out in the open state during its final shot. R1 locks out at t_6 . This then triggers the downstream device R2 to open (at t_7) isolating the faulted section between R1 and R2. R2 is prevented from attempting shots since it is triggered by a lockout from R1. The NOP is then closed (at t_8) to restore power to the healthy section between the NOP and R2. The operation of the network remains the same for all fault locations within a feeder section. The relays are current-time co-ordinated to ensure that only the first circuit breaker upstream to the fault location trips.

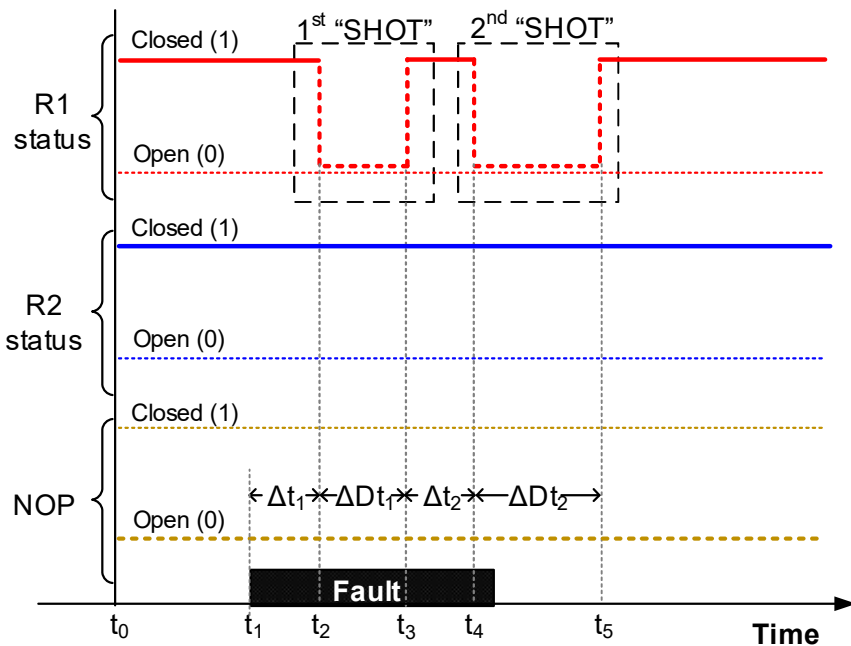


Figure 4.2 Sequence of D-FA events for a temporary fault

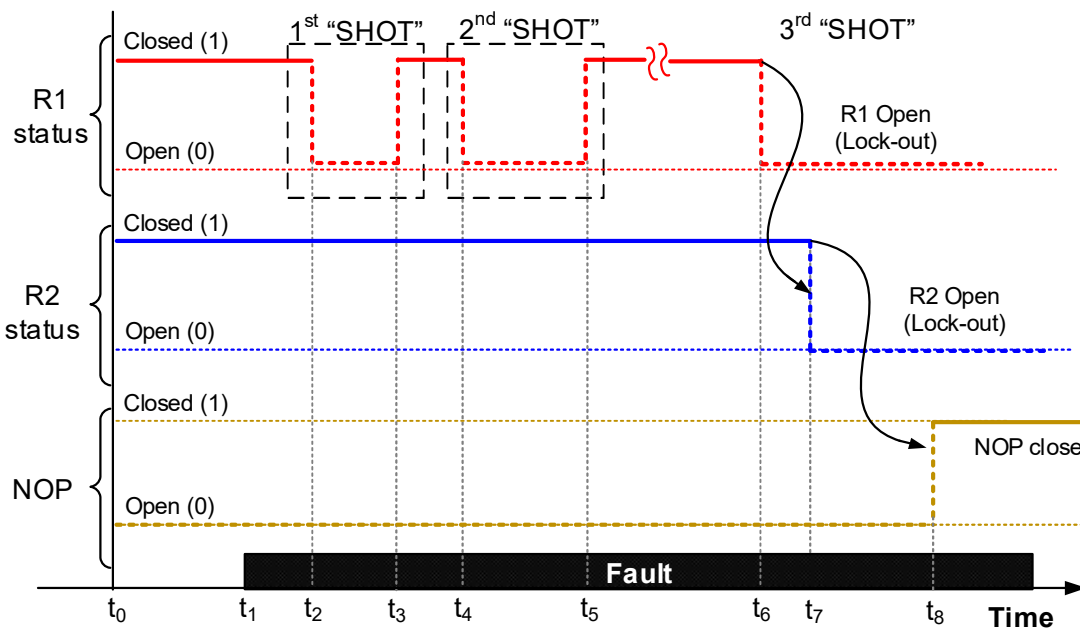


Figure 4.3 Sequence of D-FA events for a permanent fault

4.2.2 Impact of using SOP on conventional D-FA scheme

The network shown in Figure 4.4 is used to study the interactions between an SOP and a D-FA scheme. The NOP in the network shown in Figure 4.1 is replaced by an SOP and the behaviour of the network is then analysed during a balanced fault assuming that the SOP remains operational and connected to the network throughout the fault. The operation of the network with a NOP/tie switch (without the SOP) described in Section 4.2.1 is used as a base case for comparison. Interactions between FA and the SOP are analysed considering two scenarios:

- a) During a faulted condition: when the auto-recloser is opening; and
- b) After the fault is cleared: during the reclosing attempt.

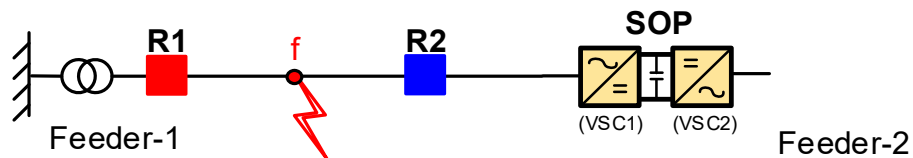


Figure 4.4 Typical distribution network with SOP

4.2.2.1 Behaviour of a network during auto-recloser opening (During fault)

This case focuses on the network behaviour with the SOP when the auto-recloser interrupts the fault current. A fault of one second duration is applied at location 'f', at $t = 2$ s of simulation time. The VSC connected to the faulted feeder (i.e. VSC1) can be operated either in the P - Q mode or V_{dc} - Q mode. Simulation results are reported for both control modes of the VSC.

1. Fault in Feeder 1 when VSC1 is in P - Q control and VSC2 is in V_{dc} - Q control.

If the SOP has zero power transfer (i.e. $P_1^* = 0$ and $Q_1^* = 0$) through VSC1 prior to the fault, R1 isolates the fault. The SOP does not contribute any current to the faulted feeder. In this case the sequence of events in the feeder automation scheme is not interrupted. During the fault VSC2 can continue to provide reactive power support to the unfaulted Feeder 2.

However, feeder automation is disrupted for non-zero power exchange through VSC1 prior to the fault. Considering the SOP set points of $(P_1^*, Q_1^*) = (-0.5 \text{ MW}, -0.5 \text{ MVar})$ and $(V_{dc}^*, Q_2^*) = (35 \text{ kV}, -0.5 \text{ MVar})$ as a typical operating scenario, the status of auto-reclosers R1 (designated R1_st) and R2 (designated R2_st) is observed during a fault on Feeder 1. Figure 4.5 shows the phase current (I_g) flowing through the SOP grid connection point. During a fault, R1 responds to the fault current and opens according to the FA scheme. A steady rise in the current is observed flowing from the SOP, and continues to flow into the fault even after R1 opens. The current rises until it reaches a threshold i_{max} . However, this current flowing into the faulted network is greater than the pick-up current of R2. R2 opens to interrupt the current from the SOP disrupting the sequence of FA operation.

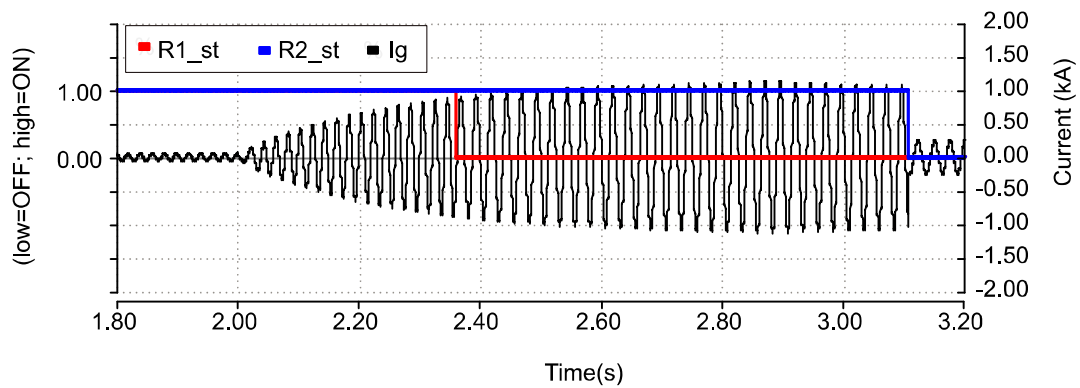


Figure 4.5 Recloser status and converter current for a temporary fault on feeder connected to P - Q controlled VSC.

2. Fault in Feeder 1 when VSC1 is in V_{dc} - Q control and VSC2 is in P - Q control.

The SOP retains its pre-fault state when $P_2^* = 0$ and $Q_1^* = 0$, making no contribution to the faulted feeder. For non-zero set points, the SOP injects current into the fault even after the opening of R1, as observed in the P - Q control. Figure 4.6 shows the phase current (I_g) flowing through the SOP grid connection point. The status of auto-reclosers R1 and R2 for a typical set points of $(V_{dc}^*, Q_1^*) = (35 \text{ kV}, -0.5 \text{ MVar})$ and $(P_2^*, Q_2^*) = (-0.5 \text{ MW}, -0.5 \text{ MVar})$. The rise in SOP current disrupts the sequence of FA operation. In addition, there is a drop in the DC link voltage as illustrated in Figure 4.7. Consequently, R2 opens faster than when the VSC was in P - Q mode.

It is notable that the direction of initial power transfer impacts the tripping time of R2. However, disruption of the feeder automation is independent of the initial direction of power transfer (*i.e.* polarity of set points).

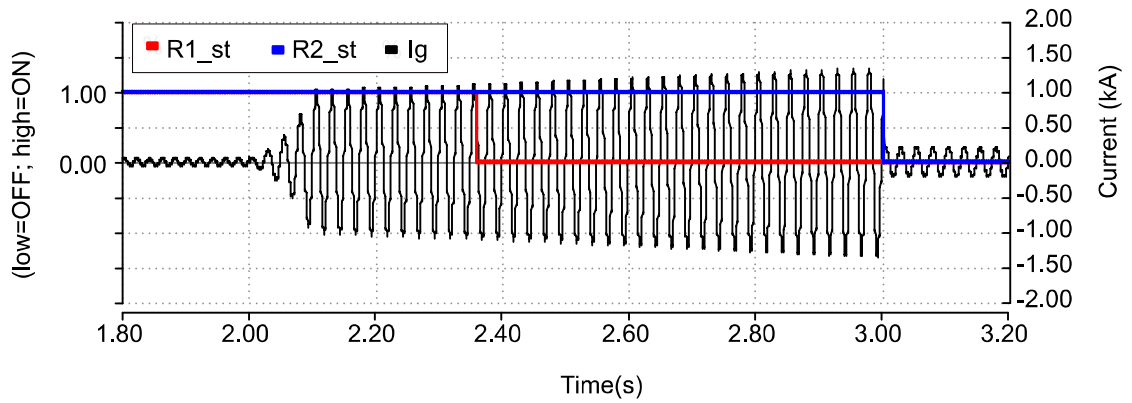


Figure 4.6 Recloser status and converter current for a temporary fault on feeder connected to V_{dc} -Q controlled VSC.

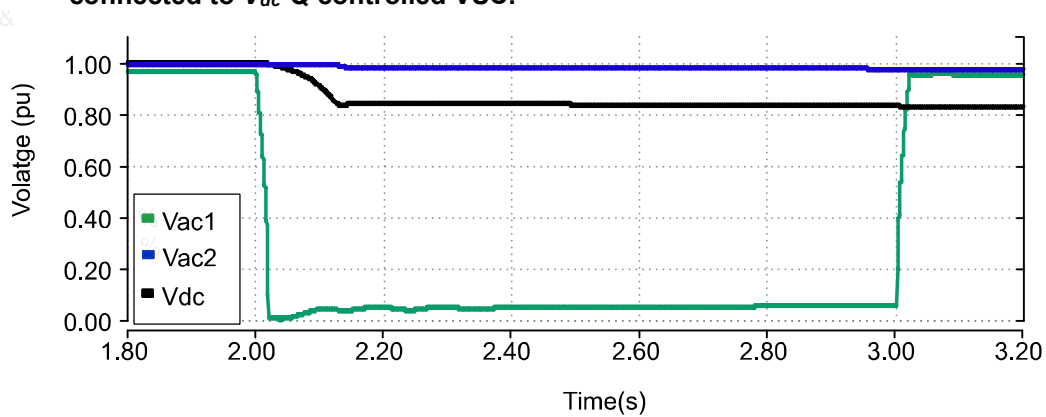


Figure 4.7 Voltages during temporary fault on feeder connected to V_{dc} -Q controlled VSC.

4.2.2.2 Behaviour of a network during reclosing attempt (Fault cleared)

Following the opening of R1 after a fault, the voltage at the grid connection point (V_{ac}) is not sustained. The power transfer from the VSC terminals to the feeder is not possible and the energy is stored in the reactor. The VSC controller responds by increasing the magnitude of the control signals (i.e. i_d^* and i_q^*) to compensate the difference between the actual power flowing through its terminals and the active and reactive power set points. The rate of increase depends on the gains of the PI controller.

R1 attempts to reclose during its first shot after a dead time (of 1s in this simulation). Ignoring the disruption to FA sequence during fault interruption, the SOP is engaged to a live bus following a temporary fault on Feeder 1. The voltage at the converter terminals attempts to build up to transfer power. It is observed that the SOP loses synchronisation with the grid. A non-sinusoidal voltage is produced, leading to disruption of the network as shown in Figure 4.8. A transient current rise is observed due to variations in the phase angle of the grid voltage and the phase angle of the reference

voltage. This variation leads to an improper voltage reference for the PLL during and after the fault.

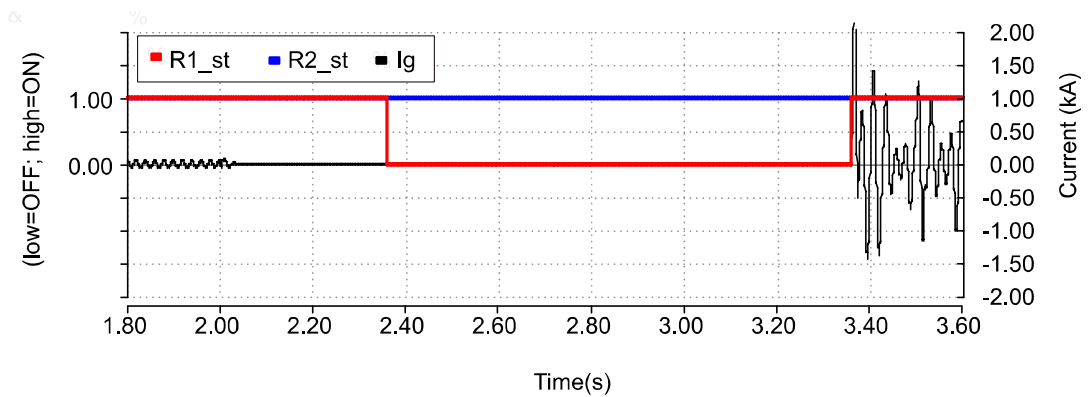


Figure 4.8 Recloser status and converter current during reclosing after a temporary fault.

4.3 Conventional D-FA scheme with SOP

In conventional operation the SOP has no role during a fault on the AC network [77]. An SOP acts as a current source during a fault on the network as discussed in Chapter 3. Therefore, the SOP is simply disassociated from the FA sequence to prevent disruptions caused by the current injected from the SOP. Network restoration is then achieved through manual switching between power control mode and restoration mode of the SOP [51], [73]. The two operating modes are discussed in further details in the following subsections. In a classical vector-control method that is used to operate the VSCs, the variables in the direct (i_d) and quadrature (i_q) axis allow independent control of parameters such as real power, reactive power, frequency, AC terminal voltage and DC link voltage. The control parameters are selected based on the operating mode of the SOP.

1. Power control mode

An SOP is operated in the power control mode during unfaulted, grid-connected condition. Control philosophy of this operating mode was discussed in Chapter 3 and it was shown to comprise of a two-level cascaded control system that includes an outer power loop and an inner current loop. The VSC control schemes are switchable between the P - Q , V_{dc} - Q , V_{dc} - V_{ac} and P - V_{ac} while operating in the power control mode. The converter terminal voltages (V_a , V_b , V_c) are calculated through inverse Park's transformation of the voltage reference signals, which are then used as the modulating signals to fire the IGBTs.

2. Restoration mode

Restoration mode is used when there is a grid fault, and the circuit breakers and/or reclosers have isolated the fault. The SOP is then used to supply the section of network without power supply. This mode is used to resume power supply to the unfaulted out-of-service loads.

When one of the SOP terminals is disconnected from the main grid the voltage at the grid connection point of the VSC is no longer dictated by the grid. This leads to a voltage and/or frequency excursion in the network. Therefore a strategy to control the terminal voltage and the grid frequency is employed [73]. The voltage is controlled through the variable in the direct axis (V_d^*), and the frequency is controlled through the variable in quadrature axis (V_q^*) of the synchronously rotating reference frame. This control scheme is applicable to the VSC connected to the feeder but disconnected from the grid. The VSC connected to the unfaulted feeder that is supplied from the main grid continues to operate in the V_{dc} -Q or V_{dc} - V_{ac} control scheme. It is essential to maintain the DC voltage, which in turn ensures the balance of active power flowing through the SOP.

Figure 4.9 shows the control scheme for the restoration mode. V_d^* is controlled at a value of $V_d = \sqrt{2/3} V_{ac}$ and the V_q at zero using closed loop control. V_{ac}^* is the desired line-line RMS voltage for the islanded network operation. The multiplication factor is used since Parks transformation is based on the peak phase voltage. The angular frequency reference is generated using the same voltages as the PLL inputs. This ensures a stable voltage reference since $\Delta\omega$ remains zero. The restoration mode controller is not impacted by the cross-coupling inductances in voltage loop [51], [73]. The outputs of the controllers form the voltage reference signals which are then used to generate the converter terminal phase voltages (V_a, V_b, V_c) through inverse Park's transformation similar to the power control mode.

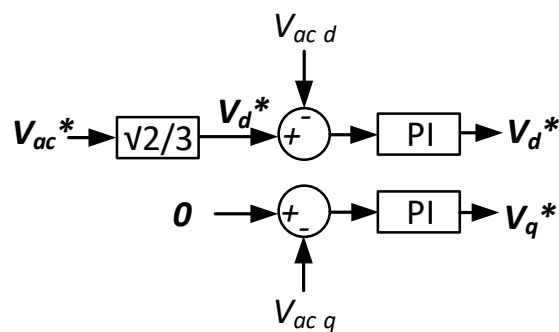


Figure 4.9 Control scheme for the restoration mode

4.3.1 Sequence of events in a conventional D-FA Scheme with SOP.

Figure 4.10 illustrates the conventional operating sequence of a D-FA scheme on a network with an SOP. The SOP normally operates in the power control mode. The SOP is isolated when a fault is detected. Typically, grid-connected VSCs have fault ride-through capability. However, this is applicable for transient faults in the range of few milliseconds [80]. For faults of longer durations, the VSC connected to the faulted feeder is isolated from the network using separate fault management devices [94]. The network protection devices then operate in a sequence governed by the FA scheme.

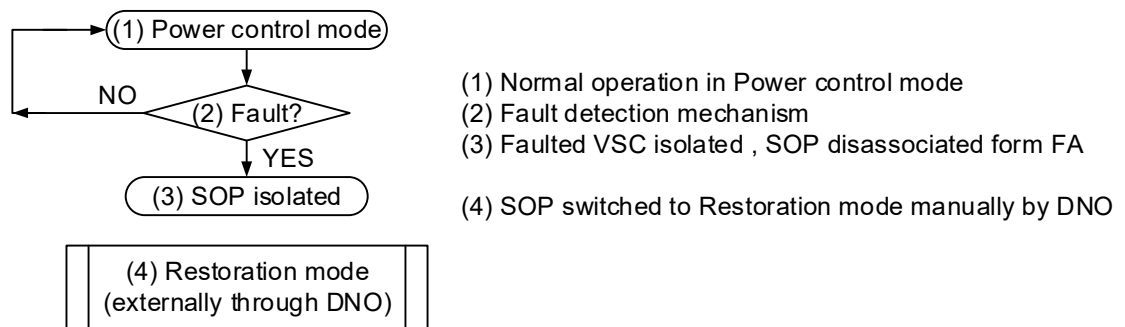


Figure 4.10 Conventional sequence of operation in a network with SOP

Figures 4.11 and 4.12 illustrate the sequence of operation followed by a network with an SOP (shown in Figure 4.4) during temporary and permanent faults respectively. When there is a fault at 'f', R1 starts the programmed open-close sequence following the disconnection of the SOP. The sequence of operation followed by the network is identical to the FA sequence in a network without an SOP. The relay operating times (Δt_n) and dead times ($\Delta D t_n$) remain unaltered. The sequence continues until either the network is restored for a temporary fault or the auto-recloser locks out in case of a permanent fault. The network operator then reconnects the SOP to the network after the sequence is completed. The applicable operating mode for the SOP is selected; the power control mode for grid-connected healthy network operation or the restoration mode to resume power supply to the un-faulted out-of-service loads. However, in both cases reconnection of the SOP is not a part of the FA sequence of events. External intervention from the DNO is needed to make this reconnection.

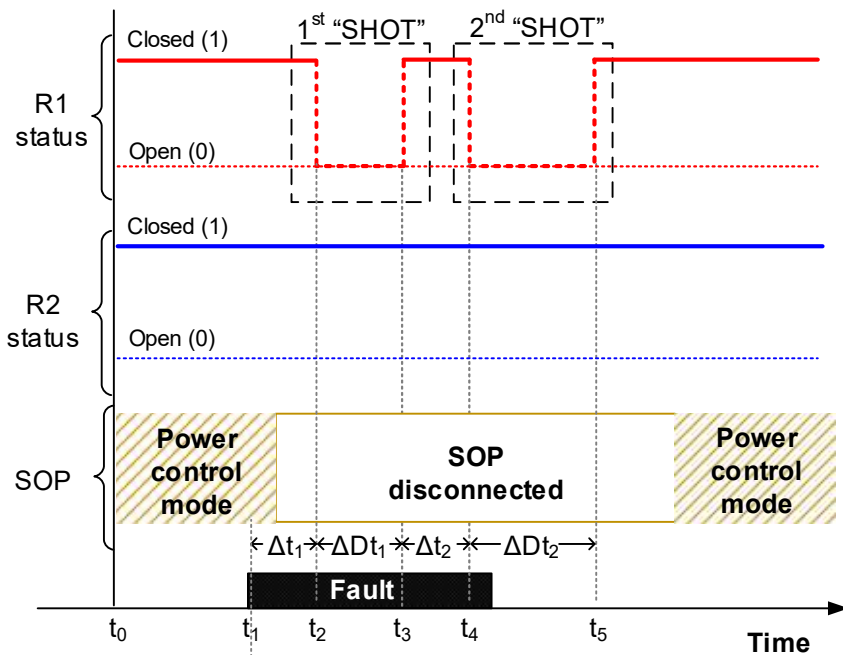


Figure 4.11 Sequence of D-FA events in a network with SOP for a temporary fault

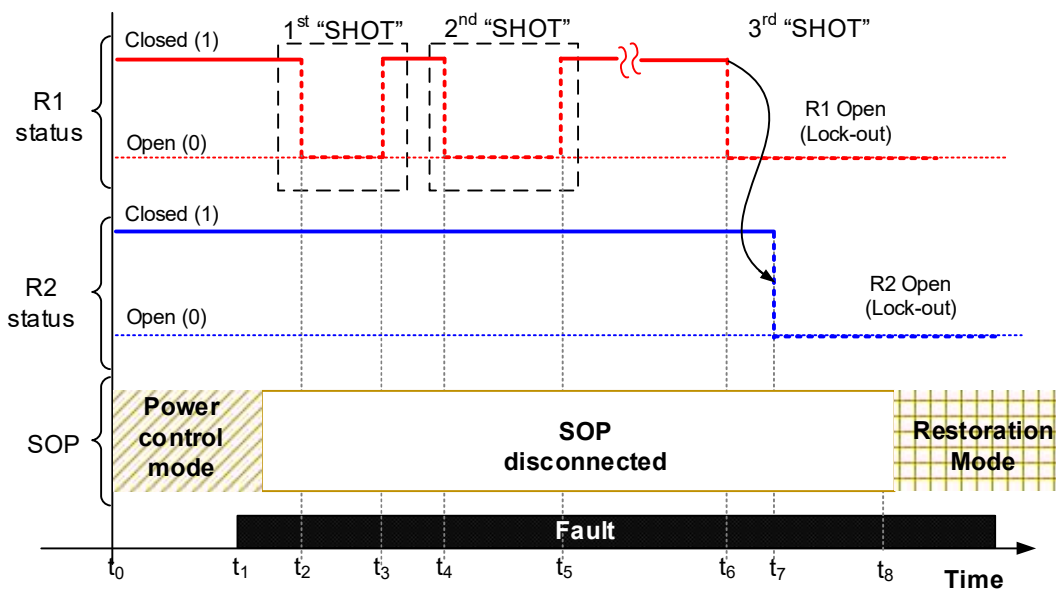


Figure 4.12 Sequence of D-FA events in a network with SOP for a permanent fault

4.3.2 Drawbacks of D-FA schemes using auto-reclosers

Conventional D-FA schemes using auto-reclosers have a number of disadvantages. As a consequence, networks have longer restoration times and result in considerable degradation of the network assets. Furthermore there are no improvements in the FA performance with the inclusion of an SOP. The main disadvantages and limitations of the conventional FA scheme are listed below.

1. Fixed dead times: The minimum dead time between each shot is calculated based on the dielectric strength of the interruption medium and the historical data of fault durations on a given network [32], [95]. Insufficient dead time will lead to incomplete discharge of stray charges on the switching contacts and thus reduce the fault interrupting capacity of the device. In addition, when reclosers are coupled with classical electromechanical relays, time needed for the induction discs to rotate should also be taken into consideration. Therefore the restoration time is limited by the dead time of the auto-recloser which is in the range of 0-5s for first shot, 11-20s for second shot and 10-30s for the third shot [32].
2. Total Number of shots: Operation of auto-reclosers varies according to the manufacturers, age and programmed logic within the controller. Selecting the number of recloser shots is a trade-off between the probability of network restoration and the asset degradation. In many networks it is common to operate auto-reclosers on three shots. The device is de-rated if it is operated more than the set number of shots or if operated within the dead times [96].
3. Degradation of the equipment: Auto-reclosers are typically designed to operate up to 2500 operations [22]. The number may vary slightly depending on the manufacturer specifications. Repeated shots lead to degradation of auto-reclosers' switching contacts and require more maintenance. In addition network components (i.e. cables, wires, transformers and connectors) are subjected to thermal and mechanical stress during each shot [96].
4. Voltage sag on adjacent networks: An auto-recloser closes on to a fault during each shot. Consequently, there could be a voltage sag on its adjacent circuits. Typically, a strong grid can ride through this sag. However, the magnitude and duration of the sag are dependent on the device used and can be detrimental to the network [96].

4.4 Network diagnostics using SOP

4.4.1 Diagnostic mode of SOP operation

The diagnostic mode is defined to operate the SOP during a fault, after the primary network protection devices open and before the network restoration is carried out. This mode is applicable for the VSC connected to the faulted feeder. The other VSC remains connected to an unfaulted feeder and controls the DC link voltage. Throughout this study it is assumed that only one of the feeders connected to the SOP is faulted. The diagnostic mode is not applicable if both the feeders connected to the SOP are faulted.

In the diagnostic mode, balanced three phase voltages are used as the modulating signals for the VSC connected to the faulted feeder. This VSC is operated in an open loop configuration at a low modulation index. A nominal operating voltage of 0.1pu of the network rated voltage is selected. A low operating voltage of the diagnostic mode enables continuous operation of the SOP during a fault. This ensures that the power electronic switches and other devices are not damaged throughout the diagnostic process. This study focuses on investigating the capability of an SOP to perform fault diagnostics. Determination of the optimum operating voltage of the SOP in the diagnostic mode is not in the scope of this thesis.

During the diagnostic mode operation, the voltage at the grid connection point follows the converter since the feeder is no longer connected to the main grid. Therefore, prevalent network condition in the section between the converter and the open circuit breaker is characterised by the current and the voltage at the grid connection point of the SOP. The currents flowing through the SOP terminals and the corresponding voltage drop at the grid connection point are quantified to distinguish between a faulted and an unfaulted condition of the network. The current and voltage measurements are then used to determine the type and location of a fault in the radial distribution network. In the following subsections details of individual protection aspects of the diagnostic mode are described.

4.4.1.1 Fault detection

Figure 4.13 illustrates a typical radial feeder having a fault at section 2. Z_g represents the line impedances of each section and Z_c is the converter impedance. $L1$ and $L2$ are two three-phase balanced loads. Shortly after a fault at point 'f', the section of the feeder including loads $L1$ and $L2$ is islanded since the circuit breaker (R1) is open.

The SOP is then operated in the diagnostic mode. The VSC1 connected to the faulted feeder behaves as a voltage source. The voltages and currents are measured at the grid connection point (GCP1) of the SOP and the faulted Feeder-1. The sequence components of the measured voltages and currents are calculated and then used as a decision variable for network diagnostics.

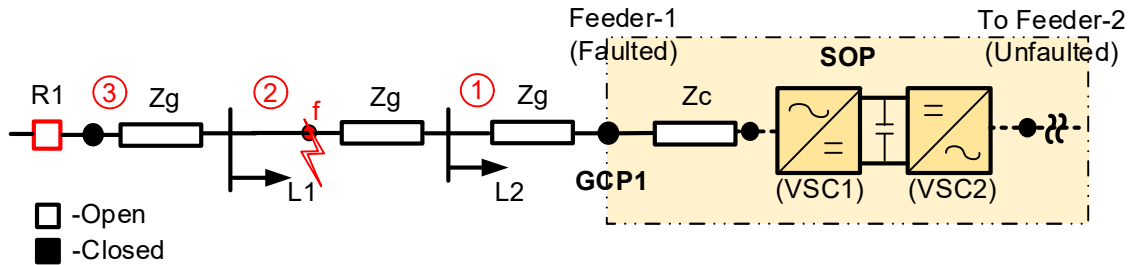


Figure 4.13 A typical radial feeder connected to an SOP in diagnostic mode (during an AC fault)

The fault analysis technique using sequence components described in Chapter 3 is extended to the diagnostic mode. The mathematical formulation of the Fault-Index (F) defined in the Section 3.4.3 is applicable for the diagnostic mode after a minor modification. Instead of using the network rated voltage, the nominal voltage of the diagnostic mode operation is used to normalise the sequence voltages. The F is defined in Equation. (4.1).

$$FI_x = \frac{(V_{xRMS}^p - (V_{xRMS}^n + V_{xRMS}^z))}{(V_{xN}^p)} \quad (4.1)$$

where x represents phases a, b, or c. V_{RMS}^p is the root mean square value of positive sequence voltage, and V_{RMS}^n is the RMS value of the negative sequence voltage and V_{RMS}^z is the zero-sequence voltage. V_{xN}^p is the nominal RMS voltage of the VSC during diagnostic mode, and it is assumed to be 0.1pu in this study. The threshold defined for F in power control mode is applicable for the diagnostic mode. Therefore a F value less than 0.9 indicates the presence of a fault on the network.

4.4.1.2 Determination of fault location and fault type

A number of algorithms are described in the literature to determine fault location in power networks. Common methods include the impedance method, travelling wave method and method using digital fault recorders [97], [98]. In the diagnostic mode, the location of a fault is estimated by calculating the apparent impedance of the network with

single-end measurement, similar to a distance relay. The algorithm based on impedance calculation using single-end measurement is advantageous since it is simple to implement, does not require any communication or remote measurements and can deliver reasonably accurate results [97].

Figure 4.14 illustrates an equivalent single line diagram of the radial feeder shown in Figure 4.13. The SOP operating in the diagnostic mode is shown as a voltage source connected at one end of the feeder. V_g and I_g are the respective phase voltage and line current measured at the grid connection point GCP1. 'd' is the per unit distance of the fault from GCP1 defined with the total feeder length (D) as base. I_f is the fault current at point f and R is the fault resistance. Z_{app} is the apparent positive sequence impedance as seen from the GCP1. Using Kirchhoff's law, the impedance seen from GCP1 can be calculated according to Equation. (4.2) [99].

Assuming the fault resistance is negligibly small, Equation. (4.3) is generalised for all types of short circuit faults. Therefore, the distance of the faulted section (d) from the measurement point can be estimated as a ratio of the total line impedance ($Z_D = Z_{app} + Z_l$).

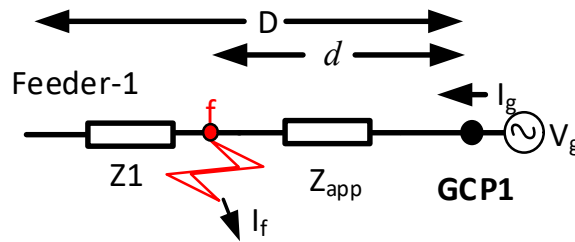


Figure 4.14 Equivalent single line diagram of the radial feeder in diagnostic mode

$$Z_{app} = \frac{V_g}{I_g} = dZ_D + R \frac{I_f}{I_g} \quad (4.2)$$

$$d = \left(\frac{Z_{app}}{Z_D} \right) \text{ (in pu)} \quad (4.3)$$

The voltage and current in the network depend on the fault type which is uniquely characterised by three conditions of line currents and the respective phase voltage. The conditions for a line-to-ground fault (L_a-G), a line-to-line fault (L_a-L_b), and a three-phase fault ($L_a-L_b-L_c$) fault in a network are listed in Table 4.1. Similar equations can be written for faults involving other phases.

Classical fault studies described in Chapter 3 are used to calculate the sequence currents and voltages applicable for each type of fault. The apparent positive sequence impedance can be calculated by using the fault-loop in the equivalent sequence network applicable for the respective fault type. The corresponding equations to calculate V_g and I_g values are shown in Table 4.2.

Table 4.1 Fault type determination criteria [89]

| Fault type determination criteria (without loads) | | |
|--|--------------------|-----------------------|
| Type of fault | Voltage conditions | Current conditions |
| L _a -G | $V_a = 0$ | $I_b = I_c = 0$ |
| L _a -L _b | $V_a = V_b$ | $I_a = -I_b; I_c = 0$ |
| L _a -L _b -L _c | $V_a = V_b = V_c$ | $I_a + I_b + I_c = 0$ |

Table 4.2 Equations for voltage and current at GCP1 for respective faults [97], [98]

| Voltage and Current at GCP1 | | |
|--|-------------|---|
| Type of fault | V_g | I_g |
| L _a -G | V_a | $I_a + \left(\frac{Z_D^z - Z_D^p}{3Z_D^p} \right) I_g^z$ |
| L _a -L _b | $V_a - V_b$ | $I_a - I_b$ |
| L _a -L _b -L _c | | |

Z_D^z is the zero-sequence line impedance and Z_D^p represents positive sequence line impedance. For earth faults, the phase to neutral voltage and line current including its zero-sequence component (I_g^z) are used. For phase faults, phase to phase voltages and currents are used. Any two phases can be used for a three phase fault [89].

4.4.2 The proposed D-FA scheme with the sequence of events coordinated by the SOP

An FA scheme using SOP is achieved by combining the diagnostic mode operation of an SOP with the power control and restoration modes described in Section 4.3. The SOP in the diagnostic mode is used to coordinate the FDIR process such that automatic transition between operating modes can be achieved. Figure 4.15 illustrates the operating sequence using diagnostic mode. Following an AC fault on the network, the SOP switches to the diagnostic mode (after the main circuit breaker opens) and determines the presence, type and the location of the fault. This enables the SOP to automatically select the desired operating mode following a fault without intervention of the DNO.

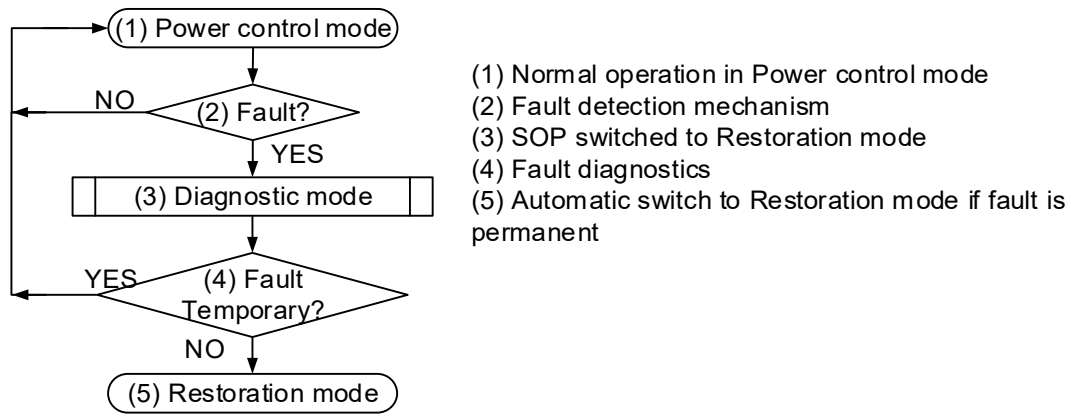


Figure 4.15 Proposed sequence of operation using diagnostic mode

In this scheme, when the SOP is operated in the power control mode during grid-connected operation, AC faults are detected using the FI threshold discussed in Chapter 3. Following the fault ride-through period, an error suppressor is engaged in the controller to prevent the VSC from injecting currents into the fault. The firing signals of the IGBTs are subsequently blocked. The VSC connected to the faulted feeder remains blocked until the contacts of auto-recloser/circuit breaker open to isolate the fault current flowing from the grid. This is necessary since an SOP responds faster than conventional protection devices. Blocking the VSC ensures that the SOP is dissociated from the faulted network but remains connected to the feeder. The auto-recloser is prevented from attempting reclosing shots and the control units are programmed to wait for a remote close command to be received from the SOP. The SOP is then unblocked allowing its operation in the diagnostic mode.

Figure 4.16 shows the sequence of operation for a temporary fault on the radial network shown in Figure 4.4. The VSC connected to the faulted feeder is blocked following the detection of a fault at time $t = t_1$. The VSC remains blocked for a duration of ΔT_1 , till R1 opens at $t = t_2$. The opening of R1 triggers the SOP to be unblocked in the diagnostic mode of operation. The SOP operates continuously in the diagnostic mode. The fault diagnostics is carried out as described earlier. The network is said to be healthy when the value of FI is maintained above the threshold for a duration of six AC cycles ($\Delta T_r = 0.12$ s). This time is sufficient for the value of FI to reach a steady state. Following the confirmation time ΔT_r , a remote close command is issued to R1. The SOP is switched back to power control mode. A hard switch from diagnostic mode to the power control results in momentary current spike at the grid connection point. Therefore a synchronous controller is used for smooth transition between control modes. The details of the design of the synchronous controller are described in [73]. During reconnection the set points of SOP are initially maintained at zero. These are then ramped up to desired levels after

voltage phase angle and magnitudes are synchronised with the original feeder in order to avoid excessive transients. The network then resumes normal operation.

Figure 4.17 illustrates the sequence of events for a permanent fault. The operation of the network and SOP is similar to the steps described above. If the value of FI is below the threshold for a pre-defined duration ΔT_p , the fault is said to be permanent. The value of ΔT_p is defined by the network operator. The faulted section is determined within ΔT_p by the SOP in the diagnostic mode. An open command is issued to R2. The faulted section is thus isolated between R1 and R2. The SOP is then operated in the restoration mode to feed the healthy network between the SOP and R2.

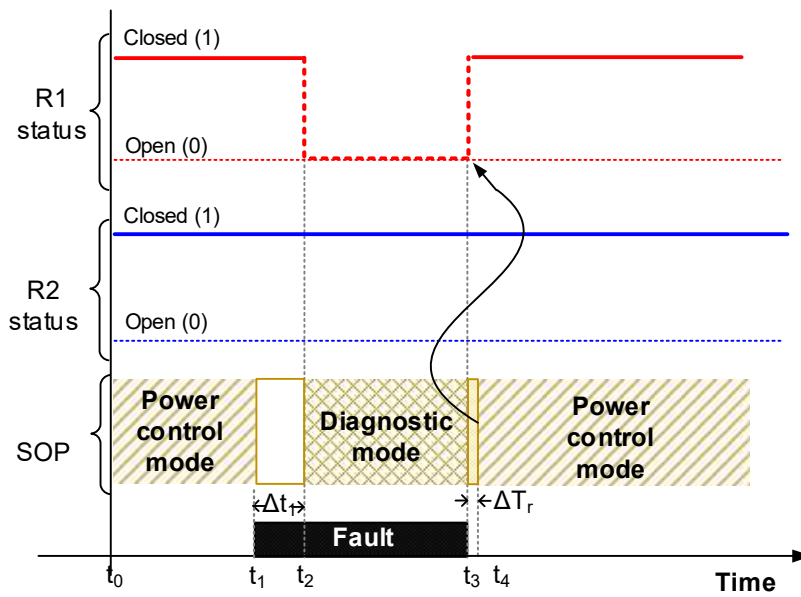


Figure 4.16 FA scheme using diagnostic mode of SOP for a temporary fault

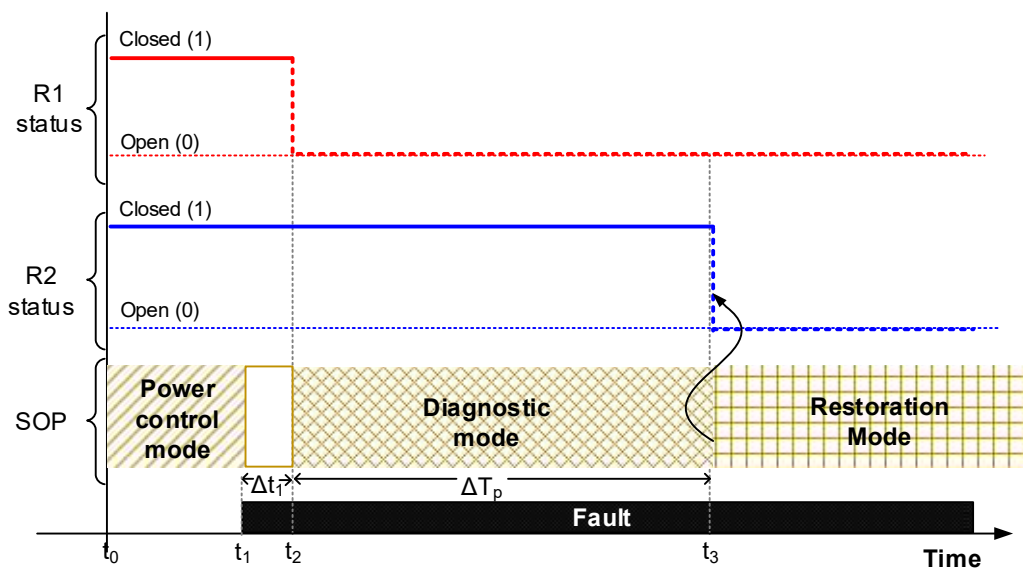


Figure 4.17 FA scheme using diagnostic mode of SOP for a permanent fault

4.4.3 Benefits of using SOP for FA in comparison to using auto-reclosers

Using SOP for fault diagnostics helps overcome the disadvantages of the conventional D-FA scheme. The main benefits of using SOP in comparison to an FA scheme using auto-reclosers are listed below.

1. No dead time: The diagnostic mode operation in an SOP is carried out through IGBT switch operation. There are no concerns of dielectric strength of switching contacts like in mechanical switches. Therefore, the restoration is no longer subject to the limitations of dead time of D-FA. Suitable restoration times may be selected by the operator based on the requirement of the network.
2. Elimination of Shots: Due to the continuous operation of the diagnostic mode the need for shots is eliminated. Consequently, the repeated disturbances on the network are also eliminated.
3. Improvement in the CML: In the UK, the regulator OFGEM specifies the customer minutes lost (CML) targets for the DNOs. CML is a performance index defined as the ratio of the sum of durations of all customers interrupted to the total number of connected customers, during a given period. The continuous operation of diagnostic mode directly translates to an improvement in the restoration time and consequently reduces CML.
4. Flexibility to choose restoration time: Selection of the restoration time (total number of shots in the conventional method) is no longer associated with the asset degradation. The pre-set time to determine a permanent fault may be optimised to best suit the requirements of the network.
5. Longer lifetime of existing assets: The assets are predominantly operated within the normal operational limit during the diagnostic mode operation. Therefore, degradation of assets due to repeated exposure to fault current is eliminated.
6. Elimination of repeated voltage sag on adjacent networks: There is no stress on the adjacent feeder(s) or on the SOP through the restoration process since the SOP operates within normal operational limits, and without repeated shots.
7. Economical and not exclusive to specific switching device: This scheme does not require specific switching devices in a network. Desired network operation can be achieved using remote controlled switches that are usually substantially cheaper than auto-reclosers.

4.5 Simulation results

4.5.1 Test network

The test network shown in Figure 4.18 is used to simulate a network with an SOP. The network was modelled in PSCAD/EMTDC. The test network consists of two radial feeders connected through an SOP of 6 MVA capacity. Feeder 1 has three sections, each has a length of 1km. Feeder 2 (not shown in the figure) is identical to Feeder-1. The line parameters are taken from a 11 kV generic UK distribution network [92]. Z_g represents the line impedance of a section. Each 1km section has a positive (Z_g^p) and negative sequence impedance (Z_g^n) of $0.164+j0.321 \Omega$, and zero sequence impedance (Z_g^z) of $0.542+j0.426 \Omega$ [93]. $L1$ and $L2$ are two three-phased balanced lumped loads of 3 MW, at a power factor of 0.9. R1 is an overcurrent-based circuit breaker in open status after interrupting a fault on the network. S1 is a remotely operated switch, which remains in closed position until an open command is received. Simulations are carried out for different types of faults on feeder sections 1, 2 and 3.

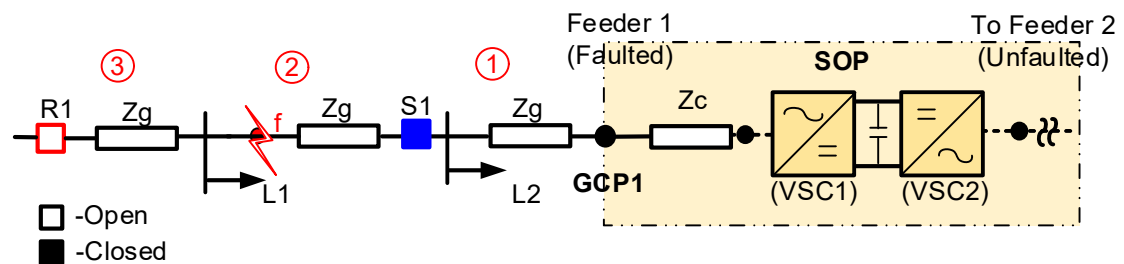


Figure 4.18 Test Network

4.5.2 Case 1: Fault type identification

Figures 4.19, 4.20 and 4.21 illustrate the fault type identification based on the voltage and current phasors at the grid connection point. Figure 4.19 illustrates the voltage and current values during a L_a -G fault, Figure 4.20 is during a L_a - L_b fault and Figure 4.21 is during a L_a - L_b - L_c fault. In each case the fault is simulated at location f , (i.e. section 2 of the test network). The current and voltage values for respective faults are compared with the criteria in Table 4.1. The measured V_g and I_g values follow the behaviour shown in Table 4.1 and are indicative of the respective fault type. It can be observed that the currents and voltages are never zero during any of the faults. This is because the criteria listed in Table 4.1 correspond to a network with no connected loads. In reality, the presence of loads results in a small non-zero current (≈ 27 A/phase) and correspondingly a small voltage at GCP1. Load currents are typically ignored in classical fault studies. Therefore, taking the load currents into account the conditions are

applicable since the behaviour remains consistent and can be uniquely characterised for each type of fault. The same criteria are applicable for faults on sections 1 and 3 on the test network.

Determination of the fault type is usually not a priority for the DNOs. Switching contacts are calibrated to open based on pre-defined current verses time curves. Typically, all three poles of the device are opened regardless of the fault type on the medium voltage level. However, it can be advantages to identify faulted phases, especially in the operation of distribution networks at lower voltages. SOPs in the diagnostic mode can be used for this purpose which in turn allows for the possibility of single phase operation (if applicable).

4.5.3 Case 2: Detection of fault and determination of fault location

The value of FI under different types of faults at section 1, 2 and 3 are listed in Table 4.3. The FI varies between 0.11-0.29 for a ground fault, 0.09-0.23 for phase faults fault and 0.09-0.23 for a balanced fault. The FI was well below the threshold of 0.9 for all types of faults and different fault location. In addition, after the fault is cleared, the FI is well above the threshold when the SOP is monitoring a healthy network.

The apparent impedance (Z_{app}) is obtained by substituting the measured current and voltage values at GCP1 into Equation. (4.2). Fault location (d) for each iteration is then estimated using Equation (4.3). The actual fault location is 0.33, 0.66 and 0.99 pu for faults on section 1, 2 and 3 respectively, since each section is assumed to have equal impedance. The error in the estimated location as compared to the actual location is expressed in percentage. The apparent impedance, fault location and error in estimation for faults at sections 1, 2 and 3 of the Feeder-1 are summarised in Table 4.4

The estimated fault location for each case is estimated. A maximum error of 3% is observed in the fault locations estimated. The errors are negligible, since the distribution feeders are significantly shorter as compared to transmission networks and determination of the exact fault location is not required. The achieved accuracy is sufficient to determine the faulted section in an MV distribution feeder. However, errors may be introduced in the single-end measurement-based impedance methods due to large load currents. Improved impedance methods such as modified Takagi method and Eriksson method can be used to reduce the error [97]. However, these methods involve a relatively higher complexity of calculation than the single-end measurement-based method and are not used in this study.

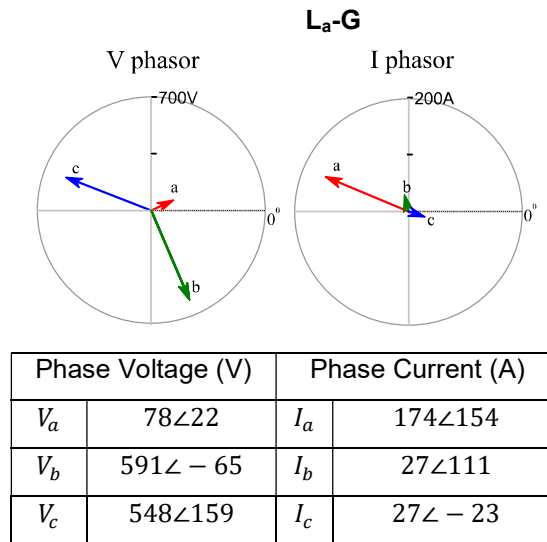


Figure 4.19 Voltage and current phasors for L_a-G fault.

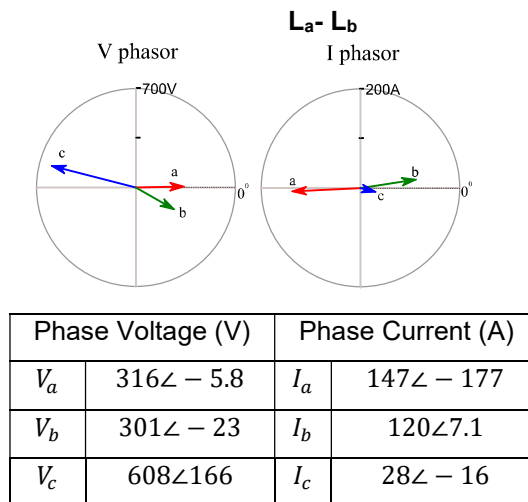


Figure 4.20 Voltage and current phasors for L_a-L_b fault.

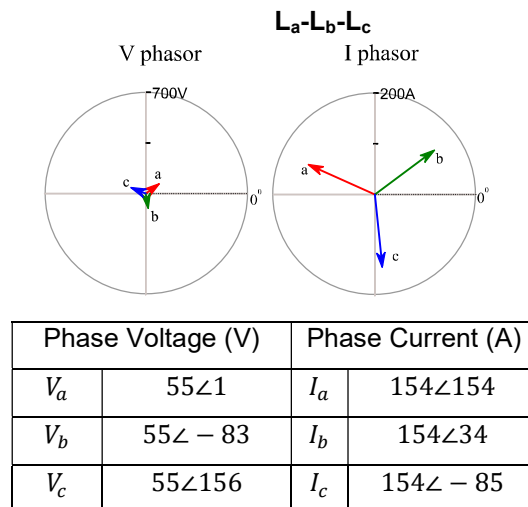


Figure 4.21 Voltage and current phasors for L_a-L_b-L_c fault.

Table 4.3 Values of Fault-Index, during and after a fault

| Fault Section | Type of Fault | <i>FI</i> (during a fault) | <i>FI</i> (after fault clears) |
|---------------|--|-------------------------------|-----------------------------------|
| Section- 1 | L _a -G | 0.29 | 0.98 |
| | L _a - L _b | 0.23 | 0.98 |
| | L _a -L _b -L _c | 0.23 | 0.98 |
| Section- 2 | L _a -G | 0.21 | 0.98 |
| | L _a - L _b | 0.16 | 0.98 |
| | L _a -L _b -L _c | 0.17 | 0.98 |
| Section- 3 | L _a -G | 0.11 | 0.98 |
| | L _a - L _b | 0.09 | 0.98 |
| | L _a -L _b -L _c | 0.09 | 0.98 |

Table 4.4 Calculated values of apparent impedance, estimated location and error in location estimation

| Fault Section | Type of Fault | *Z _{app} (Ω) | Estimated Fault location <i>d</i> (pu) | Error (%) |
|---------------|--|-----------------------|--|-----------|
| Section- 1 | L _a -G | 0.36∠ - 118 | 0.337 | 2% |
| | L _a - L _b | 0.20∠ - 118 | 0.330 | 0% |
| | L _a -L _b -L _c | 0.21∠ - 118 | 0.337 | 2% |
| Section- 2 | L _a -G | 0.724∠ - 118 | 0.680 | 3% |
| | L _a - L _b | 0.709∠ - 118 | 0.668 | 1.2% |
| | L _a -L _b -L _c | 0.710∠ - 118 | 0.669 | 1.3% |
| Section- 3 | L _a -G | 1.08∠ - 119 | 1.01 | 2% |
| | L _a - L _b | 1.06∠ - 118 | 1 | 1% |
| | L _a -L _b -L _c | 1.06∠ - 118 | 1 | 1% |

4.5.4 Case 3: Improvements in restoration time

This case illustrates improvements in the restoration time achieved by the using the SOP to coordinate the FDIR process. Simulations were carried out on the test network for L_a -G fault at location f , on section 2. A line-to-ground fault is used since it is most commonly occurring on a distribution network. However similar results can be expected for other types of faults because the operating sequence remains the same for all types of faults. Restoration times achieved by conventional D-FA scheme using reclosers and the proposed D-FA scheme coordinated by SOP using the diagnostic mode are compared.

The restoration times are compared for different fault durations varying from 1 s to 22 s in steps of 1 s. A dead times of 1 s is selected for the first (ΔDt_1), 11 s for the second (ΔDt_2) and 10 s, third (ΔDt_3) auto-recloser shots. These are the minimum recommended dead times for a distribution network below 35 kV [32]. R1 and R2 use the IEC standard-inverse curve. The details of the tripping curves settings used for the auto reclosers are given in the Appendix-B. The communication time required to issue a close command from SOP to the switching device is not considered. The results are illustrated in Figure 4.22

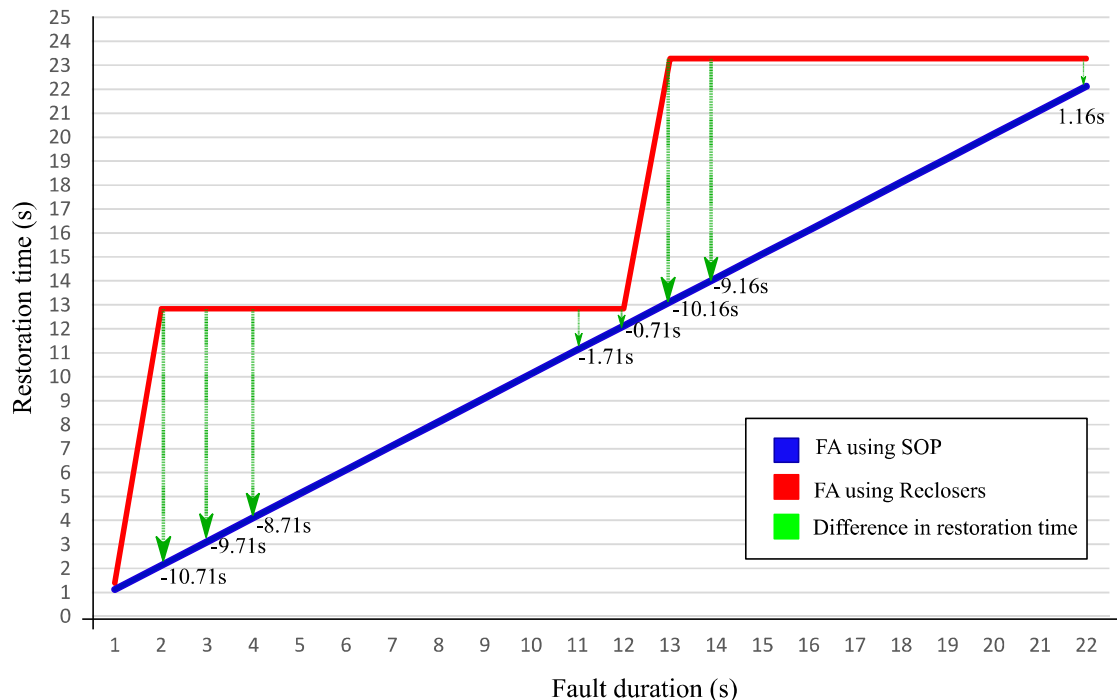


Figure 4.22 Comparison of restoration times between conventional FA and FA using SOP in diagnostic mode

The restoration time in the conventional FA scheme is a summation of operation times and dead times for the respective shots. A fault duration of 3 s is used as a typical case for a sample calculation. The operating times of the auto-recloser were $\Delta t_1 = 0.38$ s for the first shot and $\Delta t_2 = 0.45$ s for the second shot. Therefore the total restoration time including the first and second shot is $(\Delta t_1 + \Delta Dt_1 + \Delta t_2 + \Delta Dt_2)$ and is found to be 12.38 s. Restoration of the network using an SOP takes 3.12 s for the same fault. Resulting in an improvement of 9.17 s as compared to the former scheme. The restoration time is significantly reduced for fault durations slightly greater than the dead time of a specific shot. Using the SOP for FA eliminates the dead times and therefore the restoration time linearly follows the fault duration. The restoration times for faults of duration 2 s to 12 s remain 12.83 s in the conventional FA scheme due to the fixed dead time. A maximum improvement of 10.7 s and a minimum improvement of 0.71 s is achieved using SOP in diagnostic mode as compared to a two shot restoration using auto-reclosers (with minimum recommended dead times).

4.6 Summary

The sequence of events in a D-FA scheme with and without an SOP was discussed in detail. Interactions between FA and the SOP were studied assuming that SOP was not immediately isolated following a fault. It was obvious that the SOP disrupts the D-FA sequence of events due to the current injected from it during a fault. The drawbacks of conventional FA scheme using auto reclosers were also discussed.

The diagnostic mode was proposed to operate the SOP during a fault on one of its connected feeders, after the primary network protection devices opens. The efficacy of using SOP to determine the presence of a fault, fault type and fault location on a radial distribution network was investigated. Symmetrical components of the voltage and current measured at the grid connection point of the SOP and the faulted feeder were used for this purpose. Software simulations were carried out to verify the diagnostic mode operation of an SOP. A D-FA scheme was proposed such that the SOP participated in the FA sequence of events during network restoration. This was achieved by combining the diagnostic mode with other operating modes in the literature (power control and diagnostic mode). The FA scheme using the diagnostic mode provided significant improvement in restoration times. In addition, other drawbacks and limitations of using auto-closer based FA can be overcome.

5

Experimental Validation of Fault Diagnostics Capability of Soft Open Point

Chapter 5 Experimental Validation of Fault Diagnostics Capability of Soft Open Point

5.1 Introduction

In this chapter, a hardware-in-the-loop experimental setup is described to validate the fault diagnostic capabilities of back-to-back VSC based SOP proposed in the previous chapters. A real-time digital simulator (RTDS) interfaced with a VSC is used for this purpose.

The power hardware-in-the-loop setup used for this experiment is discussed. Details of the VSC prototype used to study the performance of an SOP are presented. Salient features of real-time simulations and the RTDS are briefly discussed. An 11kV generic distribution network was modelled on the real-time simulator interface (RSCAD) and connected to the VSC prototype using a four-quadrant power amplifier. This experimental setup was then used to validate the SOP operation in the diagnostic mode. The capability of SOP to determine the presence of a fault, fault type and fault location on a radial distribution network was validated.

5.2 Description of the experimental setup

Figure 5.1 shows the experimental setup used in this chapter to validate the fault diagnostic capability of an SOP. It consists of four major components;

- 1) VSC prototype (hardware under test);
- 2) Real-time digital simulator (RTDS);
- 3) Power interface (power amplifier and current probes);
- 4) Host computer

Operation of the SOP is validated using a VSC prototype that is connected to a distribution network modelled in the real-time simulator. The simulator and the VSC are interconnected through a power interface comprising of a power amplifier and current probes. The following subsections describe each of these components in further details.

5.2.1 VSC prototype (Hardware under test)

The hardware under test (HuT) consists of a three phase VSC prototype that is enclosed in an insulated box. The VSC prototype connected with an external constant DC voltage source (make and model: MAMEG-HM7042-5) represent an SOP in this experiment, as shown in Figure 5.2.

As described in the previous chapter, the diagnostic mode operation is only applicable to the VSC that is connected to the faulted feeder. The second VSC in the SOP is responsible for maintaining the DC link voltage and is assumed to be connected to a healthy feeder. Therefore, to validate the fault diagnostic capabilities of the SOP, it is sufficient to analyse the behaviour of the VSC connected to the faulted feeder. In this experiment, the VSC prototype represents the VSC that is connected the faulted feeder and is controlled independently in preferred operating mode. The DC voltage source ensures that the desired voltage level (V_{dc}) is maintained at the nominal value. This is equivalent to the second VSC of the SOP connected to a healthy feeder.

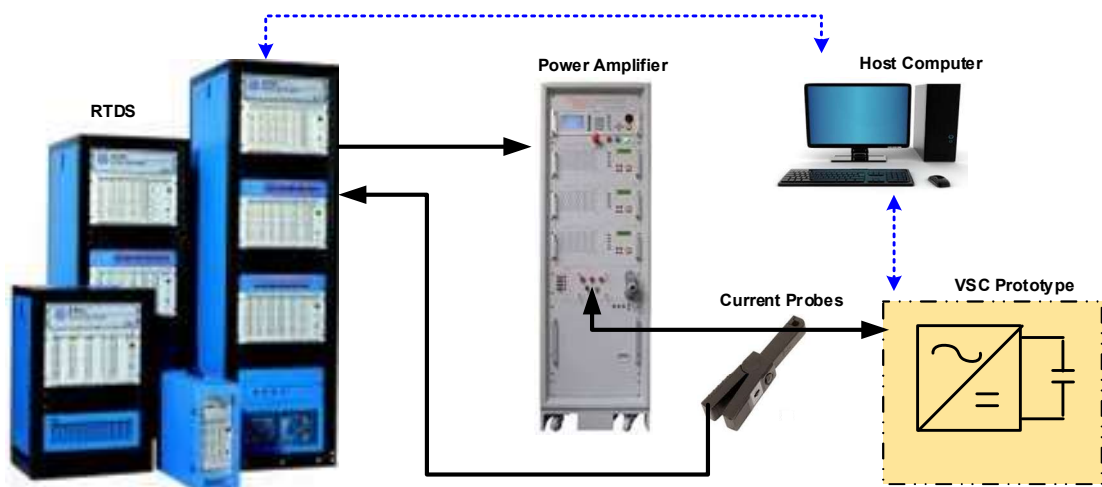


Figure 5.1 Experimental setup

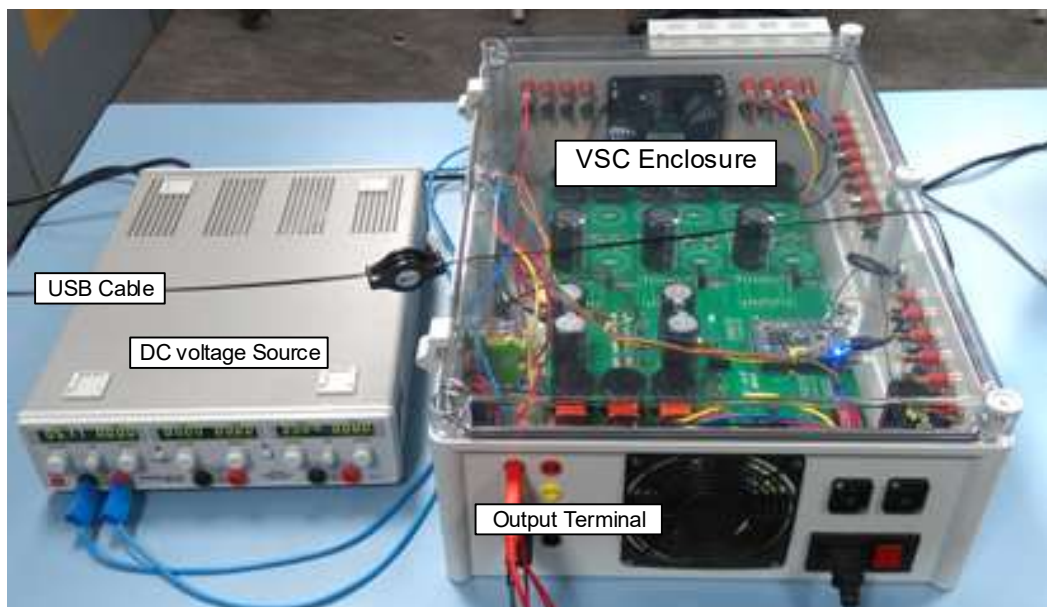


Figure 5.2 The HuT: VSC prototype and the DC voltage source

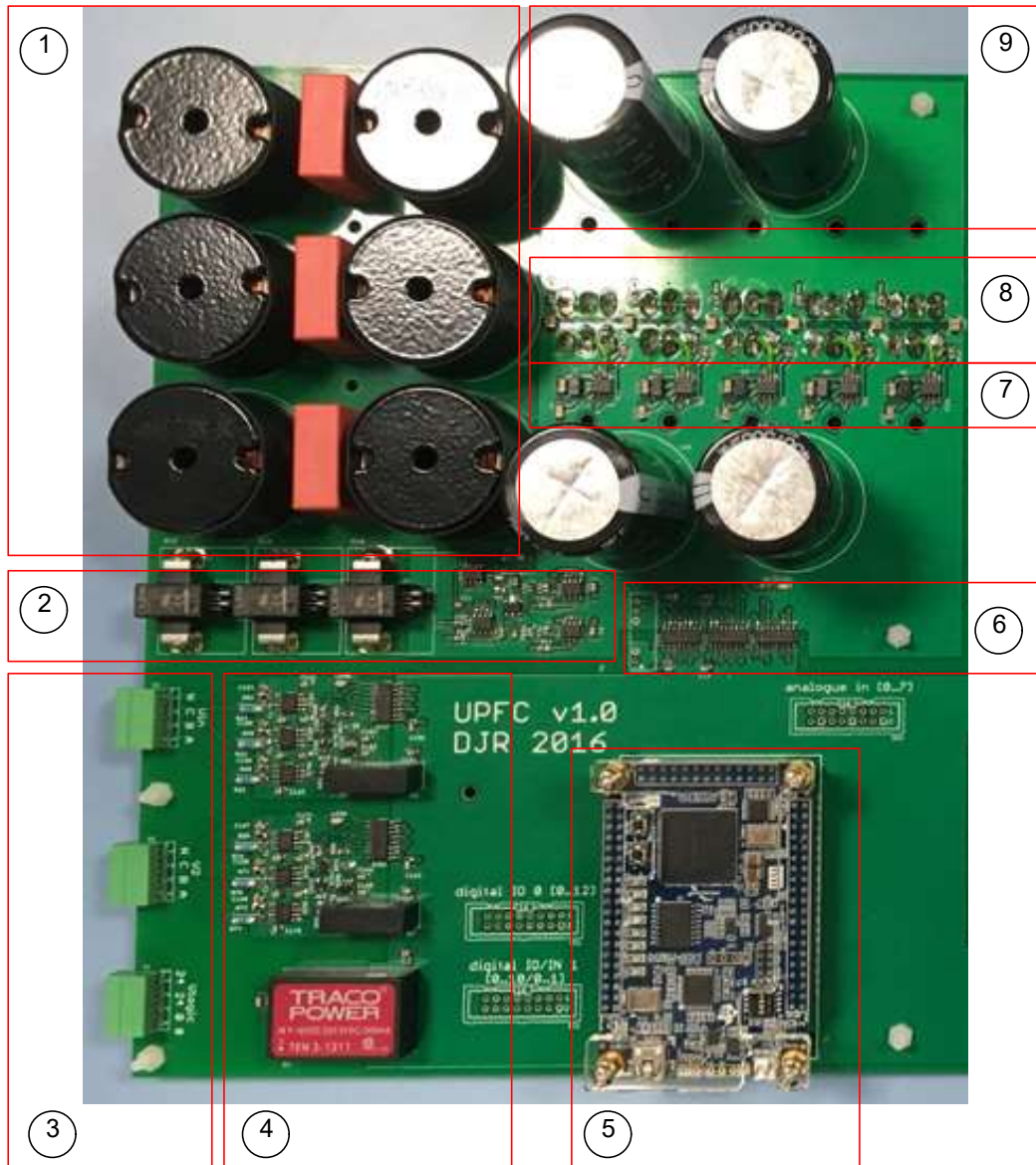
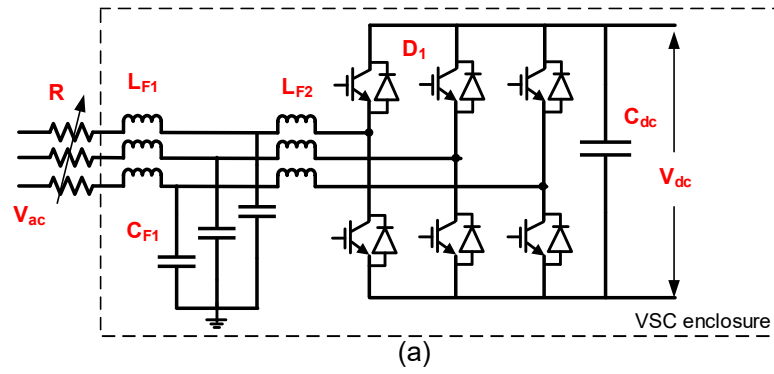
The main component of the HuT, is a voltage source converter. Figure 5.3 shows the circuit topology and the circuit board of the VSC used in this experiment. It consists of six IGBTs connected in a bridge configuration and are mounted at the underside of the circuit board (labelled (8)). The bridge constitutes the three arms of IGBTs of one VSC. These IGBTs are commutated using firing pulses generated through gate drivers (labelled (7)). The DC link consists of DC capacitor bank (labelled (9)). Therefore the combination of IGBTs and DC link represents one VSC of the SOP.

An Altera DE0 Nano development board (labelled (5)) is used to control the VSC. Details regarding the architecture and programming of this board are described in the next subsection. Digital isolators (labelled (6)) are used to isolate the controller auxiliary circuit from parts of the VSC that process power. An external power supply module (not shown in the figure) is used to supply 5 V that is needed to operate the auxiliary circuit of the VSC. The auxiliary circuit employs a number of current sensors (labelled (2)), voltage sensors and corresponding analogue to digital converter (labelled (4)). These measurements are connected to the I/O ports of the development board.

The outputs of the VSC are connected to three power terminals (labelled (3)) through an LCL filter (labelled (1)). An isolation relay (not shown in the figure) is connected between the VSC output terminals and the power connectors on the enclosure. This is used as a safety measure to isolate the VSC enclosure from the power amplifier in case of an over voltage/current or unexpected faults. The system parameters of the VSC are listed in the Table 5.1. The VSC prototype is not optimised for this experiment, therefore the parameters (e.g., maximum voltages/currents) are oversized.

Table 5.1 System parameters

| Parameter | Designed Values | Used values |
|--|--------------------------|-------------------------|
| System voltage (L-L RMS) V_{dc} | 220 V AC 440 V DC | 2.4 V AC 8 V DC |
| System frequency | 50 Hz | 50 Hz |
| L_{F1} and L_{F2} | 33 mH | 33 mH |
| R | 2-200 Ω | 3.8 Ω |
| C_{F1} | 4.4 μ F | 4.4 μ F |
| D_1 Drain-Source voltage Gate-Source voltage Current rating (at 25°C) | 1200 V 5-20 V 10 A | 1200 V 5-20 V 1 A |
| C_{dc} | 4x560 μ F | 4x560 μ F |



- ① Output L-C filter
- ② Voltage and current measurement sensors
- ③ 3 Ph AC Output terminal
- ④ A/D converters and Auxiliary DC power source
- ⑤ Controller-Altera DE0 Nano
- ⑥ Digital isolators
- ⑦ IGBT firing pulse drivers
- ⑧ IGBT bridge (Mounted on the underside of the board)
- ⑨ DC Link Capacitance

(b)

Figure 5.3 (a) Circuit topology; (b) Circuit board of the VSC

5.2.1.1 VSC controller

Figure 5.4 shows the Altera DE0-Nano development board used to control the VSC. This board consists of a compact-sized field programmable gate array (FPGA) development platform. Individual components on the controller are labelled on the figure. It features an Altera Cyclone IV FPGA, 32 MB of SDRAM, 2 Kb EEPROM, and a 64 Mb serial configuration memory device. It is equipped with an 8-channel, 12-bit A/D converter, two 40-pin headers which provide 72 I/O pins for external communication. The chip is externally powered by USB type mini-AB port (5V), DC 5 V pin for each header (two 5 V DC pins) and a 2-pin external power header (3.6-5.7 V) [100].

The operational block diagram adopted to program the Altera Nano controller is shown in Figure 5.5. The VSC control logic is designed in MATLAB/Simulink. Blocks that are compatible with VHDL Hardware Description Language (VHDL) are selected from the Simulink library for the design of the control logic. Simulink compiles this design into a Cyclone model that can be automatically translated to a VHDL code. The control logic can be designed directly on the interface available on the Quartus compiler using a hardware description language (e.g. VHDL, Verilog). However, Simulink model is used for convenience.

The VHDL design is then compiled using Quartus-II software in the host computer. The Quartus compiler then generates a bit stream with specific executable design [100]. The FPGA is programmed through the Quartus-II programmer by selecting a configuration bit stream file with the “.sof” file extension. The bit stream is communicated through a USB Mini-B cable connected between the host computer and the DE0-Nano development board. The program remains functional in the FPGA until the device is reprogrammed. However, the configuration information will be lost when the power is switched off.

The Cyclone model also has a direct interface with the FPGA through the USB cable. This is used for plotting and graphing the desired signals at the selected ports, when the program is running. Furthermore, this interface is used to communicate real-time commands with the FPGA, using designated I/O ports on the development board while running.

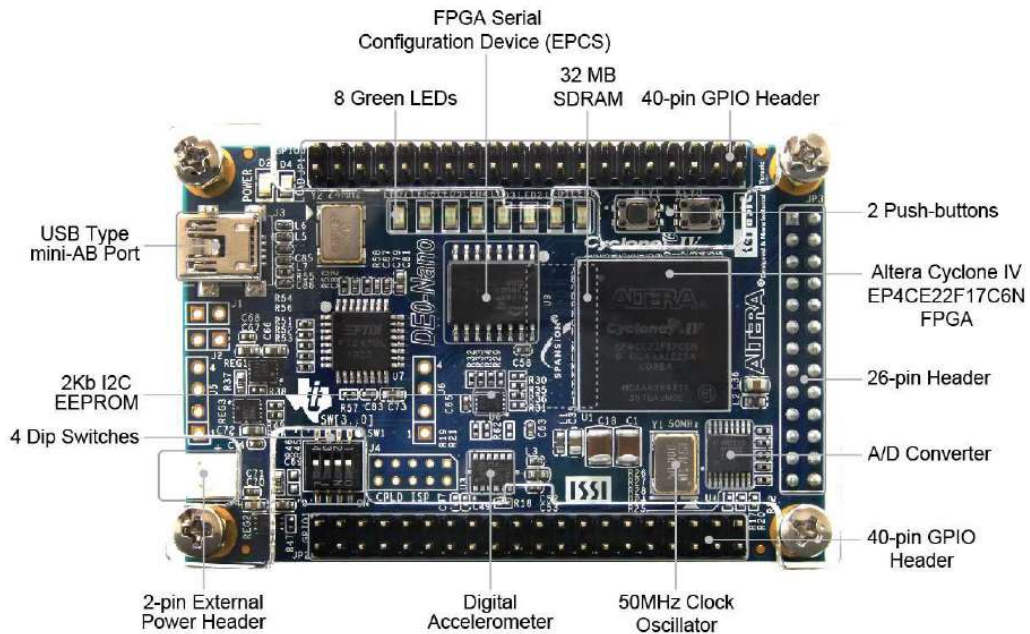


Figure 5.4 Altera DE0 Nano development board, used as the VSC controller; reproduced from [100].

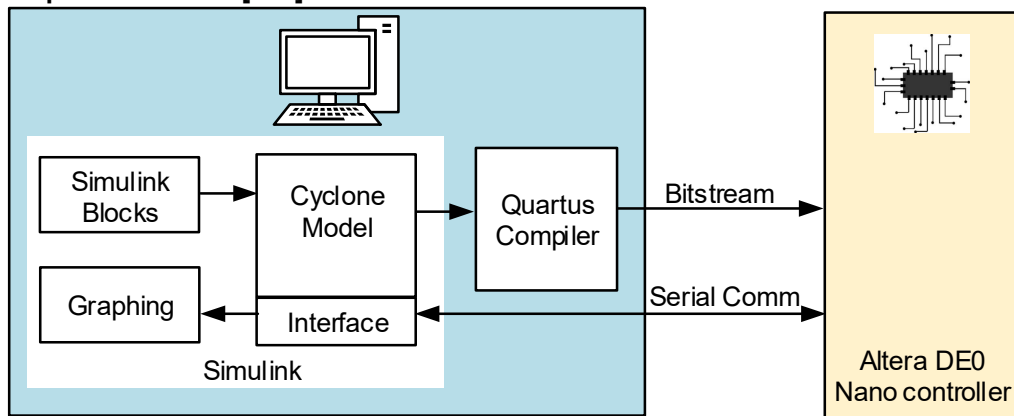


Figure 5.5 Operational block diagram of the VSC controller

5.2.2 Real-time digital simulator

The second component of the experimental setup is a test distribution network modelled in a real-time simulator which is an advanced computer that perform complex mathematical computation for one discrete time-step within the same time in real-world clock. Real-time simulators represent the behaviour of a real power system being modelled, such that the outputs (voltages and currents) are reproduced with the desired accuracy in real time [101]. Other solving techniques that use variable time-steps also exist but are unsuitable for real-time simulations. Such techniques are mainly used for solving high frequency dynamics and non-linear systems [102].

Software simulations are generally fixed time-step simulations, with discrete-time and constant step duration where the time progress in incremental steps [103], [104]. Typically, their objective is to obtain results as fast as possible which usually depends upon the available computational power and the mathematical complexity of the modelled system. Therefore, for a non-real-time simulation the execution time for an individual calculation is either less or more than the duration of one real time step [105]. However, in real-time simulation, the computation and real times are identical for every discrete time-step. In order to achieve this the real-time simulator needs to solve the model equations and generate desired system states for each time-step within the same time in real-world clock. This includes the time required for other relevant operations (e.g. driving the inputs and outputs, communication between external devices) that are to be performed by the simulator. Interfacing with external devices are discussed in Section 5.2.3). For each time-step, the simulator executes the same series of tasks:

- 1) Reading inputs and generating outputs;
- 2) Solving model equations;
- 3) Exchanging results with other simulation nodes;
- 4) Waiting for the start of the next step.

The states of the simulated system are computed and communicated to external devices once per time-step. Any idle time in the real-time computation cannot be carried over to the next discrete time-step. The simulator waits for the next iterative time-step and starts the computation again. The real-time simulation is considered erroneous if the simulation is too complex to be completed in one discrete time step. In such cases the simulator prompts a system overrun message. Real-time simulation is said to be successful if the system states are computed accurately at discrete times with acceptable resemblance to real world parameters, without overruns [101]. Therefore, it is best suited for experimental validation of network protection studies and network automation systems [106].

The RTDS simulator, developed by RTDS [105] Technologies is used to carry out the real-time simulations in this chapter. This simulator uses the ‘Dommel algorithm’ to perform digital computations of electromagnetic transients of an electric power network modelled with constant or distributed parameters [107], [108]. The algorithm converts differential equations to linear algebraic equations using the trapezoidal rule of integration. This allows all elements in a network to be represented by an equivalent current source and a conductance. RTDS simulators use this algorithm to perform real-time power system simulation using digital-computer time-domain solution.

5.2.3 Power interface

In this experiment the HIL setup is adopted. This form of real-time simulations uses a combination of a model developed in RTDS and a physical hardware prototype [105]. The hardware prototype is called hardware under test (HuT) and the software model is called rest of system (ROS) [110]. Interfaces (e.g. analogue-to-digital (A/D) converters, digital-to-analogue (D/A) converters, filters, and amplifiers) are used to link the HuT and the ROS.

HIL experiments are classified into two categories based on the power exchange between the HuT and the ROS. The HIL experiments without power transfer to or from the HuT are called controller hardware-in-the-loop (CHIL) experiments, as illustrated in Figure 5.7(a) These are typically adopted for rapid control prototyping (RCP) and testing of protection relays, where a network is modelled on the simulator and only control signals are communicated in and out of the simulator [111]. Figure 5.7 (b) illustrates the Power-HIL (PHIL) architecture which is used to test real-world hardware prototypes and is adopted in this chapter for the experimental study. PHIL experiments involves the exchange of power between the HuT and real-time simulator [110]. In addition to the real-time simulators and the HuT, a power interface is needed in order to either generate or absorb power.

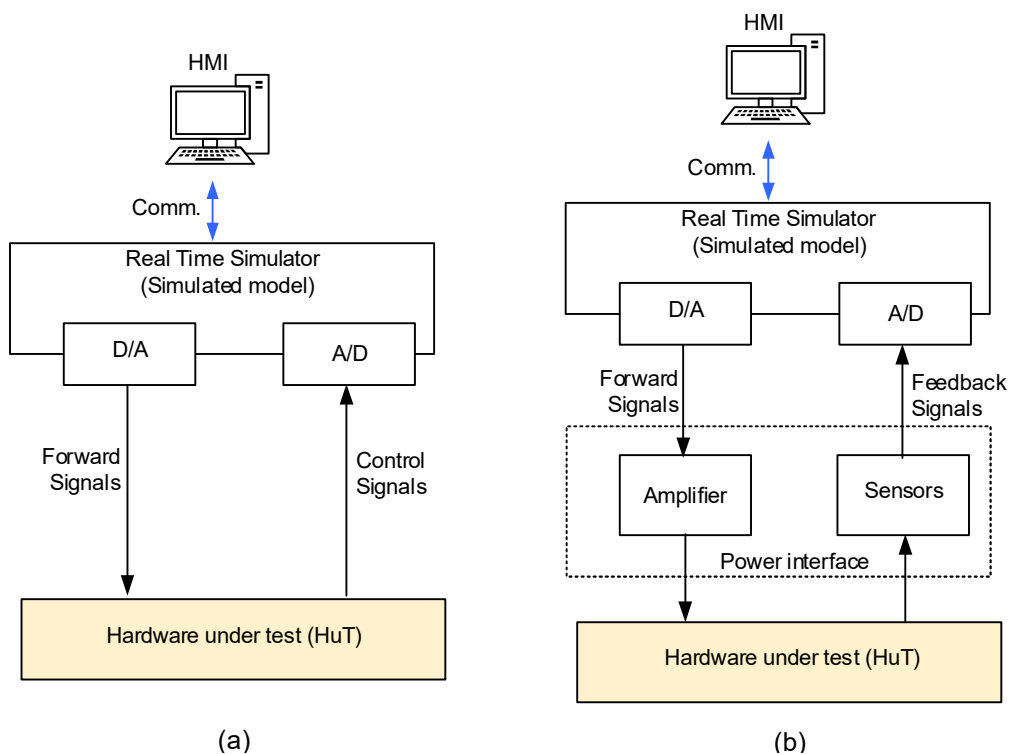


Figure 5.7 Basic HIL experiment architectures (a) CHIL (b) PHIL [105]

The functional setup of the power interface between the RTDS and the VSC enclosure (HuT) is illustrated in Figure 5.8. The terminal voltage in the RTDS test network is connected to a four-quadrant controlled voltage amplifier [112]. Power cables are connected from the 5 V, 16-bit D/A converters on the RTDS rack to the input terminals of the power amplifier. The magnitude of the voltage generated at the terminals of the power amplifier is proportional to the reference signal generated within the RTDS model. A scaling factor is used to define the operating voltage at the output terminals of the power amplifier that are connected to the HuT. Line currents flowing to/from the VSC are measured using three Hall-effect current probes. The probes are connected to the GT-I/O-analogue input ports of the RTDS A/D converter. This feedback path completes the power loop in this PHIL experimental setup.

The operation of this setup is explained with the help of an equivalent circuit shown in Figure 5.9. The test network (ROS) modelled in the RTDS is represented as a voltage source (V) with an equivalent line impedance Z . The HuT is represented by an impedance Z_L . The HuT is connected in series with the ROS. The terminal voltage (V_g) of the ROS is scaled down by a voltage scaling factor of K_1 , through a controlled voltage amplifier. Therefore, 11 kV AC in the ROS corresponds to 24 V AC at the power amplifier output terminals. The current I_g flowing through Z_L is measured and then fed back into the ROS. This is reflected in the equivalent circuit as $K_2 I_g$ flowing through the ROS, where K_2 is the current scaling factor. These scaled values of the measured currents are incorporated as a current source in the RTDS model, as shown in the Figure 5.8.

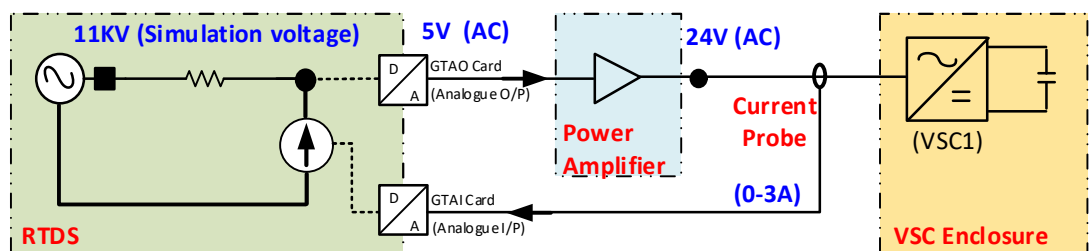


Figure 5.8 Functional setup of the HIL experiment [112]

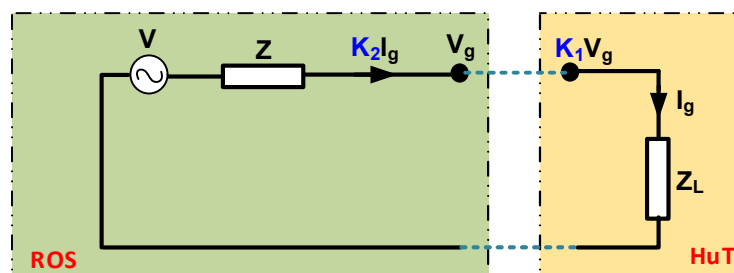


Figure 5.9 Equivalent circuit of the HIL experimental setup

5.3 Simulation results

Simulations are carried out on the experimental setup described in Section 5.2. The experimental test rig is shown in Figure 5.10. The performance of a network with SOP under various type of network faults are assessed using this rig. The behaviour of network is studied under three cases.



Figure 5.10 The experimental test rig

5.3.1 Case 1: Fault detection during normal operation (grid-connected)

This case is used to validate the fault detection method developed in Chapter 3. The performance of a network with SOP in the power control mode is investigated during a fault. Figure 5.11 shows the functional setup of the experiment. The distribution network is connected to the grid with circuit breaker R1 in closed status. The VSC is operated in the power control mode with a constant DC link voltage maintained by the regulated power source. The FI at the GCP1 is monitored for L_a-G , L_a-L_b and $L_a-L_b-L_c$ faults. The sequence filter in the RSCAD library is utilised to generate the positive, negative and zero sequence voltages needed to calculate the FI .

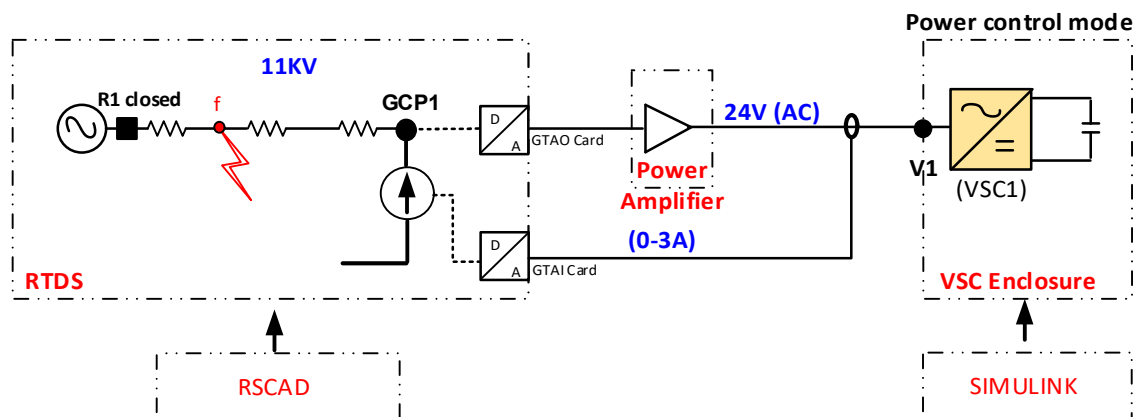


Figure 5.11 Test setup for Case 1: Fault detection for normal operation (grid-connected)

Faults are simulated at location f in the RTDS model for a duration of 0.3 s. The RTDS simulation output is plotted in the RSCAD-Runtime interface for 1 s with the fault occurring at 0.5 s. The FI is calculated for the faults using sequence voltage values measured at 0.6 s. Table 5.2 shows the FI for the L_a-G , L_a-L_b and $L_a-L_b-L_c$ faults. Only the scenario with real power injected into the feeder from the SOP is simulated, since the DC link voltage is maintained by the DC power source.

The FI is well below the threshold of 0.9 for different type of faults. Furthermore, the values of FI on an un-faulted healthy network (before and after the fault) were also within the expected range. From the results it can be observed that the values are in line with the expected levels and are in concurrence with the software simulations.

Table 5.2 FI for a grid-connected system with SOP in power control mode.

| Power flow scenerio | Type of fault | RTDS Simulations | |
|--------------------------|--|-------------------|----------------------|
| | | FI (During fault) | FI (Healthy network) |
| Power injecting from SOP | L _a -G Fault | 0.24 | 0.98 |
| | L _a -L _b Fault | 0.17 | 0.98 |
| | L _a -L _b -L _c Fault | 0.07 | 0.98 |

5.3.2 Case 2: Fault detection and type identification during diagnostic mode operation

This case validates the diagnostic mode operation of an SOP that was described in Chapter 4. Fault detection and the fault type identification, with SOP in the diagnostic mode are investigated in this case. Figure 5.12 shows the functional setup of the experiment. The test network modelled in the RTDS is disconnected from the grid supply with R1 open. The VSC is operated in the diagnostic mode. The IGBTs are commutated such that a fixed voltage of 2.4 V is maintained at the output terminal of the power amplifier. This corresponds to 0.1 pu of the 24 V, rated voltage of the VSC. The positive, negative and zero-sequence voltage and currents are monitored at GCP1 during L_a-G, L_a-L_b and L_a-L_b-L_c faults. The FI is then calculated for each of the iteration to investigate the presence of a fault. Correspondingly, the phase voltages and line currents are monitored at the grid connection point GCP1 and are then used to determine the type of fault on the network.

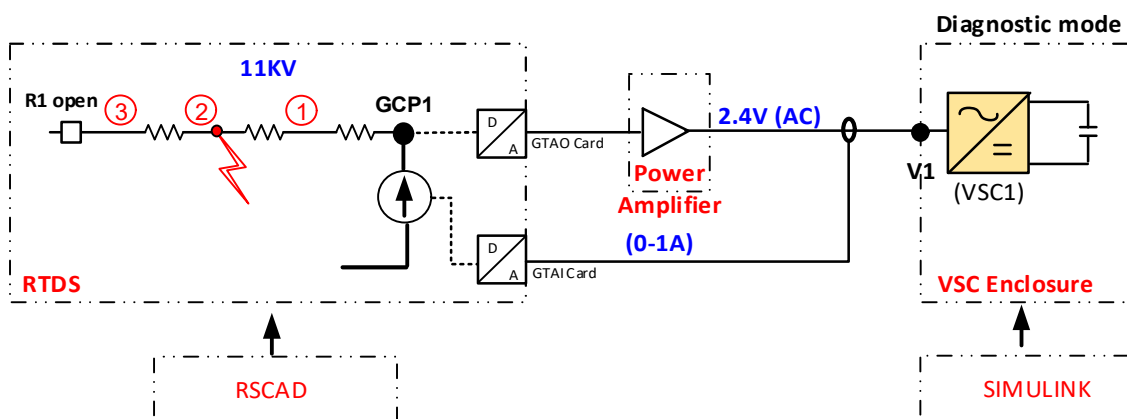


Figure 5.12 Test Setup for Case 2 and 3: Fault detection, type identification and determination of fault location during diagnostic mode operation

Faults of 0.3 s durations are simulated at section 1 in the RSCAD model. The RTDS simulation output is plotted on the RSCAD-Runtime interface for 1 s with the fault occurring at 0.5 s. The fault duration is selected such that the occurrence of a fault and the clearance of the fault are both captured in one simulation runtime of one second on the RSCAD interface. This time is used to demonstrate the operation of this mode. However, this method can be effectively applied for any fault duration since the SOP remains functional continuously during a fault. The FI is calculated for various faults using sequence voltages measured at GCP1, at 0.6 s of runtime. The experiments are repeated for faults at section 2 and 3.

Table 5.2 shows the FI for the L_a -G, L_a - L_b and L_a - L_b - L_c faults at sections 1, 2 and 3 of the feeder in RTDS. The FI values during and after the fault is cleared (healthy network) are shown in the table. A snapshot of the RSCAD-Runtime interface for the FI is shown in Figure 5.13 which illustrates the dynamic response of FI over the runtime of one second, for a L_a -G fault at section 2. It is clear that the FI values are below the define threshold of 0.9 during a fault on the network. The value of FI are within the range of 0.9 and 1 during healthy unfaulted network operation.

Figures 5.14 - 5.16 illustrate the fault type discrimination based on the voltage and current phasors at the grid connection point. The phasor diagrams are plotted for faults on section 2. Figure 5.14 illustrates the phase voltages and line currents values during a L_a -G, Figure 5.15 corresponds to a L_a - L_b fault and Figure 5.16 corresponds to a L_a - L_b - L_c fault.

The current and voltage phasors are compared with the corresponding criteria listed in Chapter 4 (in Table 4.2). Similar to the software simulation results the presence of loads results in a non-zero current (≈ 27 A/phase), and consequently a non-zero voltage at GCP1 during faults. The experimental results are not numerically identical to the values obtained in software simulations. However, their behaviour remains consistent. The voltage (V_g) and (I_g) values follow the expected behaviour for the respective fault type. Experimental results are consistent with the theoretical analysis and simulation results analysed in the previous chapters. The conditions are applicable for faults on section 1 and 3 of the test network.

Table 5.3 *FI* for an isolated system with SOP in the diagnostic mode

| Faulted Section | Type of fault | RTDS Simulations | |
|-----------------|--|-----------------------------|--------------------------------|
| | | <i>FI</i> (During fault) | <i>FI</i> (Healthy network) |
| Section 1 | L _a -G | 0.01 | 0.98 |
| | L _a -L _b | 0.02 | 0.98 |
| | L _a -L _b -L _c | 0.04 | 0.98 |
| Section 2 | L _a -G | 0.06 | 0.98 |
| | L _a -L _b | 0.03 | 0.98 |
| | L _a -L _b -L _c | 0.04 | 0.98 |
| Section 3 | L _a -G | 0.02 | 0.98 |
| | L _a -L _b | 0.05 | 0.98 |
| | L _a -L _b -L _c | 0.04 | 0.98 |

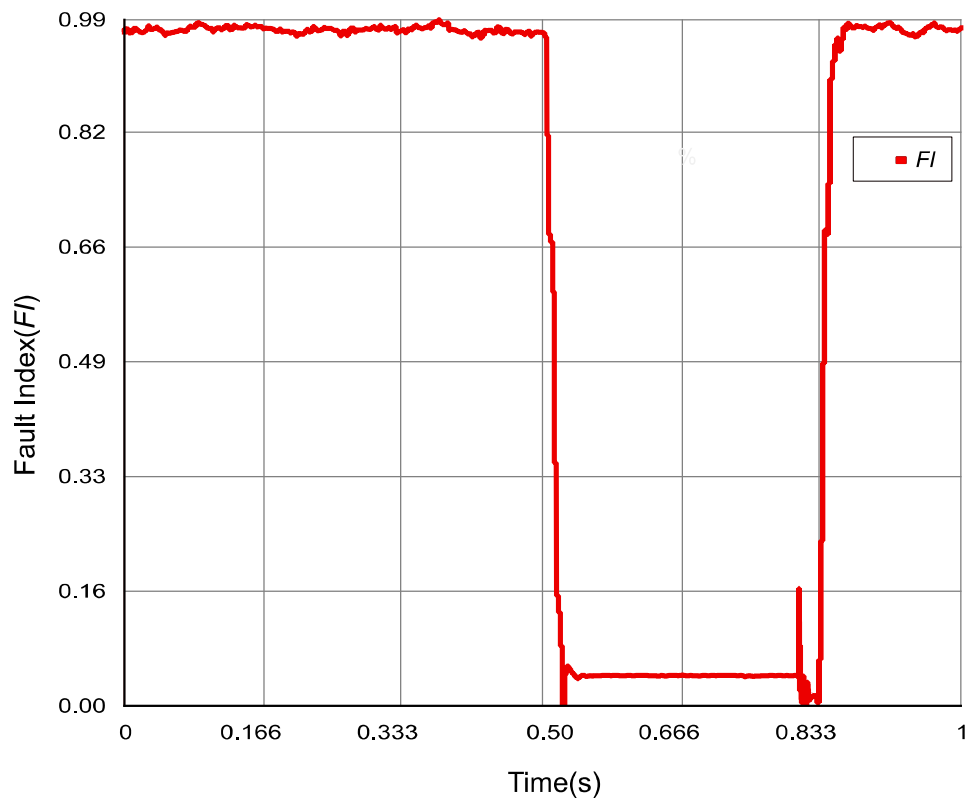


Figure 5.13 Dynamic response of *FI* for a L_a-G fault at section 1

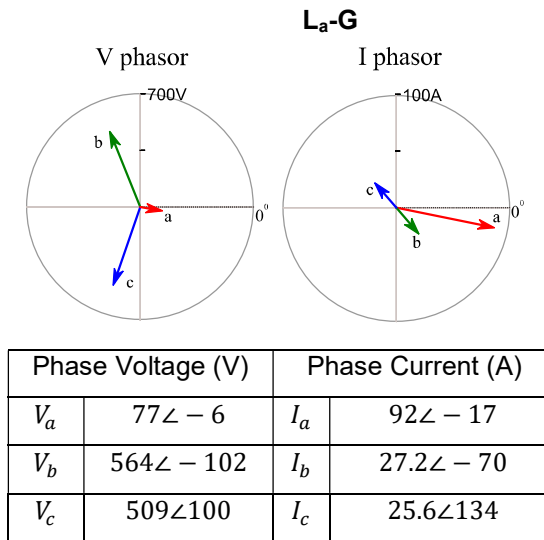


Figure 5.14 Voltage and current phasors for L_a-G fault.

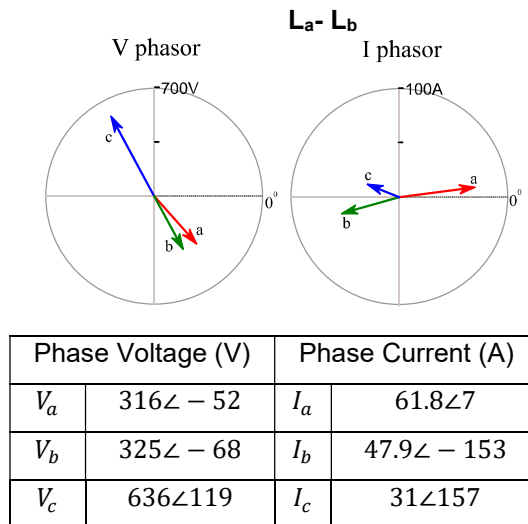


Figure 5.15 Voltage and current phasors for L_a-L_b fault.

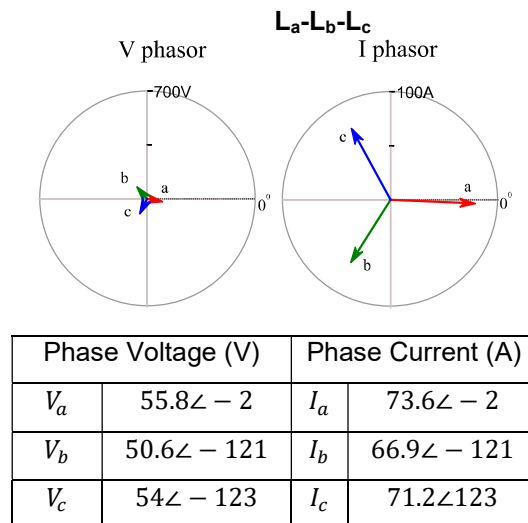


Figure 5.16 Voltage and current phasors for L_a-L_b-L_c fault.

5.3.3 Case 3: Fault location estimation during diagnostic mode operation

This case is used to validate the use of SOP in the diagnostic mode to estimate the fault location using measurements at GCP1. The testing setup used for Case 2 (as illustrated in Figure 5.12) is applied for this case. The experimental results are analysed for L_a -G, L_a - L_b and L_a - L_b - L_c faults on sections 1, 2 and 3 individually.

The apparent impedance (Z_{app}) of the network as viewed from the point of measurement (GCP1) is calculated using Equation (4.2) (in Chapter 4). Fault location (d) is then estimated using Equation (4.3). The testing network used in this experiment is identical to the network used for software simulation in Chapter-4. Each section in the test network is assumed to have equal impedance and therefore the actual fault location is 0.33, 0.66 and 0.99 pu for faults on section 1, 2 and 3 respectively. The deviation of the estimated value from the actual fault location is expressed in percentage. The calculated values of impedance, estimated fault location and the error in estimation are summarised in Table 5.4. The errors in the location calculated from the real-time PHIL experiment is greater than the errors obtained during software simulation. However, the errors are marginal (generally $\leq 10\%$) and the obtained accuracy is sufficient to determine the faulted section in MV distribution feeder.

Table 5.4 Calculated values of apparent impedance, estimated location and error in location estimation

| Fault Section | Type of Fault | RTDS Simulations | | |
|---------------|-----------------------|--------------------------|---------------------------------|-----------|
| | | * Z_{app} (Ω) | Estimated Fault location x (pu) | Error (%) |
| Section 1 | L_a -G | 0.40 \angle 177 | 0.377 | 13.1% |
| | L_a - L_b | 0.38 \angle 179 | 0.358 | 7.5% |
| | L_a - L_b - L_c | 0.38 \angle 178 | 0.358 | 7.5% |
| Section 2 | L_a -G | 0.759 \angle - 178 | 0.716 | 7.3% |
| | L_a - L_b | 0.734 \angle - 179 | 0.692 | 3.7% |
| | L_a - L_b - L_c | 0.759 \angle - 166 | 0.716 | 7.3% |
| Section 3 | L_a -G | 1.116 \angle - 176 | 1.05 | 5.1% |
| | L_a - L_b | 1.05 \angle - 177 | 0.99 | 0% |
| | L_a - L_b - L_c | 1.115 \angle - 176 | 1.05 | 5.1% |

5.4 Summary

The efficacy of using SOP for network protection was investigated. The SOP operating philosophy developed in earlier chapters were validated using a power hardware-in-the-loop experiment. Details of the major components of this experimental setup were discussed. These include a VSC prototype (HuT) connected to a DC voltage source representing an SOP, a network model developed in the RTDS and a power interface that connects the RTDS to the HuT.

The fault diagnostic capability of the SOP is validated using this experimental setup. A number of case studies have been implemented to validate the performance of the network with an SOP. The *FI* for different types of faults during a grid-connected operation with the SOP in the power control mode was investigated. The experiment was repeated for phase-to-ground faults, phase-to-phase faults and three phase faults. Experimental results from this case were consistent with the fault detection method proposed in the Chapter 3. The fault detection, fault type identification and estimation of fault location in the diagnostic mode were then investigated. The results obtained using this real-time PHIL experiment were consistent with the behaviour observed during the software simulation carried out in the Chapter 4. The experiment successfully demonstrated the use of SOP for protection of the network.

6

Conclusions and Future Work

Chapter 6 Conclusions and Future Work

6.1 Conclusion

Soft open points (SOPs) are power electronic devices installed in place of normally-open or normally-closed points in electrical power distribution networks. These devices are able to provide active power flow control, reactive power compensation and voltage regulation under normal network operating conditions.

In addition to their benefits during normal network conditions, SOPs have a potential to significantly improve fault response of a distribution network. In this thesis, the performance of a back-to-back voltage source converters (VSC) based SOP was investigated during network faults. A new application of SOPs was developed in the protection of MV distribution networks. The basic principle of integrating SOP into fault analysis was studied. In addition, the impact of using SOP on existing distributed feeder automation (D-FA) scheme was investigated. Equivalent sequence networks were formulated for different types of faults. They were further utilised to develop a method to detect the presence of faults, determine the type of faults and estimate the location of fault. The effectiveness of this method was verified using software simulation. The proposed operation of SOP was then validated in the laboratory using a PHIL experimental setup consisting of a VSC prototype and a distribution network modelled in a real-time digital simulator.

The results illuminate the role of SOP in distribution network protection, without the use of additional external devices. The protection features are easy to implement since the inputs require only the local measurements at the SOP grid connection point. SOPs were found to be able to enhance the network performance during faulted network conditions. The inclusion of fault diagnostic capability substantially improves the functional portfolio of an SOP. The details and key findings of the work carried out in this thesis are discussed below.

6.1.1 Fault analysis of a network with SOP

A fault analysis technique was developed to integrate the SOP into fault studies on distribution networks. The conventional fault analysis technique using symmetrical components was extended such that it can be applied on a simple distribution network with an SOP. The dynamic operation of an SOP during normal and faulted network conditions were observed. Equivalent sequence networks were developed for a network with SOP by incorporating the current contribution from the SOP. Equivalent networks were developed for different type of faults, including phase-to-ground faults, phase-to-phase faults and three-phase faults. They were individually verified for L_a -G, L_a - L_b and L_a - L_b - L_c faults using software simulations carried on a generic UK distribution network. A fault detection method was formulated by quantifying the sequence voltages at the SOP grid connection point while the SOP was operated in the power control mode.

Based on the fault analysis and simulations conducted the following key findings are listed below.

- It was observed that the measured values were consistent with the expected values, based on the equivalent sequence network for the respective faults. The fault analysis was found to be independent of the control mode of the SOP. The voltage at the grid connection point of faulted feeder was linearly correlated to the pre-fault set points of the SOP. However, the impact of set points was different for each of the symmetrical components. The correlation of the current injected by the SOP into the fault and the pre-fault set points were nonlinear and varying for different types of faults. Therefore, fault detection based on current measurements at the grid connection points was found to be unsuitable for a network with an SOP.
- The symmetrical voltages at the grid connection point of the faulted feeder were used as decision variables for fault detection. The Fault-Index (FI) was found to be an effective method to detect phase-to-ground faults, phase-to-phase faults and three-phase faults. During grid-connected operation the FI values were found to be within the defined limits for unfaulted network conditions and were well below the threshold (of 0.9) during faults. Fault detection using FI was effective for different control modes and pre-fault set points of the SOP. In addition, it was found to be applicable on distribution networks with different loading conditions. FI is a generic expression applicable for all voltage levels since it is normalised by the nominal voltage of the network.

6.1.2 Role of SOP in Feeder Automation

Distribution networks typically have some form of protection arrangement and automation to ensure minimal impact of network faults on the connected customers. The impact of the SOP dynamics on a conventional D-FA scheme was analysed during fault interruption and reclosing attempt. The diagnostic mode was developed to operate an SOP during network faults. A new D-FA scheme was proposed, in which the network diagnostic capability of SOP was utilised to coordinate the FA sequence. The key findings of the study are listed below.

- It was observed that the FA scheme was not disrupted when the SOP is operated in power control mode, at zero P and Q set points (i.e. when no power is exchanged through the terminals of the SOP). However, for non-zero set points, the current contributed from the SOP during network faults, disturbs the protection co-ordination of the network which in turn disrupts the sequence of FA scheme. Furthermore, the SOP loses synchronisation with the grid during an auto-reclose attempt following a temporary fault. A non-sinusoidal voltage was produced, leading to disruption of the network.
- It was found that network protection features can be achieved when the SOP was operated in the diagnostic mode by utilising the equivalent sequence networks of the faulted network. The operation of the diagnostic mode was achieved using only the local voltage and current measurements at the grid connection point of the faulted feeder and the SOP.
- Software simulations were carried out for L_a -G, L_a - L_b and L_a - L_b - L_c faults at different location on the feeder. Results showed that the SOP is able to detect the presence of a fault, determine the type of fault and estimate the faulted section on a radial distribution network.
- The proposed D-FA scheme incorporated the diagnostic mode operation with the existing operating modes of the SOP to improve the performance of the network during a fault. It was found that the FA scheme coordinated using SOP had substantial benefits in comparison to the existing D-FA schemes using auto-reclosers which include improvements in restoration times, user defined operation times and improved asset life.

6.1.3 Experimental validation

The fault diagnostic capability of an SOP was validated using a PHIL experimental setup. A VSC prototype connected to a stable DC voltage source was used

to emulate an SOP. This VSC prototype was integrated with a distribution network modelled in RTDS and was subjected to different faults.

Fault detection using FI was validated for the L_a-G , L_a-L_b and $L_a-L_b-L_c$ faults with the SOP operating in both power control and diagnostic modes. Other protection features of the diagnostic mode operation, including fault type identification and estimation of fault location were validated using this experiment. The results obtained using the real-time PHIL experiment were consistent with the software simulations. The results presented prove the capability of SOP to participate in the protection of distribution networks.

6.2 Future work

Recommendations to further extend the work reported in this thesis are grouped into three main categories.

- 1) Improvements in the diagnostic mode operation.
- 2) Broader scope of SOP applications
- 3) Supplementary analysis to justify the methods proposed.

6.2.1 Improvements in the diagnostic mode operation

The diagnostic mode operation proposed in the thesis was used to demonstrate the capability of SOP to participate in network protection. However, this work does not optimise the performance of SOP during fault diagnostics. It would be of value to assess the impact of feeder lengths and other network topologies on the results. Therefore, further analysis is required to optimise the operating voltage of a VSC in the diagnostic mode. In addition, there is a scope of improvement in estimating the location of the fault. Errors are introduced in the fault location algorithm due to the assumptions in single-end measurement method (e.g. ignoring the fault resistance and large load currents). Improvements in the accuracy of the results could be investigated by incorporating alternative methods for the estimation of fault location into the diagnostic mode operation of the SOP.

As discussed in the literature review SOP constructions exist with and without isolation transformers. However, the presence of isolation transformers (and their grounding arrangements) impacts the fault response of the SOP. Usually in HVDC applications, the choice of isolation transformer windings is dominated by the cost of insulation and the converter topology. However, this is not necessarily the case for MV networks. The cost of insulation is substantially cheaper for distribution networks due to

lower operating voltages. Furthermore, in most cases the choice of transformer grounding arrangements at lower voltage levels reflect the need of the interconnected AC networks. Currently, there are no standards or guidelines regarding the selection of isolation transformers. Determining the optimum winding arrangement for isolation transformers in MV networks should be undertaken as future work to this thesis. This is important to ensure coherent operation and control of the SOP during network faults.

The PHIL experimental setup used for the validation of SOP operation in the diagnostic mode can be modified to include a communication layer which will enable the demonstration of the D-FA scheme proposed. The I/O ports of Altera DE0 Nano development board can be programmed to coordinate with the RTDS model to demonstrate the desired operating sequence of the FA scheme.

6.2.2 Broader scope of SOP applications

This thesis focused on the operation of an SOP. However, it is clear from the study that the proposed operation is not limited to SOPs. The diagnostic mode operation could be applicable to other, more common power electronics converter applications. For example, power electronic converters that are usually used to integrate renewable energy resources to the network. Therefore, this study needs to be extended to broader VSC based applications and other SOP topologies to further explore its effectiveness.

The interaction of an SOP with a D-FA scheme was investigated in this thesis. However, the interactions of an SOP with other FA schemes were not explored. SOPs are suitable for other forms of automation since operation of the SOP is considerably faster in comparison to switching devices typically deployed in the network. Distribution networks use combinations of many devices to achieve FA. It is important to examine the co-ordination between various types of switching devices and the SOP. Individual FA schemes need to be analysed separately to achieve coordinated network operation in the presence of an SOP. In addition, a detailed study is required to investigate the impacts of the ICT infrastructure and its role in the deployment of SOPs in future smart grids.

Domestic and some commercial customers connected to the distribution network at LV level usually have single-phase connections. It is usually desirable to have single phase operation in such networks. The SOP in the diagnostic mode is able to identify the faulted phase during a fault. The control of SOP that allows for single phase operation needs to be investigated to ensure an optimum performance. Various types of low

impedance short circuit faults were investigated in this thesis. However, in order to incorporate single phase operation, fault analysis for open circuits and high impedance faults must also be included and can be extended to investigate single phase operation in FA schemes.

6.2.3 Supplementary study to justify the methods proposed

The technical application of using SOPs for the protection of distribution networks was the main focus of this thesis. A detailed analysis including the capital costs and other known benefits of SOP deployment is needed to build a business case. A purely economic evaluation of including protection features into an SOP needs to be carried out. Benefit quantification of this application gives better indication about the feasibility of this technology. This analysis is needed to ensure the wider deployment of this technology and its progress to higher technology readiness levels.

References

- [1] 'Global Warming and Climate Change Effects: Information and Facts', 2015. [Online]. Available: <https://www.nationalgeographic.com/environment/global-warming/global-warming-effects/>. [Accessed: 21-Jan-2018].
- [2] United Nations Framework Convention of Climate Change, 'Kyoto Protocol', 1998. [Online]. Available: http://unfccc.int/kyoto_protocol/items/2830.php. [Accessed: 18-Nov-2017].
- [3] T. Overbye, 'The Electric Power Industry and Climate Change : Power System Research Possibilities', 2007.
- [4] DECC, 'National Renewable Energy Action Plan for the United Kingdom Article 4 of the Renewable Energy Directive', *Dep. Energy Clim. Chang.*, pp. 1–160, 2009.
- [5] Great Britain. Department of Energy and Climate Change., 'The UK renewable energy strategy', 2009.
- [6] European Commission, 'EU Energy ,Transport and GHG emission trends 2050', 2013.
- [7] J. Ekanayake, N. Jenkins, K. Liyanage, and A. Yokoyama, *Smart Grid : Technology and Applications*. Wiley, 2012.
- [8] ETP SmartGrids, *European technology platform smart grids: vision and strategy for Europe's electricity networks of the future*, vol. 19, no. 3. 2006.
- [9] P. M. Connor, P. E. Baker, D. Xenias, N. C. Balta-Ozkan, C. J. Axon, and L. Cipcigan, 'Policy and regulation for smart grids in the United Kingdom', *Renew. Sustain. Energy Rev.*, vol. 40, pp. 269–286, Dec. 2014.
- [10] Electricity Networks Strategy Group - Reports, 'Electricity Networks Strategy: Smart Grid Route map', 2010. [Online]. Available: <http://webarchive.nationalarchives.gov.uk/20100919181612/http://www.ensg.gov.uk/index.php?article=126>. [Accessed: 18-Nov-2017].
- [11] H. Farhangi, 'The path of the smart grid', *IEEE Power Energy Mag.*, vol. 8, no. 1, pp. 18–28, Jan. 2010.
- [12] 'Low Carbon Networks Fund | Ofgem'. [Online]. Available: <https://www.ofgem.gov.uk/electricity/distribution-networks/network-innovation/low-carbon-networks-fund>. [Accessed: 18-Nov-2017].
- [13] 'Network innovation | Ofgem', 2017. [Online]. Available:

- <https://www.ofgem.gov.uk/electricity/distribution-networks/network-innovation>.
[Accessed: 18-Nov-2017].
- [14] Western Power Distribution (WPD) South West, 'Low Carbon Networks Fund Full Submission: LCN Fund Tier 2 Bid 2014 WPDT206/2R'. [Online]. Available: https://www.ofgem.gov.uk/sites/default/files/docs/2014/11/low_carbon_networks_fund_submission_from_wpd_-_ne.pdf. [Accessed: 18-Nov-2017].
- [15] 'Electricity Network Innovation Competition: 2015 funding decision | Ofgem'. [Online]. Available: <https://www.ofgem.gov.uk/publications-and-updates/electricity-network-innovation-competition-2015-funding-decision>. [Accessed: 18-Nov-2017].
- [16] N. Jenkins, C. Long, and J. Wu, 'An Overview of the Smart Grid in Great Britain', *Engineering*, vol. 1, no. 4, pp. 413–421, 2015.
- [17] UKPN, 'Flexible Urban Networks – Low Voltage Project Closedown Report Flexible Urban Networks – Low Voltage', 2017.
- [18] D. M. Staszkesky, D. Craig, and C. Befus, 'Advanced feeder automation is here', *IEEE Power Energy Mag.*, vol. 3, no. 5, pp. 56–63, Sep. 2005.
- [19] C. Beard, *Smart Grids for Dummies*. John Wiley and Sons, Ltd, Publication, 2010.
- [20] J. Northcote-Green and R. Wilson, *Control and automation of electrical power distribution systems*. CPC Press; Taylor and Francis Group, 2013.
- [21] R. Cordwell and M. Adolphus, 'Engineering Design Standard Eds 08-0136 Lv Network Design Standard This Is an Uncontrolled Document , the Reader Must Confirm Its Validity Before Use', 2014.
- [22] Cooper Power Systems, 'Eaton's Cooper Power Systems catalog: Reclosers and controls', 2015. [Online]. Available: http://www.eaton.com/ecm/idcplg?IdcService=GET_FILE&allowInterrupt=1&RevisionSelectionMethod=LatestReleased&Rendition=Primary&dDocName=PCT_1130880. [Accessed: 05-May-2017].
- [23] 'Switchgear, High-Voltage. "Controlgear—Part 203: Gas-Insulated Metal-Enclosed Switchgear for Rated Voltages Above 52 kV :IEC Standard (2003): 62271-203'.
- [24] 'Common specifications for high-voltage switchgear and control gear standards: IEC 60694-2002.'
- [25] *IEEE Std C37.20.2-2015 (Revision of IEEE Std C37.20.2-1999) - Redline: IEEE Standard for Metal-Clad Switchgear - Redline*. IEEE, 2015.

- [26] S. Koul, 'Comparative requirements of IEC and IEEE standards for medium-voltage switchgear', *IEEE Trans. Power Deliv.*, vol. 24, no. 4, pp. 1912–1923, 2009.
- [27] 'Quality of Service Incentives | Ofgem', 2015. [Online]. Available: <https://www.ofgem.gov.uk/electricity/distribution-networks/network-price-controls/quality-service/quality-service-incentives>. [Accessed: 14-Dec-2017].
- [28] F. Mekic, K. Alloway, C. Angelo, and R. Goodin, 'Fault Detection Isolation and Restoration on the Feeder(FDIR): Pick Your Technology', in *21th Int. Conf. on Elec. Distribution CIRED.*, 2011, no. 366, pp. 6–9.
- [29] I. Hwang, S. Kim, Y. Kim, and C. E. Seah, 'A survey of fault detection, isolation, and reconfiguration methods', *IEEE Trans. Control Syst. Technol.*, vol. 18, no. 3, pp. 636–653, 2010.
- [30] D. S. Popovic, L. R. Glamocic, and M. D. Nimrihter, 'The optimal automation level of medium voltage distribution networks', *Int. J. Electr. Power Energy Syst.*, vol. 33, no. 3, pp. 430–438, 2011.
- [31] A. R. Weller, L. Waters, and B. D'Albertanson, 'Centralised Automation of the East of England Network', in *Electricity Distribution, 2005. CIRED 2005. 18th International Conference and Exhibition*, 2005, pp. 1–5.
- [32] 'C37.104-2012 - IEEE Guide for Automatic Reclosing of Circuit Breakers for AC Distribution and Transmission Lines', *IEEE Std C37.104-2012 (Revision of IEEE Std C37.104-2002)*. pp. 1–72, 2012.
- [33] C. Kriger, S. Behardien, and J.-C. Retonda-Modiya, 'A Detailed Analysis of the Generic Object-Oriented Substation Event Message Structure in an IEC 61850 Standard-Based Substation Automation System', *Int. J. Comput. Commun. Control*, vol. 8, no. 5, p. 708, 2013.
- [34] P. Parikh, I. Voloh, and M. Mahony, 'Distributed fault detection, isolation, and restoration (FDIR) technique for smart distribution system', *2013 66th Annu. Conf. Prot. Relay Eng. CPRE 2013*, pp. 172–176, 2013.
- [35] A. Apostolov and B. Vandiver, 'IEC 61850 GOOSE applications to distribution protection schemes', in *2011 64th Annual Conference for Protective Relay Engineers*, 2011, pp. 178–184.
- [36] M. Lehtonen, M. Fotuhi-Firuzabad, S. Kazemi, and R. J. Millar, 'Application of pulse closing technology for automatic loop restoration', in *22nd International Conference and Exhibition on Electricity Distribution (CIRED 2013)*, 2013, pp. 0197–0197.

- [37] T. Taylor, T. Fahey, T. Royster, and D. Engler, 'New recloser functionality enhances feeder automation', in *Transmission and Distribution Exposition Conference: 2008 IEEE PES Powering Toward the Future, PIMS 2008*, 2008, pp. 1–8.
- [38] C. A. McCarthy, 'New technology for looped distribution feeders', in *2008 IEEE/PES Transmission and Distribution Conference and Exposition: Latin America*, 2008, pp. 1–5.
- [39] J. P. H. Knauss, C. Warren, and D. Kearns, 'An innovative approach to smart automation testing at National Grid', *Proc. IEEE Power Eng. Soc. Transm. Distrib. Conf.*, pp. 1–8, 2012.
- [40] T. Green and N. Jenkins, 'HubNet Position Paper No 3 - Issues for Distribution System Operation at 2030 - Version 4.0', 2014. [Online]. Available: <http://hubnet.org.uk/filebyid/523/2030GridOperation.pdf>. [Accessed: 27-Jan-2017].
- [41] Y. L. Tan, 'Analysis of line compensation by shunt-connected FACTS controllers: a comparison between SVC and STATCOM', *IEEE Power Eng. Rev.*, vol. 19, no. 8, pp. 57–58, 1999.
- [42] R. Silversildes, T. Green, and T. Luth, 'HubNet Position Paper No 6 - Power Electronics in Distribution System Management - Version 2.0', 2015. [Online]. Available: http://hubnet.org.uk/filebyid/535/PE_Distribution.pdf. [Accessed: 27-Jan-2017].
- [43] 'UK Power Networks - Flexible Urban Networks - Low Voltage', 2017. [Online]. Available: <http://innovation.ukpowernetworks.co.uk/innovation/en/Projects/tier-2-projects/Flexible-Urban-Networks-Low-Voltage/>. [Accessed: 18-Nov-2017].
- [44] Scottish Power Energy Networks, 'Electricity NIC submission: SP Energy Networks – ANGLE-DC', 2016. [Online]. Available: <https://www.ofgem.gov.uk/publications-and-updates/electricity-nic-submission-sp-energy-networks-angle-dc>. [Accessed: 15-Dec-2016].
- [45] Scottish Power Energy Networks, 'Electricity Network Innovation Competition Screening Submission-LV Engine', 2017. [Online]. Available: <https://www.ofgem.gov.uk/ofgem-publications/56848/national-gridelec-nicmsb.pdf>.
- [46] Ofgem, 'Network Innovation Competition 2017 Funding Decisions Decision', 2017.
- [47] J. Flottesmesch and M. Rother, 'Optimized energy exchange in primary distribution networks with DC links', 2004, vol. 1, pp. 108–116.
- [48] C.-Y. Tang, Y.-F. Chen, Y.-M. Chen, and Y.-R. Chang, 'DC-Link Voltage Control Strategy for Three-Phase Back-to-Back Active Power Conditioners', *IEEE Trans. Ind. Electron.*, vol. 62, no. 10, pp. 6306–6316, Oct. 2015.

- [49] M. Barragán-Villarejo, E. Romero-Ramos, A. Marano-Marcolini, J. . Maza-Ortega, and A. Gómez-Expósito, 'Voltage source converter-based topologies to further integrate renewable energy sources in distribution systems', *IET Renew. Power Gener.*, vol. 6, no. September 2011, pp. 435–445, 2012.
- [50] W. Cao, J. Wu, and N. Jenkins, 'Feeder load balancing in MV distribution networks using soft normally-open points', in *IEEE PES Innovative Smart Grid Technologies, Europe; Istanbul, Turkey*, 2014, pp. 1–6.
- [51] W. Cao, J. Wu, N. Jenkins, C. Wang, and T. Green, 'Operating principle of Soft Open Points for electrical distribution network operation', *Appl. Energy*, vol. 164, pp. 245–257, 2016.
- [52] W. Cao, 'Soft Open Points for the Operation of Medium Voltage Distribution Networks', PhD Thesis; Cardiff University, 2015.
- [53] J. M. Bloemink and T. C. Green, 'Benefits of Distribution-Level Power Electronics for Supporting Distributed Generation Growth', *IEEE Trans. Power Deliv.*, vol. 28, no. 2, pp. 911–919, Apr. 2013.
- [54] M. Saeedifard, M. Graovac, R. F. Dias, and R. Iravani, 'DC power systems: Challenges and opportunities', *IEEE PES Gen. Meet.*, pp. 1–7, 2010.
- [55] M. Othman, A. Rajabi-Ghahnavieh, and M. Fotuhi-Firuzabad, 'Optimal unified power flow controller application to enhance total transfer capability', *IET Gener. Transm. Distrib.*, vol. 9, no. 4, pp. 358–368, Mar. 2015.
- [56] C. Wang, G. Song, P. Li, H. Ji, J. Zhao, and J. Wu, 'Optimal siting and sizing of soft open points in active electrical distribution networks', *Appl. Energy*, vol. 189, pp. 301–309, 2017.
- [57] C. Wang, G. Song, P. Li, H. Ji, J. Zhao, and J. Wu, 'Optimal Configuration of Soft Open Point for Active Distribution Network Based on Mixed-integer Second-order Cone Programming', *Energy Procedia*, vol. 103, no. April, pp. 70–75, 2016.
- [58] L. Bai, T. Jiang, F. Li, H. Chen, and X. Li, 'Distributed energy storage planning in soft open point based active distribution networks incorporating network reconfiguration and DG reactive power capability', *Appl. Energy*, no. (In press), 2017.
- [59] H. Ji, C. Wang, P. Li, J. Zhao, G. Song, F. Ding, and J. Wu, 'An enhanced SOCP-based method for feeder load balancing using the multi-terminal soft open point in active distribution networks', *Appl. Energy*, vol. 208, no. August, pp. 986–995, 2017.
- [60] E. Romero-Ramos, A. Gómez-Expósito, A. Marano-Marcolini, J. M. Maza-Ortega, and J. L. Martinez-Ramos, 'Assessing the loadability of active distribution networks in the

- presence of DC controllable links', *Gener. Transm. Distrib. IET*, vol. 5, no. 11, pp. 1105–1113, 2011.
- [61] Q. Qi, J. Wu, and C. Long, 'Multi-objective operation optimization of an electrical distribution network with soft open point', *Appl. Energy*, vol. 208, no. September, pp. 734–744, 2017.
- [62] W. Cao, J. Wu, N. Jenkins, C. Wang, and T. Green, 'Benefits analysis of Soft Open Points for electrical distribution network operation', *Appl. Energy*, vol. 165, pp. 36–47, 2016.
- [63] L. J. Thomas, A. Burchill, D. J. Rogers, M. Guest, and N. Jenkins, 'Assessing distribution network hosting capacity with the addition of soft open points', in *5th IET International Conference on Renewable Power Generation (RPG) 2016*, 2016, p. 32 (6 .)-32 (6 .).
- [64] C. Long, J. Wu, L. Thomas, and N. Jenkins, 'Optimal Operation of Soft Open Points in Medium Voltage Electrical Distribution Networks with Distributed Generation', *Appl. Energy*, vol. 184, pp. 427–437, 2016.
- [65] S. Khan and S. Bhowmick, 'Impact of DC link control strategies on the power-flow convergence of integrated AC-DC systems', *Ain Shams Eng. J.*, vol. 7, no. 1, pp. 249–264, 2016.
- [66] J. M. Bloemink and T. C. Green, 'Increasing distributed generation penetration using soft normally-open points', in *IEEE PES General Meeting; Minneapolis, USA*, 2010, pp. 1–8.
- [67] P. Li, H. Ji, C. Wang, J. Zhao, G. Song, F. Ding, and J. Wu, 'Coordinated Control Method of Voltage and Reactive Power for Active Distribution Networks Based on Soft Open Point', *IEEE Trans. Sustain. Energy*, vol. 8, no. 4, pp. 1430–1442, 2017.
- [68] J. M. Bloemink and T. C. Green, 'Increasing photovoltaic penetration with local energy storage and soft normally-open points', in *2011 IEEE Power and Energy Society General Meeting; Detroit, USA*, 2011, pp. 1–8.
- [69] G. Bathurst, G. Hwang, and L. Tejwani, 'MVDC - The New Technology for Distribution Networks', *11th IET Int. Conf. AC DC Power Transm.*, no. Dc, pp. 1–5, 2015.
- [70] S. Giannelos, I. Konstantelos, and G. Strbac, 'Option value of Soft Open Points in distribution networks', in *2015 IEEE Eindhoven PowerTech*, 2015, pp. 1–6.
- [71] A. Aithal and J. Wu, 'Operation and performance of a medium-voltage DC link', *CIGRE - Open Access Proc. J.*, vol. 2017, no. 1, pp. 1355–1358, Oct. 2017.
- [72] P. Li, H. Ji, C. Wang, J. Zhao, G. Song, F. Ding, and J. Wu, 'Optimal Operation of Soft Open Points in Active Distribution Networks Under Three-Phase Unbalanced Conditions',

- IEEE Trans. Smart Grid*, pp. 1–1, 2017.
- [73] W. Cao, J. Wu, and Z. Huang, 'Use of Soft Open Points for Supply Restoration in Medium Voltage Distribution Networks', in *IEEE PES Asia-Pacific Power and Energy Engineering Conference; Brisbane, Australia*, 2015, pp. 1–6.
- [74] P. Li, G. Song, H. Ji, J. Zhao, C. Wang, and J. Wu, 'A supply restoration method of distribution system based on Soft Open Point', in *2016 IEEE Innovative Smart Grid Technologies - Asia (ISGT-Asia)*, 2016, pp. 535–539.
- [75] A. Kirakosyan, M. S. El Moursi, and V. Khadkikar, 'Fault ride through and grid support topology for the VSC-HVDC connected offshore wind farms', *IEEE Trans. Power Deliv.*, vol. 32, no. 3, pp. 1592–1604, 2017.
- [76] A. Moawwad, M. S. El Moursi, and W. Xiao, 'Advanced Fault Ride-Through Management Scheme for VSC-HVDC Connecting Offshore Wind Farms', *IEEE Trans. Power Syst.*, vol. 31, no. 6, pp. 4923–4934, 2016.
- [77] S. Mortazavian, M. M. Shabestary, and Y. A. R. I. Mohamed, 'Analysis and Dynamic Performance Improvement of Grid-Connected Voltage-Source Converters under Unbalanced Network Conditions', *IEEE Trans. Power Electron.*, vol. 32, no. 10, pp. 8134–8149, 2017.
- [78] W. Kou and S.-Y. Park, 'Generalized direct phase-coordinates control of inverter-interfaced distributed energy resources on fault ride through strategies', in *2017 North American Power Symposium (NAPS)*, 2017, pp. 1–6.
- [79] C. Kim, T. Bialek, and J. Awiylika, 'An initial investigation for locating self-clearing faults in distribution systems', *IEEE Trans. Smart Grid*, vol. 4, no. 2, pp. 1105–1112, 2013.
- [80] C. A. Plet and T. C. Green, 'Fault response of inverter interfaced distributed generators in grid-connected applications', *Electr. Power Syst. Res.*, vol. 106, pp. 21–28, 2014.
- [81] A. Yazdani and R. Iravani, 'Grid Imposed Frequency VSC system: Control in dq-Frame', in *Voltage-sourced converters in power systems: modeling, control, and applications*, John Wiley & Sons, 2010, pp. 204–245.
- [82] C. L. Trujillo, D. Velasco, J. G. Guarnizo, and N. Díaz, 'Design and implementation of a VSC for interconnection with power grids, using the method of identification the system through state space for the calculation of controllers', *Appl. Energy*, vol. 88, no. 9, pp. 3169–3175, 2011.
- [83] M. Kalantar and S. M. Mousavi G., 'Dynamic behavior of a stand-alone hybrid power generation system of wind turbine, microturbine, solar array and battery storage', *Appl.*

- Energy*, vol. 87, no. 10, pp. 3051–3064, 2010.
- [84] A. Egea Álvarez, A. Junyent Ferré, and O. Gomis Bellmunt, 'Active and reactive power control of grid connected distributed generation systems', in *Modeling and Control of Sustainable Power Systems*, Springer Berlin Heidelberg, 2012, pp. 47–81.
- [85] J. Alcalá, V. Cardenas, A. R. Ramirez-Lopez, and J. Gudino-Lau, 'Study of the bidirectional power flow in Back - to - Back converters by using linear and nonlinear control strategies', in *2011 IEEE Energy Conversion Congress and Exposition*, 2011, pp. 806–813.
- [86] R. Teodorescu, M. Liserre, and P. Rodriguez, *Grid Converters for Photovoltaic and Photovoltaic and Wind Power Systems*, Vol 29. John Wiley & Sons., 2011.
- [87] B. Y. C. Fortescue, 'The Measurement of Power in Polyphase Circuits', *J. Am. Inst. Electr. Eng.*, vol. 42, no. 3, p. 205–218., 1923.
- [88] B. M. Weedy, B. J. Cory, N. Jenkins, J. B. Ekanayake, and G. Strbac, *Electric power systems*, 5th ed. Wiley, 2012.
- [89] ALSTOM Grid, 'Network Protection & Automation Guide', 2011. [Online]. Available: <http://electrical-engineering-portal.com/download-center/books-and-guides/electrical-engineering/automation-guide>. [Accessed: 22-Dec-2016].
- [90] S. Lotfi-fard, J. Faiz, and M. R. Iravani, 'Improved overcurrent protection using symmetrical components', *IEEE Trans. Power Deliv.*, vol. 22, no. 2, pp. 843–850, 2007.
- [91] The Electricity Council, 'Planning Limits for Voltage Unbalance in the United Kingdom', *Engineering Recommendation P29*, 1990. [Online]. Available: <http://www.nienetworks.co.uk/documents/Security-planning/ER-P29.aspx>. [Accessed: 27-Jan-2017].
- [92] C. Foote, P. Djapic, G. Ault, J. Mutale, and G. Strbac, 'United kingdom generic distribution system (UKGDS)', *DTI Centre for Distributed Generation and Sustainable Electrical Energy*, 2010. [Online]. Available: <https://github.com/sedg/ukgds>. [Accessed: 27-Jan-2017].
- [93] S. Ingram, S. Probert, and K. Jackson, 'Impact of Small Scale Embedded Generation on operating parameters of Distribution Networks, Department of Trade and Industry & Renewable Energy Program', *K/EI/00303/04/01 URN 03/1051*, 2003. [Online]. Available: http://webarchive.nationalarchives.gov.uk/20100919181607/www.ensg.gov.uk/assets/22_01_2004_phase1b_report_v10b_web_site_final.pdf. [Accessed: 27-Jan-2017].
- [94] J. Candelaria and J. D. Park, 'VSC-HVDC system protection: A review of current methods',

- 2011 *IEEE/PES Power Syst. Conf. Expo. PSCE 2011*, pp. 1–7, 2011.
- [95] ABB Inc., *OVR outdoor vacuum reclosers 15-38 kV Innovative designs ensure system reliability*. 2012.
- [96] L. L. Grigsby, *The Electric Power Engineering Handbook: Electric Power Generation, Transmission, and Distribution*, Third Edit. CRC Press, Taylor & Francis Group, 2012.
- [97] S. Das, S. Santoso, A. Gaikwad, and M. Patel, 'Impedance-based fault location in transmission networks: Theory and application', *IEEE Access*, vol. 2, pp. 537–557, 2014.
- [98] 'IEEE Guide for Determining Fault Location on AC Transmission and Distribution Lines IEEE Power and Energy Society-IEEE Std C37.114™-2014', 2014.
- [99] M. M. Saha, J. Izykowski, and E. Rosolowski, *Fault Location on Power Networks*, vol. 48, no. January 2010. 2010.
- [100] User Manual, *DE0-Nano*, 2013th ed. Terasic Technologies Inc, 2013.
- [101] J. Belanger, P. Venne, and J.-N. Paquin, 'The What, Where and Why of Real-Time Simulation', *Planet RT*, vol. 1, no. 0, pp. 37–49, 2010.
- [102] H. Dommel, 'Nonlinear and Time-Varying Elements in Digital Simulation of Electromagnetic Transients', *IEEE Trans. Power Appar. Syst.*, vol. PAS-90, no. 6, pp. 2561–2567, Nov. 1971.
- [103] K. S. Amitkumar, R. S. Kaarthik, and P. Pillay, 'A versatile power-hardware-in-the-loop based emulator for rapid testing of electric drives', in *2017 IEEE Energy Conversion Congress and Exposition (ECCE)*, 2017, pp. 5468–5474.
- [104] P. M. Menghal and A. J. Laxmi, 'Real time simulation: Recent progress & challenges', in *2012 International Conference on Power, Signals, Controls and Computation*, 2012, pp. 1–6.
- [105] M. D. Omar Faruque, T. Strasser, G. Lauss, V. Jalili-Marandi, P. Forsyth, C. Dufour, V. Dinavahi, A. Monti, P. Kotsampopoulos, J. A. Martinez, K. Strunz, M. Saeedifard, Xiaoyu Wang, D. Shearer, and M. Paolone, 'Real-Time Simulation Technologies for Power Systems Design, Testing, and Analysis', *IEEE Power Energy Technol. Syst. J.*, vol. 2, no. 2, pp. 63–73, 2015.
- [106] Z. Tan, F. Gong, H. Tang, H. Chen, and F. Zhao, 'Research on distribution grid simulation and test based on RTDS and simulation tools', in *2017 IEEE 3rd Information Technology and Mechatronics Engineering Conference (ITOEC)*, 2017, pp. 794–798.

- [107] R. Iracheta-Cortez and N. Flores-Guzman, 'Developing automated Hardware-In-the-Loop tests with RTDS for verifying the protective relay performance', in *2016 IEEE 36th Central American and Panama Convention (CONCAPAN XXXVI)*, 2016, pp. 1–9.
- [108] H. Dommel, 'Digital Computer Solution of Electromagnetic Transients in Single-and Multiphase Networks', *IEEE Trans. Power Appar. Syst.*, vol. PAS-88, no. 4, pp. 388–399, Apr. 1969.
- [109] P. Forsyth and R. Kuffel, 'Utility applications of a RTDS Simulator', *Int. Power Eng. Conf. 2007*, pp. 112–117, 2007.
- [110] C. S. Edrington, M. Steurer, J. Langston, T. El-Mezyani, and K. Schoder, 'Role of Power Hardware in the Loop in Modeling and Simulation for Experimentation in Power and Energy Systems', *Proc. IEEE*, vol. 103, no. 12, pp. 2401–2409, Dec. 2015.
- [111] A. Spina, R. Palaniappan, D. Hilbrich, U. Hager, and C. Rehtanz, 'Comparison between CHIL simulation and hardware test of a Dynamic Power Flow Controller', in *2017 IEEE Manchester PowerTech*, 2017, pp. 1–6.
- [112] RTDS_Technologies, 'Power Hardware in the Loop (PHIL)', 2013.

Appendix A

Appendix A-1

The Park transformation matrix $\mathbf{T}(\theta)$ is

$$\mathbf{T}(\theta) = \begin{bmatrix} \cos(\theta) & \cos(\theta - \frac{2\pi}{3}) & \cos(\theta + \frac{2\pi}{3}) \\ \sin(\theta) & \sin(\theta - \frac{2\pi}{3}) & \sin(\theta + \frac{2\pi}{3}) \\ 1/2 & 1/2 & 1/2 \end{bmatrix}$$

Appendix A-2

$$\mathbf{V}_x = \mathbf{v}_x^p + \mathbf{v}_x^n + \mathbf{v}_x^z ; \text{ where } \mathbf{v}_x = [v_a \quad v_b \quad v_c]^T ;$$

$$\begin{bmatrix} v_a \\ v_b \\ v_c \end{bmatrix} = \begin{bmatrix} v_a^p & v_a^n & v_a^z \\ v_b^p & v_b^n & v_b^z \\ v_c^p & v_c^n & v_c^z \end{bmatrix} \begin{bmatrix} 1 \\ 1 \\ 1 \end{bmatrix}$$

$$\begin{bmatrix} v_a^p \\ v_b^p \\ v_c^p \end{bmatrix} = \frac{1}{3} \begin{bmatrix} 1 & -1/2 & -1/2 \\ -1/2 & 1 & -1/2 \\ -1/2 & -1/2 & 1 \end{bmatrix} \begin{bmatrix} v_a \\ v_b \\ v_c \end{bmatrix} - \frac{1}{j2\sqrt{3}} \begin{bmatrix} 0 & 1 & -1 \\ -1 & 0 & 1 \\ 1 & -1 & 0 \end{bmatrix} \begin{bmatrix} v_a \\ v_b \\ v_c \end{bmatrix}$$

$$\begin{bmatrix} v_a^n \\ v_b^n \\ v_c^n \end{bmatrix} = \frac{1}{3} \begin{bmatrix} 1 & -1/2 & -1/2 \\ -1/2 & 1 & -1/2 \\ -1/2 & -1/2 & 1 \end{bmatrix} \begin{bmatrix} v_a \\ v_b \\ v_c \end{bmatrix} + \frac{1}{j2\sqrt{3}} \begin{bmatrix} 0 & 1 & -1 \\ -1 & 0 & 1 \\ 1 & -1 & 0 \end{bmatrix} \begin{bmatrix} v_a \\ v_b \\ v_c \end{bmatrix}$$

Appendix A-3

Table A.1 The set points used to simulate Scenarios 1-4 in Case 1

| Scenario No | VSC1 ($P_{1 Ref}$, $Q_{1 Ref}$) & VSC2 ($V_{dc Ref}$, $Q_{2 Ref}$) | VSC1 ($V_{dc Ref}$, $Q_{1 Ref}$) & VSC2 ($P_{2 Ref}$, $Q_{2 Ref}$) |
|-------------|---|---|
| | (MW, MVar) (kV, MVar) | (kV, MVar) (MW, MVar) |
| 1 | (0,0) (35,0) | (35,0) (0,0) |
| 2 | (0,-2) (35,0) | (35,-2) (0,0) |
| 3 | (2,-2) (35,0) | (35,-2) (2,0) |
| 4 | (-2,-2) (35,0) | (35,-2) (-2,0) |

Power flowing from SOP to Feeder-1 and Feeder-2 to SOP is assumed positive.

Appendix B

Appendix B-1

Table B.1 Protection settings for recloser R1

| Attempt no | Pick up current | Time dial setting | Curve |
|------------|-----------------|-------------------|------------------|
| Shot 1 | 0.65kA | 0.08 | Standard Inverse |
| Shot 2 | 0.65kA | 0.1 | Standard Inverse |
| Shot 3 | 0.65kA | Instantaneous | N/A |

Table B.2 Protection settings for recloser R2

| Attempt no | Pick up current | Time dial setting | Curve |
|------------|-----------------|-------------------|------------------|
| Shot 1 | 0.45kA | 0.08 | Standard Inverse |
| Shot 2 | 0.45kA | 0.1 | Standard Inverse |
| Shot 3 | 0.45kA | Instantaneous | N/A |